Made available through a Creative Commons CC-BY License

ACS Catalysis

pubs.acs.org/acscatalysis Review

MWW and MFI Frameworks as Model Layered Zeolites: Structures, Transformations, Properties, and Activity

Mariya Shamzhy, Barbara Gil,* Maksym Opanasenko, Wieslaw J. Roth, and Jiří Čejka*

Cite This: *ACS Catal.* 2021, 11, 2366−2396 Read Online

ACCESS | Metrics & More | Article Recommendations

ABSTRACT: Porous solids containing internal pores with sizes ranging from angstroms to nanometers are highly useful and valuable in the catalysis, separation, and storage of molecules because these materials provide large surface areas and void spaces for the interaction and adsorption of molecules. In particular, two-dimensional zeolites (2D, sometimes called layered zeolites) with layer thickness of 2−3 nm (1−2 unit cells) have enabled the synthesis of advanced materials and their application in catalysis for the transformation of bulky substrates unable to enter zeolite pores, thereby substantially increasing the number of zeolite applications and modifications. Accordingly, this Review aims to highlight recent developments in the synthesis, characterization, and application of 2D zeolites, focusing on the two most important representatives, **MWW** and **MFI**.

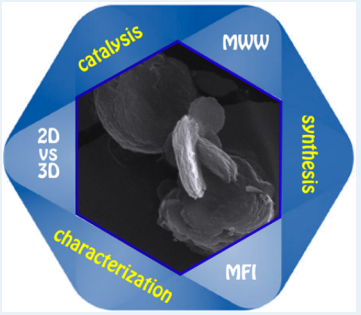

KEYWORDS: *layered zeolites, MWW and MFI frameworks, synthesis, structures, transformations, acidic properties, catalytic activity, alkylation, oxidation, biomass transformations*

See https://pubs.acs.org/sharingguidelines for options on how to legitimately share published articles.

INTRODUCTION

Porous solids have been one of the major sources of breakthroughs and innovations in catalysis and sorption. The processes involving porous catalysts are currently driving advances in key new areas, especially in green chemistry and environmental catalysis.[1] The main advantages in activity and performance have been shown by materials defined as molecular sieves with framework structures containing micropores of molecular dimensions.[2,3] In the case of zeolites, such structures can be realized in two (2D zeolites) or three (3D zeolites) dimensions.

The area of 2D zeolites is expanding rapidly with novel discoveries and insights reported continuously, which calls for timely updates. The emerging diversity justifies a focused approach as presented in this Review. The focus on two zeolites **MWW** and **MFI** (Figure 1), which are the most versatile and illustrate almost all known forms of 2D zeolites, provides a framework for analysis and development for the others. At the same time, both of them are available in highly active forms, which is rare with 2D zeolites, and can serve as representatives for analyzing catalytic activity. Importantly, the 3D forms of **MFI** and **MWW** are also industrial standards for a number of catalytic processes.

1. Zeolites and 3D Frameworks as Ideal (Micro)Porous Solids. The 3D framework structures with strictly defined micropores and channels of zeolites[4] represent ideal materials,[5−7] which have not only brought many practical benefits by themselves[8,9] but also triggered tremendous progress in related classes of material such as surfactant-templated mesoporous materials,[10,11] MOFs,[12] and low-dimensional solids, including clays and other layered materials.[13,14] The benefits from zeolites resulted in widespread industrial applications in the catalysis, separation, and storage of molecules.[15−17] Formally, zeolites can be defined as 4-connected tetrahedral frameworks composed of corner-sharing tetrahedra, TO_4, with a central T atom bonded to 4 oxygen atoms in which each tetrahedron has 4 neighbors, possibly except at the surface.[18,19] These structures contain micropores, whose sizes are of the same order as kinetic diameters of small molecules, thus exhibiting shape selective phenomena.

In the electrostatically neutral silicate framework, the inserted Al atoms generate negative centers capable of ion exchange and strong acid activity.[20] As a result of this structure, aluminosilicate zeolites exhibit high activity, shape selectivity, and chemical and thermal resistance.[21] Additionally, they are environmentally benign, inexpensive, and relatively easy to handle in large-scale synthesis and applications.[22] Among various useful aluminosilicates, with structures ranging from amorphous, through 2D clay minerals to 3D, zeolites are at the forefront in performance and quality in catalysis and sorption applications.[23]

Received: December 5, 2020
Revised: January 21, 2021
Published: February 5, 2021

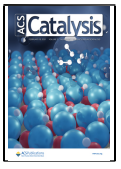

ACS Publications

© 2021 The Authors. Published by American Chemical Society

https://dx.doi.org/10.1021/acscatal.0c05332
ACS Catal. 2021, 11, 2366−2396

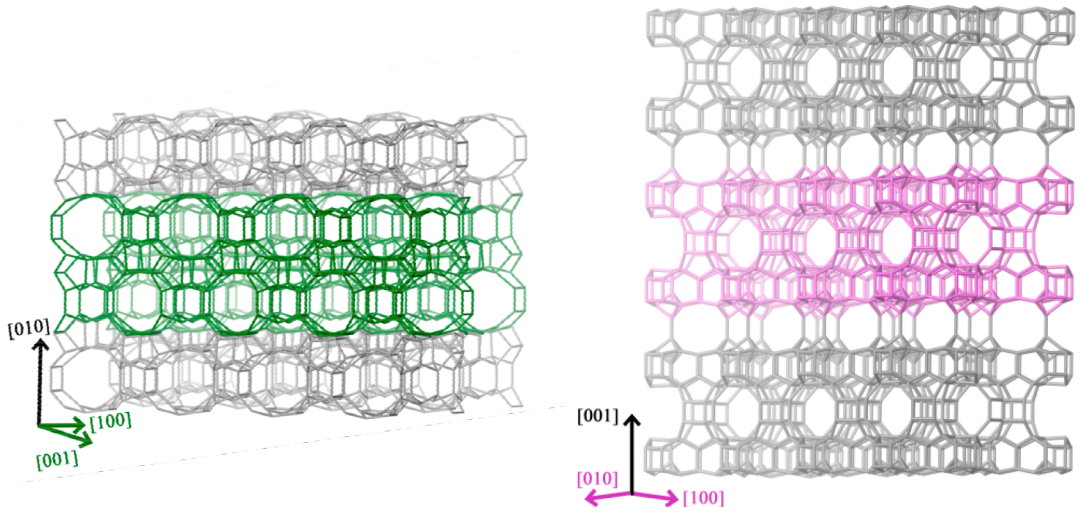

Figure 1. Structures of **MFI** (left) and **MWW** (right) zeolite frameworks showing the typical directions of layer formation (colored axes). Resulting [010] surface in **MWW** and [001] surface in **MFI** are exposed.

However, the greatest zeolite strengths arising from robust rigid structures have been also their liability. It is generally hard to modify zeolites postsynthesis, and their much-desired structure diversification has been possible almost exclusively by trial and error synthesis.[24] In contrast, 2D layered materials, which frequently compete with zeolites for the same applications (sometimes successfully), offer flexible structures with the possibility of diverse modifications: expansion, surface modification, and formation of intimate composites with other compounds.[25,26] For example, the synthesis and expansion of pillared layered clays has provided materials with pores larger than those of zeolites.[27] Yet, despite the larger pores of molecular sieves, their performance has not surpassed that of zeolites thus far. In total, there are now close to 250 approved zeolite framework topologies,[18] in addition to others pending approval (MCM-71, IPC-9),[28−30] and ca. 20 have already produced some layered form.[31,32]

2. Back to Two Dimensions—Layered Zeolite Precursors. In this context of perceived and often actual superiority of 3D structures, embodied by zeolites and their sharp differentiation from 2D solids, the discovery and even existence of 2D (i.e., layered zeolite structures) have marked a pivotal moment in the progress of these materials. The area of conventional 3D zeolites remains intact, with its benefits and dominance, at least for now, but a new dimension is added, with expanded flexibility, thus enabling structural and other modifications, including chemical alterations, which have been well developed with 2D solids.[33−36]

The recognition of 2D zeolites is directly related to the synthesis/discovery of a new framework related to the material MCM-22, later designated **MWW**, with medium-size pores and large internal supercages.[37] Zeolite **MWW** proved to be an excellent aromatic alkylation catalyst and, as such, was quickly implemented in valuable industrial process, replacing less environmentally friendly catalysts.[38,39] The syntheses of **MWW** using hexamethylenimine (HMI) as a template revealed two formation pathways: directly in 3D and via a 2D layered (zeolite) precursor named MCM-22P.[40] The latter was observed first and produced the complete 3D framework upon (topotactic) condensation of its constituent layers, approximately 2.5 nm thick. This was a surprising twist in our understanding of zeolites and was promptly confirmed in practice by the preparation of surfactant-intercalated (swollen) and silica pillared derivatives.[41] As often happens when unexpected phenomena are discovered or new materials prepared, examples of layered zeolite precursors already existed, but they were recognized only after **MWW**.[42,43]

The next significant advance was the synthesis of a precursor of the well-established 3D zeolite ferrierite,[44,45] while another milestone was reached with the synthesis of zeolite **MFI**[46,47] in a layered form. This proliferation of layered zeolite forms implied that all frameworks afford 2D precursors[31] as it is easy to imagine splitting a periodic structure into lower-dimensional fragments. The key question was how to do this. In practice, a periodic structure can be divided when the surface of a growing framework is terminated with hydroxyl groups instead of continued propagation in 3D by attachment of TO_4 tetrahedra. The problem lies in establishing conditions for such a termination, which for now remains a predominantly empirical approach although rational solutions may be found in the future. Similarly, in contrast to 3D frameworks, 2D zeolites can also be prepared via a top-down approach from previously synthesized germanosilicates. Because of labile Ge−O bonds, mostly located in double-4-rings (D4R) or double-3-rings (D3R), the parent 3D structure can be chemically selectively hydrolyzed to 2D silicate layers while preserving the original structure. Hence, further manipulations with these layers can be performed as those layered forms prepared by direct synthesis.[48−50]

As an addition to conventional zeolites, 2D zeolites neither violate the formal definition nor require revising basic tenets and concepts, but the 3D zeolite forms continue to dominate, especially in practical uses, with only approximately 20 of 250 approved frameworks yielding layered forms. As a fundamental expansion, these materials either bring forward new or broaden existing principles in a number of ways.

First, so far, zeolite layers have usually been less than a few nanometers thick, but the transition between 2D and 3D may become blurred and produce a continuum of layer thicknesses (increasing number of unit cells). The framework **MFI** has already produced layers with different thicknesses.[51,52]

Second, an expanded concept of secondary zeolite structures can be proposed to include all forms, such as various layer arrangements and composites, with nonzeolites, even amorphous components, acting as auxiliaries between zeolite layers.[31]

https://dx.doi.org/10.1021/acscatal.0c05332
ACS Catal. 2021, 11, 2366−2396

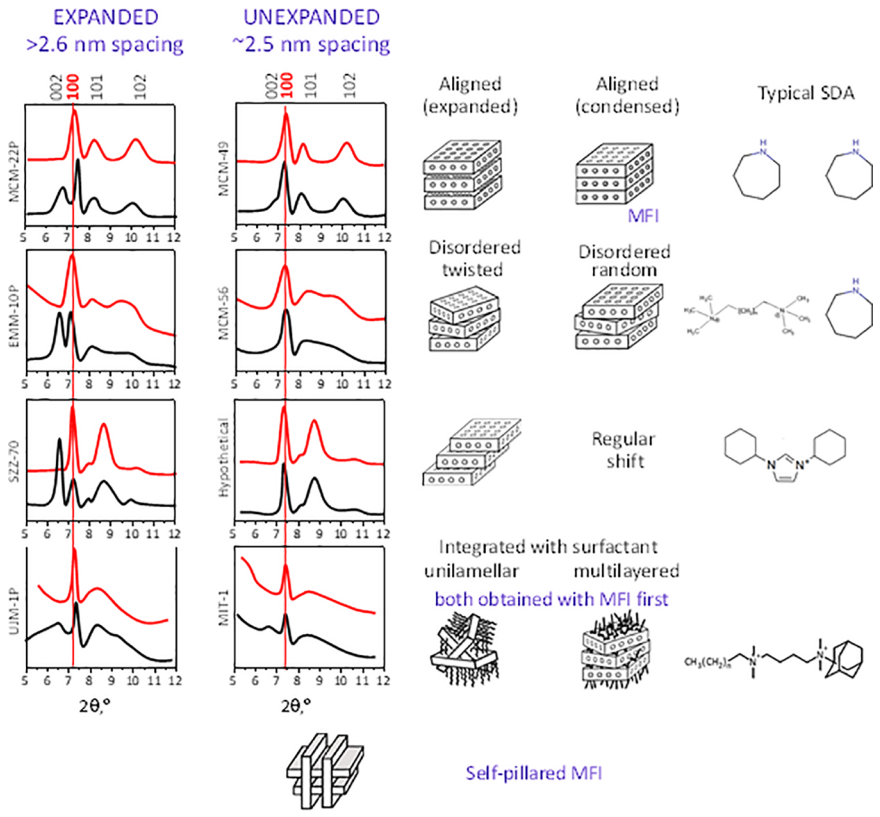

Figure 2. Different layered forms of the zeolites **MWW** and **MFI**/ZSM-5 (indicated in violet) synthesized in one-pot with XRD patterns for **MWW** as-synthesized and calcined (bottom and top, respectively), showing distinct features for identifying different materials. The reported preparation of a swollen **MWW** by direct synthesis is discussed separately. Upon calcination, the expanded **MWW** materials show XRD pattern like the unexpanded (on the right), but upon silylation (with bridging compounds like $(alkyl)_2Si(OR)_2$ referred to as stabilization) the expanded structure and corresponding XRD pattern are preserved, where applicable. All patterns are based on published experimental profiles.

Third, the practical significance of these layered zeolites lies in their greatly expanded potential for innovation: zeolites in the standard 3D form have rigid, immutable structures, but as layered materials, they can be readily modified into new architectures, topotactically functionalized, and converted into intimate composites.[33] The practical benefits from modifying 2D zeolites include increased openness with a concomitant increase in access to active sites and enhanced diffusion. These benefits are illustrated by the first material with such properties ever produced, namely the pillared layered form of zeolite **MWW**, designated MCM-36 and discussed below in the section 4.2.2 on pillared layered materials.[41,53] Several other materials showing added benefits were subsequently prepared and demonstrated.

2D zeolites raise an immediate question about their comparison with 3D frameworks in terms of activity, performance, and stability. These properties depend on specific circumstances, although we have already mentioned a pillared form that shows superior activity (MCM-36). In fact, the picture is rather mixed, as discussed below, but new opportunities for layered zeolites may entail less favorable practical factors, including complicated multistep synthesis, increased exposure of active sites, and reduced confinement impacting intrinsic activity. This will be reviewed in detail later on.

The ultimate goal of this overview is to discuss the main synthesis, textural, and structural features of 2D zeolites of the **MFI** and **MWW** types, as the two most important representatives of this class so far, and to relate their properties to selected catalytic reactions. Earlier and more general reviews have covered other frameworks,[31,54−61] which are not as broadly developed as **MFI** and **MWW** but should mimic their advances.

3. Synthesis and Structure of 2D Zeolites. *3.1. Layered Zeolite Precursors.* The term layered zeolite precursor was coined when the framework **MWW** was first converted into a layered material, that is, when the 3D zeolite **MWW** (MCM-22) was produced from the layered precursor MCM-22P upon calcination.[37,62] This ability to form a layered material was concluded from XRD patterns, as shown in the top left corner of Figure 2, depicting a congruent condensation of the layers upon contraction of the unit cell from 2.7 to 2.5 nm.

This illustrates a general pattern occurring upon condensation/calcination of layered precursors showing in-layer reflections not changing their *d*-spacing position (except mono- and triclinic) while the interlayer reflections shift to lower *d*-spacing.[45] The condensation of precursors is not always congruent and can result in disordered or incomplete structures.[63−65] This can be attributed to unfavorable vertical alignment associated with interlayer organic templates. In such cases, a more favorable arrangement can be achieved with another template through direct synthesis or by removal of the original one and reintercalation of suitable organic compounds.[66] The importance of zeolite precursors lies in the potential for modification, especially expansion to produce derivative structures with increased porosity, accessibility of acid sites, and enhanced diffusion of reactants.

The framework **MWW** shows that the number of distinct layered forms forming directly by synthesis can be considerable as illustrated in Figures 2 and 3. Thus, **MWW** layers can be

https://dx.doi.org/10.1021/acscatal.0c05332
ACS Catal. 2021, 11, 2366−2396

	Proposed notation	Different layered forms (proposed)	Schematic structure as-synthesized	Schematic structure calcined	MWW	MFI	Other frameworks with layered forms (first and/or notable reports cited)
					Representative examples		
1	ZEO	3D Framework			MCM-22 calc[37,62,85] MCM-49[40,86]	MFI/ZSM-5,[87-88] silicalite[89]	MEL,[90-91] FER[92-93]/CDO[94-95], CAS[96]/NSI[42,97], RRO[98]/HEU[99-100], SOD[101], RWR[102], AFO[103], AST[104], MTF[105-106], RTH[107], PCR[108], 'IPC-9'[30], STI[109-110], SFO[111]
2	Pre-ZEO	Precursor, multilayered, ordered (can form complete 3D framework)			MCM-22P[62] ERB-1[112] SSZ-25[113] PSH-3[114]	Not available NA	FER[45],CDO[94-95],NSI[42,97], HEU[115], RRO[98], SOD[116-117], RWR[43,118-121], AFO[122], AST[123], MTF[124], RTH[125], PCR[108], 'IPC-9'[30], STI[126], SFO[127]
3	dPre-ZEO	Disordered multilayered precursor (forms incomplete 3D framework)			EMM-10P[128] IPC-3P[129] UZM-8[130]	NA	
4	Pre-ZEOd	Multilayered precursor with shifted layers forming incomplete 3D framework	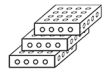		SSZ-70[74] ECNU-5[82]	NA	FER (ERS-12)[64]
5	Del-ZEO	Monolayer; delaminated			MCM-56[69-70]	NA	
6	mSurf-ZEO	Multilamellar precursor with surfactant			UJM-1P/ UJM-1[80]	Multilamellar nanosheets[47]	
7	uSurf-ZEO	Unilamellar precursor with surfactant			MIT-1[79]	Unilamellar nanosheets[131]	
8	Pre-ZEO-det	De-templated precursor forming sub-zeolite			MCM-56 analog[132]	NA	FER[133], CDO[134], NSI[135-137], SOD[138], RWR[119], PCR[139]
9	ZEO-IEZ	Stabilized ordered precursor (IEZ)			MWW-IEZ[140]	NA	FER[141], CDO[141], NSI[142], RRO[143], SOD[144], RTH[125], PCR[108], OKO[145], IPC-10[30]
10	d-ZEO-IEZ	Stabilized disordered precursor (IEZ-like)			EMM-10-IEZ (EMM-12)[146]	NA	
11	ZEO-Org	Grafted with organic groups	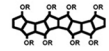		-	NA	SOD[144], RWR[147-148]
12	ZEO-Sw	Swollen precursor			Swollen MCM-22P[41]	NA	FER[149], CDO[133], NSI[135-136], SOD[150], RWR[120,138], PCR[139]
13	Sw-ZEO	Swollen precursor synthesized directly			ECNU-7P[151]	same as #6	

Figure 3. continued

https://dx.doi.org/10.1021/acscatal.0c05332
ACS Catal. 2021, 11, 2366−2396

	Proposed notation	Different layered forms (proposed)	Schematic structure as-synthesized	Schematic structure calcined	MWW	MFI	Other frameworks with layered forms (first and/or notable reports cited)
					Representative examples		
14	ZEO-Del	Delaminated swollen precursor		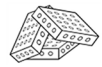	ITQ-2[152]	NA	FER/CDO[149], NSI[153], RWR[154]
15	ZEO-Pi	Pillared zeolite			MCM-36[41]	Pillared MFI[46, 155]	FER/CDO[149], NSI[135], SOD[150], PCR[156]
16	s-Pi-ZEO	Self-pillared			NA	Self-pillared MFI/MEL[157]	
17	ZEO-PCH	Porous (zeolite) heterostructures			NA	NA	RWR[158]
18	ZEO-Opi	Organic pillared			MWW-BETB[159]	NA	RWR[160], PCR[161]
19	ZEO-coll	Monolayer colloidal dispersion			[162]	NA	
20	ZEO-surf-coll	Colloidal suspension of surfactant covered layers			[163]	[163]	RWR[154],SOD[164]

Figure 3. Compilation of various layered zeolite forms (including those from Figure 2; updated based on the published version[165]) with schematic structures for **MWW**. For comparison to various **MFI** and **MWW** forms, also different layered forms of other zeolites like **FER**, **CDO**, **IPC**, **PCR**, **STI**, **SFO**, **OKO**, **SOD**, and others are summarized, see refs 85−164.

arranged as expanded and unexpanded structures, represented by columns in Figure 2. The former show apparent ca. > 2.6 nm interlayer distance (2 reflections at 1.35 and 1.24 nm *d*-spacing, ca. 6.5 and 7.1 degrees (deg) 2θ Cu Kα radiation, interlayer 002 and intralayer 100) and contain a template and/or hydrogen bonding between layers.[67,68] The unexpanded materials (2nd column in Figure 2) show only one distinct reflection, 100, that may overlap with the 002. Both the expanded and unexpanded types can further produce three different lateral arrangements: ordered stacking showing two separated peaks in the range 8−10 deg ((101) and (102)), disordered stacking, and a special case of regular shifts in the ab plane, probably due to particular features of the **MWW** structure (3rd row of patterns/structures in Figure 2). The corresponding materials can be described as follows. In addition to the MCM-22P (semiordered multilamellar precursor, condensing to ordered 3D framework) and the conventional 3D framework MCM-49/22 (fused/complete 3D framework), the additional distinct examples are illustrated by MCM-56 (monolayers),[69−71] EMM-10P (like MCM-22P disordered),[67,72] and SSZ-70 (multilayered, layers shifted by discrete vectors).[73,74] An additional structure similar to the (expanded) SSZ-70 but without interlayer separation (unexpanded) can be postulated to complete the pattern. It is already known as calcined SSZ-70, which has been assigned a separate structure code (***-SVY**[73]), but the as-synthesized equivalent has not been made yet. These different forms of layered zeolite precursors are usually prepared by hydrothermal synthesis that produces layered material instead of a 3D framework. The outcome of these direct preparations depend on the synthesis conditions, particularly the gel composition and on the templates used, as also illustrated in Figure 2.

Thus far, only **MWW** layers show such a variety of structures, and most zeolites have only three or fewer forms (ordered and disordered precursors). Since this variety of forms results from differences in layer packing, other 2D zeolites should behave similarly and produce equivalent structures. However, two general issues arise, that is, whether these various forms can in fact be obtained with other topologies and whether the initial layer arrangements affect subsequent modifications and catalytic performance.

Notably, some forms of layered zeolite precursors may be difficult to recognize. For example, the **MFI** pattern is complex and dominated by intralayer reflections. The XRD patterns of **MWW** may be unique in revealing differences in layered structures, and only some zeolite layers can offer comparably diverse packing. **MWW** has the lowest density of silanols on the surface reported so far[56] and readily forms layers with high Al content.[75] Thus, these features may be the starting point for a more in-depth analysis of different forms of layered zeolite precursors.

Preliminary findings indicate that the initial layer arrangements do affect modifications and catalysis. For example, SSZ-70 shows unique activity because of its structure with free silanols. However, upon swelling with surfactants, the regular offset of layers in SSZ-70 becomes obliterated, and the product becomes similar to other swollen **MWWs**, as shown by XRD.[76] MCM-56, an **MWW** zeolite with a high Al content obtained by direct synthesis, shows advantages in swelling with surfactants, in

https://dx.doi.org/10.1021/acscatal.0c05332
ACS Catal. 2021, 11, 2366−2396

contrast to the precursor MCM-22P, whose swelling decreases with the increase in Al content.[75] These are isolated observable differences, and it remains to be seen if they are general.

The unique variety of the **MWW** zeolite family allows a deeper analysis of the role of Al, as the key factor of acid catalysis, in the formation of 2D and 3D zeolite forms. The a-b surface of the **MWW** structure contains pyramidal T atoms terminated with silanol with a very low density of 1.12 per nm^2, in the hexagonal arrangement, at a distance of 0.81 nm.[77] The layers are relatively thick, 2.5 nm, with internal pores and channels, which can accommodate Al atoms and keep them hidden from the outside and protected by organic structure-directing agents in the as-synthesized form. In contrast, ferrierite layers are ca. 0.9 nm thick, with a silanol density of 1.8 per nm^2, and any Al present is directly accessible.[56]

The effect of Al content is illustrated by the synthesis of **MWW** with hexamethylenimine (HMI) in alkaline medium. A higher Si/Al, above roughly 12/1, favors the layered precursor MCM-22P, but as the effective Si/Al diminishes (factoring OH amount−silica dissolution increases with alkalinity and decreases Si/Al of the gel), the 3D framework, MCM-49, is obtained directly in one pot.[40] This is made more complicated by the formation of an intermediate layered product with high Al, MCM-56, but it can be rationalized by kinetic factors as described below.[75] The supposition that increasing Al concentration promotes the formation of 3D frameworks in preference to 2D forms[47] is reinforced by the fact that most layered zeolites prepared to date using hydroxide as mineralizer have a relatively low Al content. This implies that Al atoms on a surface, present most likely as $AlOH^-$, favor the formation of Al-O-Si as the propagation of a framework in 3D, over termination enabled under favorable conditions by SiOH and possibly AlF (in fluoride media high Al layered zeolite seems to form much easier than with OH mineralizer). The formation of MCM-56 can be rationalized by considering a combination of kinetic and pH effects—surface Al promotes the attachment of O-Si units, rendering a 3D structure (MCM-49), albeit at a slow rate. Presumably, MCM-49 is produced by crystallization, not layer alignment. Thus, in MCM-56, monolayer crystallization is much faster than 3D growth, enabling a full conversion of the gel into **MWW** layers. As the OH concentration becomes higher at the end of the amorphous-to-crystalline zeolite conversion, the next step, in which surface AlOH reacts with SiOH, is accelerated, initiating the growth of an adjacent layer as a 3D structure.[75] Yet, a key question remains unanswered, that is, whether the same conversion is possible with other frameworks or whether the required interplay of factors, including the concentration of pyramidal sites, pH, and kinetics, cannot be balanced to initially form only monolayers, as observed in MCM-56.

3.2. The Role of Templates in the Formation of Different Layered Structures. Templates (alternatively, structure-directing agents (SDAs)) promote the formation of a specific framework. With **MWW** zeolites, SDAs have a strong effect on layer organization, producing various structures with differences in layer spacing and order, as shown in Figure 2. Yet, the status and role of templates remain mostly unclear, to a large extent, because of the overall complexity of the problem, which has been primarily addressed using ^{13}C, or in some cases ^1H MAS NMR, temperature-programed base desorption, and modeling, as presented below.

Above (section 3.1), the formation of different **MWW** structures derived from hexamethylenimine, HMI, (MCM-22P, MCM-49, and MCM-56) has been rationalized on the basis of the Al content in the synthesis mixture. Under this assumption, HMI molecules and ions would mainly act as "pore" fillers between layers, as in the layered precursor MCM-22P, in addition to supporting the formation of the layers themselves and the filling of intralayer sinusoidal channels. Accordingly, both experimental and theoretical investigations have been conducted to test this hypothesis.

In the study by Lawton,[40] using temperature-programed base desorption and ^{13}C MAS NMR, the estimated amount of HMI in the interlayer spaces was 2 times higher in MCM-22P than in the as-synthesized 3D form MCM-49. Considering that HMI is present in both locations in the neutral and protonated forms, the interlayer SDA was initially proposed to promote the in-register alignment of silanols,[67] but an alternative geometry, disordered over several positions, was subsequently postulated on the basis of density functional theory (DFT) calculations.[68]

Diquat SDAs, such as bis(*N*,*N*,*N*-trimethyl)-1,5-pentanediaminium dibromide (diquat-C5) and the 1,6-hexanediaminium homologue, produced disordered, possibly turbostratic materials (e.g., EMM-10).[67,72] The suggested diquat arrangement consisted of two trimethylammonium head groups filling the opposite surface pockets and thus causing layer misalignment because of the long and flexible pentamethylene (C_5) and hexamethylene (C_6) chains connecting two N atoms.

The quaternary amino-adamantyl group is a strong promoter of the **MWW** layer. As such, depending on the other constituents, different types of materials were prepared, the first being SSZ-25, as an analogue of MCM-22P, templated with the trimethyladamantammonium cation ($TMAda^+$). The same SDA was used to synthesize an all-silica layered product, ITQ-1,[78] in the presence of HMI providing a "cooperative structure-directing effect"—with HMI stabilizing the 10-MR channels and a much larger $TMAda^+$—promoting large cavities. In turn, the bifunctional templates that were used to generate layered **MFI** inspired the design of analogous ions to prepare **MWW** based on amino-adamantane. The products were the house-of-cards MIT-1[79] and its multilayered derivative UJM-1.[80] A similar principle was adapted to obtain (by direct synthesis) DS-ITQ-2.[81] Another class of unique **MWW** materials has been obtained with functionalized imidazolium templates, which produced regular stacking sequences. ECNU-5 was prepared using the rapid dissolution-recrystallization route,[82] with 1,3-bis-(cyclohexyl) imidazolium hydroxide (IM^+OH^-) and with ITQ-1 as the silica source. Another example is the SSZ-70 zeolite.[83]

The breakthrough in the synthesis of 2D zeolites was made by Ryoo,[47,84] who designed and used bifunctional amphiphilic SDAs for the synthesis of layered **MFI** zeolites. This strategy was then extended to the synthesis of other frameworks, including the aforementioned zeolites of the **MWW** family, namely, DS-ITQ-2,[81] MIT-1,[79] and UJM-1.[80] Park et al.[51] conducted systematic studies to find the optimal structure of bifunctional SDAs, composed of quaternary ammonium heads and long hydrophobic tails, for the synthesis of 2D **MFI** materials. They concluded that surfactants should be equipped with at least two ammonium groups responsible for the formation of zeolite microporous structures, in addition to the amphiphilic and micelle-packing properties. They also found that the thickness of the nanosheets can be tuned according to the number of ammonium groups, noting structural differences depending on the surfactant used because $C_{22-6}N_2$ resulted in multilamellar mesostructures, whereas $C_{22-8}N_2$ yielded disordered nanosheets.

https://dx.doi.org/10.1021/acscatal.0c05332
ACS Catal. 2021, 11, 2366−2396

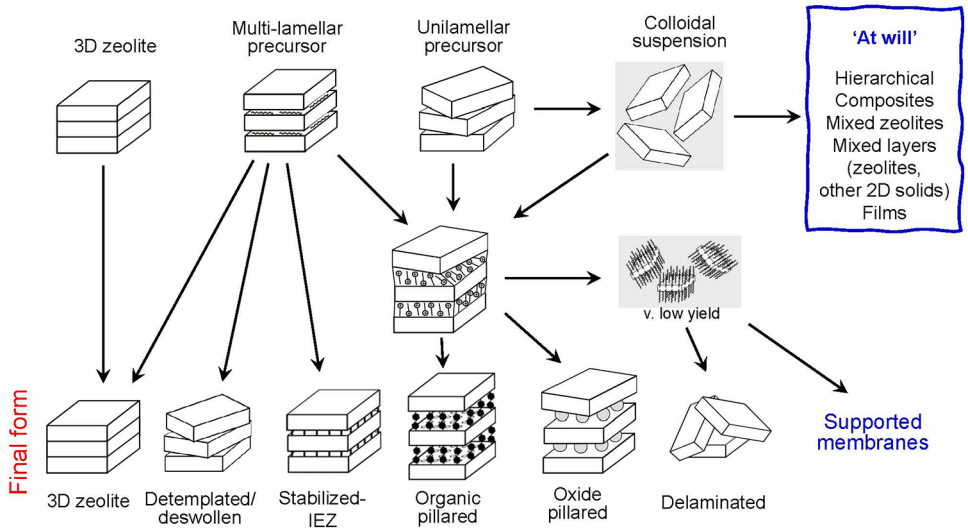

Figure 4. Principal transformations and derivative materials from layered **MWW** zeolites.

In addition to the modifications of layers arrangements mentioned above, the use of specific templates may also change the population and siting of the framework Al atoms, which affect the resulting acidity of the material (see section 5.2 and 5.3).

The other structures and forms that have been produced with **MWW** layers, approximately 15, including modifications (Figure 3), appear less "abnormal" than MCM-56 and should be easy to obtain with other frameworks.

3.3. Layered Forms of the MFI Topology. Layered forms of the **MFI** topology represent a significant milestone in the progress of layered zeolites.[47,131,157] First, 2D **MFI** materials helped to confirm the expected generality of the 2D zeolite phenomenon. Second, **MFI** is the second most important zeolite in catalysis after **FAU**, which is used in catalytic cracking (FCC) and produced in huge quantities. **MFI** and **FAU** are by far the most widely used among all commercial zeolites in catalytic processes in terms of both volume and diversity of applications.[166,167] They also dominate zeolite research activities. Third, the layered form was prepared by designing a template to produce the **MFI** topology without propagation in the third dimension. Fourth, the resulting nanosheets were active catalytically and stable, thus showing advantages over the conventional **MFI** in MTP and MTH reactions (see section 5.2.4).[47]

The template was bifunctional, consisting of a core, which directs the formation of the **MFI** structure, and tails, which prevent framework growth on top of the layer. Qualitatively, this design was different from that of other layered zeolite precursors—the template was an integral part of the layer and precluded both surface exposure and simple "detemplation", which is crucial for further transformations. The question of the formal "layered MFI" precursor, that is, its exact structure and congruent condensation to an ordered, complete **MFI**, has not been considered directly. One of the reasons may be practical, associated with XRD patterns, because **MFI** lacks prominent interlayer reflections necessary to diagnose interlayer spacing at a close distance, as well as order/disorder, in contrast to **MWW**. Almost all reflections observed in a layered **MFI** XRD pattern are intralayer, so structural details like layer packing, order, and distancing, must be determined using tools that are much more laborious and usually local (microscopy), that is, not as applicable to the bulk. These issues are illustrated by the nonordered condensation of **MFI** layers, as reported in the original study, and by the fact that the layer thickness ranges from 1 to 1.5 unit cells.[47,163] The layers with apparently one unit cell thickness are evident in TEMs of crystal cross sections, but the layers isolated by exfoliation, only in very low yield, have a thickness of 3.5 nm or 1.5 unit cells.[163] The bifunctional MFI templates produced two types of structures: stacked multilayered and monolayered house-of-cards (see Figures 2 and 3). The latter are particularly valuable considering the research goals to increase interlayer spaces and accessibility, which may be less favorable in multilayered structures without applying spacers (e.g., by pillaring).

The **MFI** structure can be regarded as consisting of 0.5−0.6 nm-thick monolayers propagated by a center of inversion.[168] The related topology **MEL** (ZSM-11) is obtained when the stacking is governed by reflection in lateral mirror planes. From this perspective, the reported one-unit-cell-thick **MFI** layers actually consist of three hypothetical "primitive" layers, which may or may not be possible to prepare. Since the differentiation between **MFI** and **MEL** by XRD can be tricky, the formation of the latter should be considered when synthesizing nominally **MFI** materials. Moreover, a third layered type material of this topology, known as self-pillared **MFI**, is a novel and apparently layered zeolite that consists of stacks of layers intergrown with a second set at right angles. This self-pillaring is enabled by the facile transition between and intergrowth of **MFI** and **MEL** topologies, which results from specific features of these two topologies, and may be limited to few comparable structures. Similar behavior was reported for the **FAU**/**EMT** frameworks, but the layers were much thicker and do not fall under the layered zeolite concept.[169,170] Most efforts toward developing lamellar **MFI** have involved the design of various templates and synthesis conditions, thereby producing various materials with different thicknesses,[60] ranging from layers with a single row of pores[171] to 5 nm-thick layers.[172]

4. Transformations of Layered Zeolites. *4.1. Modification of Layered Zeolites—General Comments.* Layered precursors can themselves provide benefits that exceed those of conventional 3D structures, as exemplified by the original **MFI** nanosheets and the **MWW** forms SSZ-70 and MCM-56. However, their most promising feature is the potential for

https://dx.doi.org/10.1021/acscatal.0c05332
ACS Catal. 2021, 11, 2366−2396

modification into new expanded architectures and other derivatives. Among all layered materials, zeolites provided for the first time 2D layers with pores inside or across the layers combined with inherent strong activity.

The following general types of modified layered zeolites materials have been reported in roughly chronological order (see also Figure 3): intercalated/swollen (expanded with surfactants),[41,112] pillared,[41] delaminated (disordered layer assemblies),[152,173,174] interlayer expanded zeolites (IEZ),[140,141] house-of-cards (**MFI**),[131] swollen with surfactants and exfoliated into liquid dispersions of individual layers (low yield),[163] exfoliated in high-yield by soft-chemical treatment[162] (Figure 4).

Most of these forms were proven conclusively and unequivocally, but in some cases, questions about their true identity and veracity/quality have not been fully resolved. Zeolite **MWW** has usually been the first in providing a specific modification, which most often can be confirmed by XRD. As found in various as-synthesized forms, **MWW** derivatives display specific XRD patterns, usually in the low angle range from 8.8 to 0.9 nm *d*-spacing (1−10 deg 2θ Cu Kα radiation, Figure 2). These features allow unequivocal identification and even quality/quantity assessment. For example, **MWW** swollen with hexadecyltrimethylammonium cation shows a (new) peak at 1.6−1.75 nm *d*-spacing (5−5.5 deg 2θ, assigned 003 Miller indices) in addition to 001 (which can be a false-positive due to an MCM-41-like contamination, as indeed occurred on occasion and was wrongly attributed to swelling). IEZs are characterized by XRD patterns after calcination similar to those of layered precursors and not to those of the condensed framework, as expected, and were termed "stabilized precursors".

The main transformations of the **MWW** materials, exemplified by the multilayered MCM-22P and monolayered MCM-56, are shown in Figure 4. Again, since the governing principle is based on arranging layers in space using suitable media, analogous modifications could be expected from the other **MWW** forms, including disordered EMM-10P and SSZ-70. Before the availability of monolayer dispersions in solution, the options for modifications were limited, but they have widened since. With exfoliated monolayers in solution,[162] materials can be designed at will, subject to limitation, which can be termed "compatibility", including charge, concentration of silanols, and other factors that will likely be better understood with time and experience.

The long-awaited ability to modify zeolites structures that has been enabled by the emergence of 2D zeolites comes with caveats and pitfalls requiring careful consideration, especially when weighing prospects for commercial significance. First, the additional steps needed to produce modified catalysts may entail significant labor and added costs, which can offset the gains. It is hard to indicate specific actions to decrease the cost of 2D zeolites production as each situation is different. As a general rule, minimalization of both additional steps and usage of organic reagents are desired, but it may affect quality. Additional processing can affect the intrinsic activity, especially the concentration of active sites, as shown with the swelling of MCM-22P and MCM-56.[175] Despite such adverse effects, the absolute activity can be maintained or enhanced, but in many cases, it does not happen (i.e., it is below state-of-the-art standard form). Third, as exemplified by MCM-22P and likely others, when increasing the Al content, transformations such as swelling and IEZ formation become less effective or not possible at all.[75] The overall activity of zeolite catalysts often increases with the Al content but at some point may reach a maximum and then decrease because of factors such as reduced stability or excessive coke formation. Results reported on the performance of pillared **MWW** materials have shown that the final activity is primarily determined by the Si/Al of the starting precursors.[75,176] Subsequent attempts at swelling, including layer preservation (at a lower temperature) or desilication and Si/Al lowering, had a minor effect. The role of Al in the formation and activity of 2D zeolites is analyzed in more detail in a separate section (see sections 5.2 and 5.3), but in short, the validation of a useful modification for large-scale applications must consider the effect of the Al content for both the 3D zeolite and the modified form. Thus, suitable benchmark materials are particularly important, especially when evaluating benefits for a commercial process. However, information on benchmarks or the materials themselves is usually unavailable (e.g., proprietary), so caution is necessary in assigning positive practical advances and prospects.

4.2. Modified Zeolite Forms—Secondary Structures and Material Types. Differences in 3D zeolite topologies (primary structures) are reflected in differences in their XRD patterns, which are the primary basis for their practical differentiation. The same principle is applicable to various **MWW** forms when recognizing different types of modifications (secondary structures). Not all patterns are unique, especially among disordered forms, in which case other distinguishing features can help to identify and differentiate forms. As a result, nearly 20 different types of zeolite materials (secondary forms) have been identified so far. As we learn more on this subject, further scrutiny and validation may be implemented toward creating systematic procedures. Among the possible forms of 2D zeolites, some are particularly important and will be discussed in more detail below.

4.2.1. Surfactant-Swollen Zeolites. Successful surfactant swelling was initially both a definite proof of the layered nature of the **MWW** zeolite and the necessary step for its practical exploitation in preparing expanded or more open materials such as MCM-36 and ITQ-2. Uncharacteristically for 2D solids in general, the efficiency of MCM-22P swelling was marginal until a highly concentrated surfactant hydroxide and exclusion of other small cations was adopted. Several factors determined the positive swelling outcome. High pH caused deprotonation of the surface silanols, and the absence of smaller cations allowed unobstracted attachment of surfactant molecules to the layers and interlayer expansion. Larger cations, such as TPA and TBA, were successfully used as bases in combination with a surfactant salt, thus suggesting that their size was unfavorable for displacing or not admitting surfactant to the surface. The severity of the process was initially justified by hydrogen bonding and strong interlayer affinity (bonding) requiring disruption. An alternative and more plausible revised reinterpretation is that **MWW** has a particularly low silanol density on the surface and at lower pH the entering surfactant molecules are simply lying horizontally, thereby causing little expansion, similarly to clays, where charge density determines surfactant packing.[177] The high pH environment generates additional SiO^--defects, which attract surfactants and produce expansion. To reduce the apparent detrimental effect of the reaction between hydroxide and **MWW** surface, a room temperature process was applied resulting in "layer structure preservation".[178] The swollen **MWW** had smaller interlayer *d*-spacing than in the initial reports, most likely because less surfactant was present between the layers, in line with the lower number of SiO^--defects. These

https://dx.doi.org/10.1021/acscatal.0c05332
ACS Catal. 2021, 11, 2366−2396

room-temperature conditions become less efficient with the increase in Al content,[75] and the activity is not dependent on swelling conditions, with or without preservation of better layers, despite significant degradation in the latter case.[176] The swelling of MCM-56, a high-Al, monolayered (delaminated) **MWW** zeolite is particularly noteworthy. In contrast to the multilayered MCM-22P precursor, it can occur under less demanding conditions (e.g., with a surfactant salt−small cation hydroxide combination). Accordingly, these results suggest a more exposed external surface, that is, the monolayered nature of MCM-56, which is further validated by the recent complete exfoliation of MCM-56 with tetrabutylammonium hydroxide (TBAOH).[162]

Swollen **MWW** can be deswollen in reactions with an acid or in a milder environment, in contact with ammonium nitrate or quaternary organic salts in water/ethanol. The product consists of randomly stacked layers.[75,178]

An analogue of postsynthesis, surfactant-swollen **MWW** materials was directly prepared using a dual template system, IM^+OH^- and the surfactant cetyltrimethylammonium bromide (CTAB), and including zeolite seeds (siliceous ITQ-1).[151]

4.2.2. Pillared Layered Zeolites. Pillared layered zeolites consist of layers permanently separated at some distance by props, known as pillars, that generate porosity between layers. Unlike the archetype pillared layered solids, clay minerals with Al-Keggin ions between layers,[27] pillared zeolites could not be obtained by a simple ion exchange of such ions or other molecular clusters into the interlayer space. The initially successful process[41] mimicked pillaring of layered oxides by the reaction between a (pre)swollen layered substrate and TEOS, as a silicon dioxide precursor, to insert the latter between layers.[179] The product, MCM-36, showed enhanced porosity, for example, doubled BET surface area, a mixture of micro- and meso-pores, and genuine activity enhancement in comparison with the 3D zeolite in iso-butane alkylation.[41,53] The performance was enhanced despite reduced concentration of the active sites due to the presence of ca. 50% inert silica as pillars. The obvious research direction was to make pillars active by incorporation of elements that add activity, like Al and other heteroatoms. Yet, so far, the activity gains have been minor, except when introducing redox centers, including Ti and Fe, among others.[180−185] The activation of pillars has not produced significant increases in performance, which is not surprising considering the generally amorphous nature of these props. The solution to this problem has been to prepare zeolitic pillars, but not much progress has been achieved yet. Zeolite pillars (**MFI**) with **MFI** layers have been reported,[46] but evidence confirming the nature of the pillars is difficult to obtain. The best confirmation will come in the form of activity enhancement in comparison with silica pillared layered zeolites. Organic molecules with functional groups have been also introduced as active pillars between MCM-22P[159] or IPC-1P[161,186,187] layers. Here, thermal instability prevents the usually desired zeolite activation up to 500 °C.

4.2.3. Interlayer Expanded Zeolites (IEZ). Most layered zeolite derivative structures and types of materials have equivalent analogues among other, traditional layered solids. IEZ structures are unique and were unanticipated[140] but appeared obvious once a suitable synthesis path has been discovered. They are obtained by connecting Si-OH groups on the surface of opposite layers with an Si atom forming the bridge O-Si(alkyl)$_2$-O with formal expansion of pores between layers by 2 SiO links (e.g., converting 10-ring into 12-ring pores). A convenient synthesis method is silylation with (alkyl)$_2$Si(OR)$_2$ reagents in acidic solutions.[141] The desired outcome is readily recognized in the XRD because the pattern is qualitatively similar to that of the precursor, without visible contraction that occurs when forming the corresponding 3D framework and maintaining peak positions. Initially, this process was referred to as (precursor) stabilization. The pore is nominally expanded by two Si-O units, but the bridging Si atoms are not four connected, having 2 groups attached (e.g., CH_3 or OH). The product is usually not a formal zeolite, whereas the additional groups on the bridging Si narrow the pore entrance. Consequently, the benefits from this enlargement are more subtle than going simply from, for example, 10-ring to 12-ring zeolites. In turn, an IEZ form of **MWW** is one of the best examples of the possible advantages of 2D zeolites over 3D. The accommodation of Ce cations by ion exchange produced a qualitative change from no activity toward CO-to-CO_2 oxidation in Ce-MCM-22 to imparting this activity in Ce-IEZ-MCM-22.[188] An example of the IEZ zeolite derivative that is a zeolite is **PCR**-IEZ.[108] In this case, the interlayer bridges are close to each other and condense to form a square as each Si becomes four connected. Further examples have been reported.[189]

As best as we could ascertain, there have been no reports of an IEZ form of **MFI**, although there is no reason to expect that it cannot be prepared. As such, the current lack of IEZ forms of **MFI** is probably temporary.

4.2.4. Delaminated Zeolites. The concept of a delaminated zeolite represents an idea of maximized exposure and accessibility of zeolite active sites (layers) to the reactants with a fixed porous structure embodied by a "house-of-cards" architecture.[152,174] The first report of a delaminated zeolite involved subjecting a swollen **MWW** to sonication, coagulation by acidification, isolation of solids, and calcination. The product, designated ITQ-2, showed higher BET surface area, pore volume, and activity toward model compounds (*n*-decene, 1,3-diisopropylbenzene, and vacuum gas-oil) than the starting material.[152] In addition, TEM revealed the presence of an isolated **MWW** layer. This idea has stimulated the pursuit of zeolite delamination in general. At that time, there was already an apparently monolayer **MWW** material disclosed in patents and later on determined to be a delaminated zeolite obtained by direct synthesis[69−71] with high Al content, albeit pronounced to be less active than ITQ-2.[174] The idea of delaminating the swollen layered zeolites was extended to the frameworks **FER** and **NSI**, providing materials designated ITQ-6, -18, and -20.[153,174] Since then, the term delaminated zeolite has been applied quite broadly to include materials with perturbed stacking of **MWW** or other zeolite layers. The typical evidence included XRD patterns, often similar to MCM-56, increased textural parameters and enhanced catalytic performance. The term delamination and its often-used equivalent exfoliation imply the potential for producing dispersion of loose layers in a liquid medium. The first evidence of such a phenomenon for zeolites was produced from swollen **MWW** and **MFI** materials, but through an elaborate procedure involving extrusion with a polymer, extraction with organic solvents, and surfactant removal.[163] The yield was very low and insufficient for use in catalysis, but the approach has been beneficial for zeolite membrane preparation.

True delamination, in a single step, with demonstration of layers in solution, has been recently reported with a preparation of MCM-56 that was obtained with a specific synthesis formulation.[162] This preparation was uniquely favorable because

https://dx.doi.org/10.1021/acscatal.0c05332
ACS Catal. 2021, 11, 2366−2396

it contained only a small amount of layer intergrowth, which are found in most known preparations and thwart significant exfoliation. The MCM-56 material produced dispersed monolayers by the same method as many oxide materials do—by treatment with TBAOH solution and centrifugation to separate the nonexfoliated fraction.[36,190] As the first case, this system was thoroughly characterized by standard and advanced methods to confirm dispersion into monolayers. The evidence also included flocculation of the suspended layers as a demonstration of its usefulness for the preparation of catalysts. In this material, the separated monolayers can be combined with other components of different functionality.

Layered zeolites house-of-cards materials with apparently intergrown layers have been obtained with bifunctional templates as shown in Figure 2, bottom.[79,131]

5. Properties and Catalytic Performance of 2D Zeolites. *5.1. Porosity.* Unmodified conventional zeolites are purely microporous materials. Thus, during potential catalytic reactions, bulky molecules can neither penetrate deeply into zeolite micropore system and efficiently reach active sites nor escape narrow channels and are thus trapped.[191] As a consequence, the products formation is difficult because of the limited number of active sites accessible on the outer rim of the crystals. Even if they are formed, the products suffer from increased residence times and can undergo secondary reactions, leading to undesired low-molecular products (low selectivity) or to coke formation (catalyst deactivation). 2D zeolites increase access to active sites and to overcome limitations of conventional zeolites. Most 2D zeolites designed to date can also be classified as hierarchical materials because they combine the intrinsic zeolite microporosity and the permanent intercrystalline mesoporosity of pillared, self-pillared, and delaminated/exfoliated forms.

To quantify the aforementioned characteristics, Perez-Ramirez et al.[192] introduced a hierarchy factor (HF), defined as the product of the relative micropore volume (V_{micro}/V_{total}) and the relative mesopore surface area (S_{meso}/S_{BET}). The higher the HF value the greater the mesopore surface area, without severely affecting the micropore volume. For layered zeolites, the HF is usually high, even if one pore system has to be sacrificed by slicing the 3D structure to obtain a 2D structure. Figure 5 shows two extreme cases, that is, zeolites with high mesoporosity and low microporosity are located at the top left corner, whereas classic 3D materials are located at the bottom right corner of the graph.

The only delaminated zeolite presented in the original graph, ITQ-18, is located at the top left corner, with HF of 0.02. The HF values of other 2D zeolites with **MFI** or **MWW** frameworks (Table 1) are scattered throughout the entire plot, with notable location of the single-layered material MIT-1 in the center right section, with HF over 0.3, or UJM-1, which is multilamellar, also in the center right section, with HF over 0.2. Overall, these findings show that mesoporosity and microporosity of 2D materials are balanced.

Thus, despite extreme reduction of crystal size in one crystallographic direction in 2D zeolites, both **MFI** and **MWW** lamellar materials maintain a significantly intact micropore system. Consequently, as a feature of 3D zeolites, selectivity is expected to remain unchanged, to some extent, in their layered derivatives.

In addition to increased total surface area or mesopore volume, which provides high accessibility to active sites, 2D zeolites present additional benefits. For the same topology (e.g., **MFI** or **MWW**), different structures, that is, architectures of layers assembly, can be produced, with modified textural features and catalytic behavior. For instance, the **MWW** family is represented by various pillared (MCM-36), postsynthetically delaminated (ITQ-2), and directly synthesized materials with different types of stacking (MCM-49, EMM-10, MCM-56, UJM-1, and MIT-1, among others). Accordingly, the **MFI** framework has provided pillared multilamellar, disordered unilamellar, and layered-like self-pillared forms.[46,84,131,171] This ability to obtain different structures makes it possible to adjust textural properties and to control other important characteristics of zeolite catalysts such as their mechanical and chemical stability, the distribution of active sites among different framework positions, the acid strength of active sites, and the confinement for potential reactants/intermediates under reaction conditions.

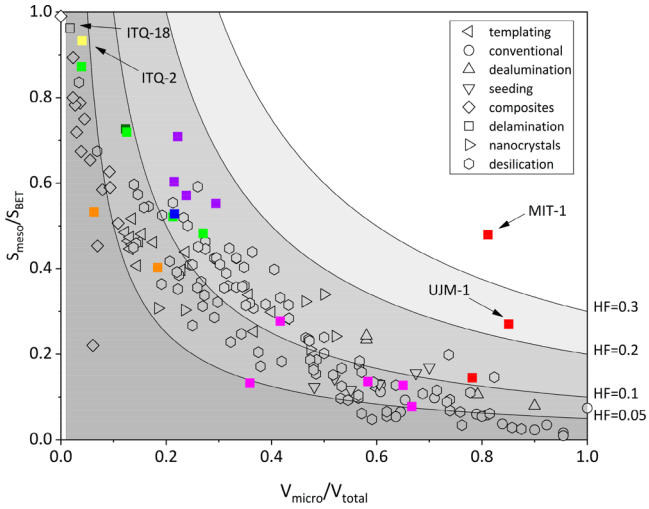

Figure 5. Hierarchy factor (HF) plotted in a contour plot as a function of the relative mesoporous surface area and relative microporous volume of different zeolite types prepared using different methods (from ref 192) and adding 2D **MFI** and **MWW** (data presented in Table 1). Colors: violet—ref 193, dark green—ref 194, green—ref 195, dark blue—ref 196, red—ref 80, magenta—ref 76, orange—ref 197, yellow—ref 198. Individual colors are also given in Table 1.

Zeolite nanosheets were shown to have high thermal and mechanical stability similarly to conventional zeolites.[171] Moreover, the 3D-to-2D transition is not expected to cause significant framework distortions in both purely siliceous and aluminosilicate forms,[199] instead likely affecting more subtle characteristics, including the number of exposed silanols, which determine catalyst hydrophilicity, or the local environment of acid sites, which influence their strength.

*5.2. **MFI** and **MWW** as Model Layered Brønsted Acid Zeolite Catalysts.* The following discussion is focused on recent studies on the characterization of acid sites in 2D vs 3D zeolites and on catalytic processes underlying fundamental differences between 2D and 3D zeolites under different reaction conditions. More comprehensive discussions of possible catalytic applications of these materials in various types of transformations can be found in earlier reviews.[2,200,201] Section 5.2 analyzes aluminosilicate **MFI** and **MWW** as model Brønsted acid layered zeolite catalysts, whereas section 5.3 addresses 2D Lewis acid zeolite catalysts. For the reader's guidance, Scheme 1 shows different surface acid sites discussed in sections 5.2 and 5.3.

5.2.1. Probing Brønsted Acidity in 2D Zeolites. Lewis acid sites (LAS) in zeolites are viewed as defects, so researchers

https://dx.doi.org/10.1021/acscatal.0c05332
ACS Catal. 2021, 11, 2366−2396

Table 1. Porosity of Different 2D MFI and MWW Materials Published in the Literature and the Corresponding Hierarchy Factor (HF)[a]

framework	sample name from referenced work	color in Figure 5	V_{micro}/V_{total}	S_{meso}/S_{BET}	HF	reference
MFI	SI-ONS-87	violet	0.294	0.552	0.163	193
	SI-ONS-50		0.222	0.709	0.157	
	SI-ONS-30		0.215	0.603	0.130	
	SI-ONS-15		0.238	0.571	0.136	
	NS-2.5	dark green	0.123	0.727	0.089	194
	ZSM-5-0.055	green	0.270	0.483	0.131	195
	ZSM-5-0.065		0.213	0.522	0.111	
	ZSM-5-0.075		0.125	0.719	0.090	
	ZSM-5-0.085		0.039	0.872	0.034	
	nanosheets	dark blue	0.216	0.528	0.114	196
MWW	UJM-1	red	0.851	0.270	0.230	80
	UJM-1-pillared		0.782	0.145	0.113	
	MIT-1		0.811	0.480	0.389	
	B-SSZ-70(4)	magenta	0.667	0.077	0.052	76
	B-SSZ-70(4)-pil		0.359	0.132	0.047	
	B-SSZ-70(25)		0.650	0.127	0.083	
	B-SSZ-70(25)-pil		0.583	0.136	0.079	
	Al-SSZ-70		0.417	0.277	0.116	
	MCM-56	orange	0.184	0.403	0.074	197
	MCM-56(D)		0.063	0.533	0.034	
	ITQ-2	yellow	0.040	0.933	0.038	198

[a]Samples are labeled according to the original publications.

Scheme 1. Possible Acid Sites on the Surface of Aluminosilicate Zeolites

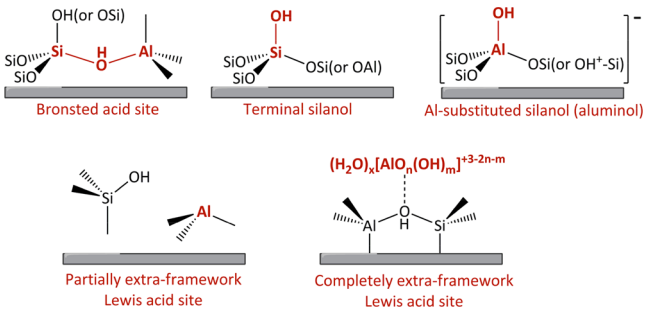

primarily focus on Brønsted acidity associated with Si-OH-Al groups. Aluminum-related Brønsted acid sites (BAS) are relatively easy to detect, in contrast to Lewis centers, using direct spectroscopic methods such as solid-state ^{1}H and ^{27}Al MAS NMR, FTIR in the OH vibration region (FTIR-OH, range 3750−3000 cm^{-1}, Figure 6a,b) and NMR- and FTIR-monitored adsorption of molecular probes. The parameters that can be determined by spectroscopy are accessibility to acid sites (most frequently evaluated in relation to the external surface/inner space when comparing 2D and 3D zeolites), their strength and number. However, the currently available methods are unable to provide accurate information about all three parameters simultaneously. As elaborated below, each approach has its own blend of advantages and disadvantages. Thus, only the combination of different spectroscopic techniques (i.e., direct detection of Si-OH-Al groups and probing with basic molecules) can distinguish differences in acidity between 3D and 2D zeolites, which depend on topology of the layers and their thickness, the heteroatom distribution, the population of surface silanol groups, and other factors.

In this section, we discuss solid-state MAS NMR and FTIR-OH. ^{27}Al NMR spectra detect framework Al atoms in tetrahedral coordination, which are usually associated with Brønsted acid sites. They are observed in the range of chemical shifts δ = 50−65 ppm. ^{27}Al MAS NMR studies of 2D **MFI** zeolites detect aluminum in tetrahedral (50−60 ppm), octahedral (0 ppm) and penta-coordinated/distorted four-coordinated positions ("the broad feature between 0 and 60 ppm").[202] The high abundance of the species results from irregular coordination of T atoms at the large external surface.

^{29}Si MAS NMR can be highly informative for zeolite materials, but the presence of Al introduces well-known complications such as peak broadening and overlap. Wu et al.[203] enhanced ^{29}Si NMR signal using the $^{29}Si-^{1}H$ CP technique when studying series of **MFI** ranging from conventional through multilamellar to unilamellar structures. It was found that the ratios of $Q^3(0Al):Q^4(0Al)$ (a measure of silanol abundance) and $Q^4(1Al):Q^4(0Al)$ (a measure of framework Al) did not change significantly, thus suggesting that neither the silanol concentration nor the framework Al abundance correlates with layer thickness.

Although chemical shifts are independent of external characteristics of materials (morphology, textural properties) for both **MFI**[194] and **MWW**[204] zeolites, solid-state spectra are difficult to interpret accurately.[205] The exact correlation between published chemical shifts and specific framework positions is typically impossible because of insufficient peak resolution and sensitivity of Al chemical shifts to the changes in the local Al atom environment (e.g., when comparing 2D and 3D zeolites with the same layer topology). Various aspects of zeolite acidity are reflected and can be readily appraised on the basis of the presence and number of OH groups observed in FTIR spectra of activated samples (in protonic form).

The main IR maxima due to bridging Si-OH-Al hydroxyls associated with BAS are observed at 3620−3625 cm^{-1} for **MWW** and at 3610 cm^{-1} for **MFI**. Also other OH groups are common to both **MWW** and **MFI**, as shown in Figure 6: (i) external, terminal silanols characterized by the IR band at 3745

https://dx.doi.org/10.1021/acscatal.0c05332
ACS Catal. 2021, 11, 2366−2396

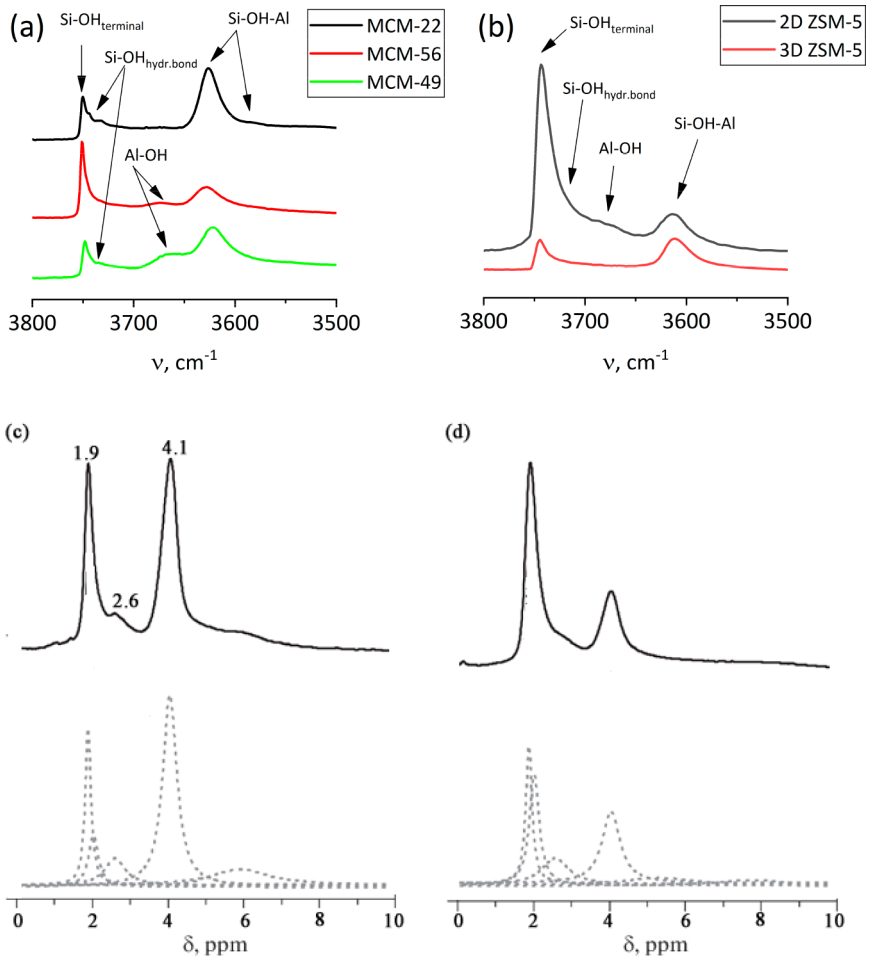

Figure 6. FTIR-OH spectra of different 2D and 3D **MWW** (a) and **MFI** (b). ^{1}H MAS NMR spectra of 3D **MWW** (c) and ITQ-2 (d). (c) and (d) Reproduced with permission from ref 206. Copyright 2016 Elsevier.

cm^{-1}; (ii) internal silanols located at the structural defects (including geminal silanols), with the maxima at ca. 3730−3740 cm^{-1}; (iii) hydroxyls associated with extra-framework or partly framework Al (3670 cm^{-1}); and (iv) wide maximum of hydrogen-bonded silanols or hydrogen-bonded Si-OH-Al groups at ca. 3300 cm^{-1} (spectra not shown).[175,207,208] The main difference between **MWW** and **MFI** is the frequency of bridging Si-OH-Al hydroxyls. For **MFI**, bridging hydroxyl groups are characterized by the band at 3610 cm^{-1}; **MWW** shows the main IR band around 3620 cm^{-1} with a shoulder at ca. 3575 cm^{-1}. Deconvolution produced three submaxima at 3628, 3618, and 3575 cm^{-1} which were assigned to bridging hydroxyls in supercages, in the 10-ring channels, and in the double six-membered rings connecting the supercages, respectively.[209] Meloni et al.[210] estimated that 50−70% of Si-OH-Al groups would be located in supercages, 20−30% in sinusoidal channels, and 10% in hexagonal prisms between two supercages. In comparison with 3D analogues, both 2D **MFI** and **MWW** show a more intense band at 3745 cm^{-1}, corresponding to terminal silanol groups (Figure 6).

Valuable information and insights have been obtained by ^{1}H NMR and NMR-monitored adsorption of probe molecules. ^{1}H MAS NMR allowed direct determination of the type and concentration of individual OH groups (protons) in 3D **MFI** and **MWW** zeolites that did not require additional information like absorption coefficients, which are necessary when working with infrared spectra (vide infra). The key to both FTIR and NMR is dehydration to eliminate strong interactions between structural OH groups and adsorbed water. Several types of OH groups have been observed in ^{1}H MAS NMR spectra of **MWW** and ITQ-2 (Figure 6c,d): SiOH in the region 1.8−2.3 ppm; Si-OH-Al groups (3.8−5.9 ppm)—whose exact chemical shift depends on the local environment near a specific OH group.[211] The 2.6−3.6 ppm signals are usually assigned to extra-framework AlOH groups,[212] although Delitala et al.[213] assigned them to protons associated with framework Al in Q^{3}(3Si,1OH) or even Q^{2}(2Si,2OH) environment for **MWW** zeolites. In contrast to FTIR-OH, ^{1}H MAS NMR spectroscopy, which is more powerful but technically demanding, is rarely used to characterize zeolites.

Despite providing information about the number of Brønsted sites, ^{1}H NMR and FTIR-OH are unable to discriminate acid centers by their strength and accessibility. To solve both issues, an approach based on the interaction of acid sites with probe molecules has been commonly used.

To distinguish acid sites by their type, strength, and accessibility, the adsorption of probe molecules is followed by NMR measurements. Hence, the signals of various nuclei (such as ^{31}P, ^{1}H, ^{13}C) or their combinations (e.g., ^{27}Al-^{31}P or ^{31}P-^{1}H) in the case of 2D (correlation) NMR spectroscopy are determined under MAS conditions.

^{31}P NMR using basic trialkylphosphine oxides (TAPO) as probes is one of the most developed techniques to assess the concentration, acid strength, and spatial distribution of Al sites

https://dx.doi.org/10.1021/acscatal.0c05332
ACS Catal. 2021, 11, 2366−2396

in **MFI** and **MWW** zeolites of different dimensionality. The last characteristic (spatial distribution) can be evaluated using titrant TAPO molecules of different sizes. The most common pair of probes, the small molecule trimethylphosphine oxide (TMPO, kinetic diameter = 5.5 Å) and the relatively bulky tributylphosphine oxide (TBPO, 8.2 Å), was first proposed by Zhao et al.[214] Although both types of molecules can interact with Brønsted sites located on highly accessible external surfaces, TBPO cannot diffuse into 10-ring micropores. The strength of acid centers in **MFI** and **MWW** materials is usually differentiated on the basis of the ^{31}P chemical shift of trialkylphosphine oxides (Figure 7),[215] whereas the concentration of Al sites is estimated

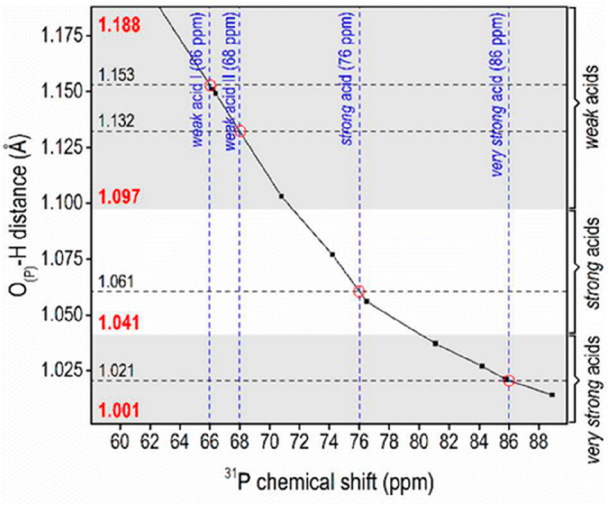

Figure 7. Correlation between acid strength (distances between protons and TMPO oxygens) and ^{31}P chemical shifts. Reproduced with permission from ref 217. Copyright 2016 American Chemical Society.

by peak integration combined with elemental analysis. Like the majority of techniques based on interaction with probe molecules, this method for the quantification of acid sites typically shows some discrepancies between the determined total Al and chemical analysis due to the presence of extra-framework Al and steric limitations. Therefore, a fraction of BAS remains undetected even when using small TMPO probe molecules, thus allowing to get information about accessibility of acid sites.[216]

The assessment of the total number of different types of acid sites (number of peaks observed in ^{31}P NMR spectra) and the apparent strength of these sites (reflected in chemical shifts) depends on sample preparation and spectral analysis, particularly on the deconvolution procedure. As a result, it is difficult to judge whether the values of chemical shifts reported for different topologies (**MFI** and **MWW**) are truly different because discrepancies between peak positions in ^{31}P NMR spectra reported for materials with the same layer topology (e.g., **MWW** obtained by different groups) can be greater than between different zeolites. For example, Luo et al. observed ^{31}P chemical shifts associated with Brønsted acid sites at δ = 85, 72, 68, and 63 ppm,[79] whereas Zhou et al.[216] observed resonance peaks related to the same acid sites at chemical shifts of δ = 82, 78, 69, 66 ppm for the same type of solid (**MWW** nanosheets). A similar region in NMR spectra of **MFI** nanolayers contains signals at δ = 86, 76, 68, 66 ppm,[194] thus suggesting that differences in exact peak positions cannot be postulated for materials of different types, at this point. The change in the arrangement of layers in different forms of 2D zeolites has no effect on the ^{31}P chemical shifts if the spectra are recorded in the same mode: MIT-1 and MCM-56 (both are 2D) and MCM-22 (3D zeolite) exhibited comparable signal positions at δ = 63−85 ppm. This range corresponds to strong Brønsted acid sites located in the 12-ring cavities or in 10-ring pores, as shown by the correlation between simulated values of proton affinities (acid strength) and the respective chemical shifts in ^{31}P NMR spectra.[79,218]

Similarly to NMR, various molecules with different sizes can be utilized as probes in FTIR to distinguish highly accessible sites on the external surface or pore mouths and centers with lower accessibility in micropores. As a representative pair of small and bulky probe molecules, pyridine and its alkyl-substituted analogues (2,6-dimethylpyridine, 1,3,5-trimethylpyridine, 2,6-di*tert*-butylpyridine) are commonly applied in FTIR monitoring. These probe molecules are usually described by kinetic diameters and sometimes by minimal dimensions (MIN-1 and MIN-2 in Table 2) as molecular size descriptors, as

Table 2. Molecular Size Descriptors for Probe Molecules and the Respective Molar Absorption Coefficients as Determined for 3D and 2D Zeolites[a]

	molecular size descriptors, Å			molar absorption coefficients		
molecule	kinetic diameter	MIN-1[219]	MIN-2[219]	IR maximum, cm^{-1}	based on intensity, cm^2/μmol	based on integrated intensity, cm/μmol
ammonia	2.6[20]	3.111	3.697	1450	0.090[208] (2D)	13.0[222] (3D)
nitrogen	3.64[20]	2.991	3.054	-	-	-
dimethyl ether	4.7[223]	4.027	4.556	-	-	-
pyridine	5.4[20]	3.339	6.475	1545	0.078[224] (3D)	1.36[226] (3D)
					0.07[225] (3D)	1.67[227] (3D)
					0.044[207] (2D)	
pivalonitrile	6.2[228]	-	-	2258−2278	0.11[229] (3D)	0.15[229] (3D)
				2269 + 2296	0.05[208] (2D)	
2,6-lutidine	6.7[230]	4.127	6.957	1652 + 1627	-	6.8[231] (3D)
2,4,6-collidine	7.2[232]	-	-	1635	-	10.1[233] (3D)
2,6-di-*tert*-butylpyridine	7.9[233]	6.454	8.294	1615	0.5[221]	5.3[221]
					(3D and 2D)	(3D and 2D)
1,3,5-trimethylbenzene	8.6[234]	4.062	8.178	-	-	-
2,4-dimethylquinoline	9.1[235]	n/a	n/a	1647	-	3.3[236] (3D)

[a]Based on refs 20,207,208,219−236.

https://dx.doi.org/10.1021/acscatal.0c05332
ACS Catal. 2021, 11, 2366−2396

Table 3. Concentration of Total Brønsted (BAS_{total}) and Lewis (LAS) Acid Sites and External Brønsted Acid Sites (BAS_{ext}) in Different 2D MWW and MFI Structures Probed by Bulky Basic Molecules[a]

zeolite		BAS_{total}, μmol/g	LAS, μmol/g	BAS_{ext}, %	probe used for accessibility studies	reference
MCM-22		697	30	22	pivalonitrile	208
		780	180	5	di-*tert*-butylpyridine	240
		187−269	52−72	14−19	dimethylquinoline	241
		330	170	12	di-*tert*-butylpyridine	129
MCM-36		330[b]		64 incl. 31[pm]	di-*tert*-butylpyridine and triphenylphosphine	239
		640[b]		10	2,2,4-trimethylpentane	242
		290−440	90−120	4−18	di-*tert*-butylpyridine	240
		126−146	65−109	18−50	di-*tert*-butylpyridine	238
		135−197	167−182	81−100	dimethylquinoline	241
MCM-56		353−1049	25−173	17−69	pivalonitrile	237
		913−930	95−154	97−100	pivalonitrile	208
		125	78	44	di-*tert*-butylpyridine	238
MCM-56-pillared		91−199	77−176	28−56	di-*tert*-butylpyridine	238
ITQ-2		21	23	40	di-*tert*-butylpyridine	243
DS-ITQ-2		n/p	n/p	n/p	di-*tert*-butylpyridine	81
MIT-1		330	55	64	tributylphosphine oxide	79
		307	n/p	n/p		80
UJM-1		899	86	100%	pivalonitrile	208
UJM-1-pillared		307	57			80
2D **MFI**	multilamellar	330[b]		n/p	-	47
	unilamellar	310[b]		n/p	-	
2D **MFI**	multilamellar	591[b]		n/p	-	195
	unilamellar	246[b]		n/p	-	
2D **MFI**		111−178	n/p	93−98	pivalonitrile	193
		n/p	n/p	100	2,4,6-trimethylpyridine	244
		72−94	54−292	30−39	di-*tert*-butylpyridine	245
2D **MFI**		21−121	26−82	-	-	246
nanolayered **MFI**		150−350	50−220	17−67	collidine	203
2D **MFI**-pil		185	n/p	38 incl. 6[pm]	di-*tert*-butylpyridine and triphenylphosphine	239
			n/p			

[a]Based on refs 47,79−81,129,193,195,203,208,237−246. Abbreviations: n/p−not provided, pm−pore mouth. [b]Brønsted + Lewis acid sites.

proposed by Breck[20] and Webster and Sing.[219,220] Table 2 lists these parameters for the most frequently used probe molecules.

The molecules with kinetic diameters below 5.4 Å (e.g., ammonium, pyridine) are small enough to enter the medium-size pores of both **MFI** and **MWW**, whereas the larger molecules (e.g., 2,6-di-*tert*-butylpyridine, 2,4-dimethylquinoline) interact exclusively with acid sites on the surface of 3D crystals or 2D nanosheets.[221]

One of the key factors when quantifying the concentration of zeolite acid centers with FTIR is the uncertainty of molar absorption coefficient values required to calculate the concentration of active sites based on the Beer−Lambert equation (Table 2). For some probes, the absorption coefficients are not known; for others, several different values have been reported and used so far. The absorption coefficient of popular probes, such as pyridine[207] or pivalonitrile,[208] may be different for 2D and 3D materials.

Since enhanced accessibility to acid sites is one of the main features of layered zeolites, comparative IR investigation of 2D and 3D zeolites is usually the method of choice.[221] Accessibility to acid sites in **MWW** zeolites has been extensively studied by several authors (Table 3) using pivalonitrile, di-*tert*-butylpyridine, 2,2,4-trimethylpentane, or dimethylquinolines, that is, molecules with kinetic diameters ranging from 6.2 to 9.1 nm. For MCM-56, composed of single **MWW** layers, the accessibility determined by pivalonitrile strongly depends on synthesis parameters, not only on the source of silica (Ludox, Ultrasil or Aerosil) but also on the crystallinity,[237] with accessibility reaching ca. 70% of all acid sites. A different study[238] has reported that MCM-56 pillaring only slightly improved accessibility, from 43% to the maximum of 56% (tested by di-*tert*-butylpyridine). In another study on the accessibility of acid sites for pillared **MWW** and **MFI** materials, Wu et al.[239] quantified not only the number of external acid sites but also the number of sites located at the pore mouth, which are nominally in the micropores but very close to the external surface. The results showed that pillared **MFI** has 32% acid sites located at the external surface, 6% at the pore mouth, and 62% internal acid sites, whereas pillared **MWW** has 33% external, 31% pore mouth, and 36% internal acid sites.

Di-*tert*-butylpiridine (DTBP) was used as a probe to quantify external acid sites in the delaminated ITQ-2 zeolite. Depending on the synthesis conditions, the concentration of the external acid sites reached 40% for the material prepared by "classic" multistep synthesis ($S_{ext} > 700\ m^2/g$),[247] but only relative values in absorbance units were provided for directly synthesized DS-ITQ-2 ($S_{ext} = 300\ m^2/g$).[81] In the multilamellar UJM-1 material, all acid sites were available for pivalonitrile sorption.[80]

Larger probe molecules display enhanced, even close to 100%, adsorption in 2D vs 3D **MFI** zeolites, as shown in 2D **MFI** samples (termed "self-interlocked ordered nanosheet stacks" or SI-ONS by the authors) with nominal Si/Al ratios ranging from 15 to 87 and BAS concentrations ranging from 195 to 514 μmol/g.[193] The percentage of accessible strong Brønsted acid sites

https://dx.doi.org/10.1021/acscatal.0c05332
ACS Catal. 2021, 11, 2366−2396

(determined by pivalonitrile sorption at 200 °C) remained almost constant in all 2D **MFI** samples (93−97%) and was higher than the percentages for the respective 3D zeolites (44−66%). Such high accessibility percentages, especially for 3D **MFI**, may be due to the relatively high temperature of adsorption, which is much higher than the ambient temperature recommended by Busca[248,249] or those used by other authors.[208,230]

Although hierarchical zeolites, including 2D forms, are characterized by enhanced accessibility to their Brønsted acid sites, they usually show lower concentrations of BAS than conventional 3D forms in response to increases in mesoporous/external surface area (Table 3). For 2D zeolites, at least two reasons may explain the lower absolute values of acid site concentration: (i) except for special cases, such as MCM-56, layered forms usually have lower Al content than can be reached with 3D forms; (ii) chemical modifications tend to reduce the number of Brønsted acid sites considerably. The reported data can be also affected by flawed measurements or sample degradation, which may account for the reported disparate concentrations of acid centers of various **MWW** materials, ranging from low to exceptionally high.[175,243] Even for MCM-56, which has a rather steady Si/Al ratio between 10 and 12, the reported concentrations range from 78 to 913 μmol/g. For **MFI** (Table 3), the acidity of the multilamellar material (310 μmol/g) did not differ significantly from that of the unilamellar analogue (330 μmol/g) and was only slightly lower than that of bulk **MFI** (360 μmol/g). Concurrently, Bleken et al.[202] reported similar concentrations (Si/Al = 60 and 50) and intensities of the Si-OH-Al maxima for 3D and 2D **MFI**. These higher values are quite rare since many authors report that both 2D **MWW** and 2D **MFI** structures show lower intensities of the Si-OH-Al maximum at 3610−3620 cm^{-1} than their 3D counterparts even for a similar Si/Al ratio.[76,237,250]

Notably, the analysis of layered zeolites is more complex considering the significant increase in surface effects and potential defects. One of these unusual effects results from the apparent presence of acidic groups, which are capable of protonating pyridine but do not contribute to the intensity of IR maximum at 3610−3620 cm^{-1} (Figure 6a,b) and therefore remain undetected by FTIR.[251] Consequently, upon pyridine desorption at 400 °C, no IR band characteristic of Si-OH-Al groups is detected at 3620 cm^{-1}, whereas the intensity of the pyridinium band at 1545 cm^{-1} decreases by ca. 10%. Onida et al.[252] also suggested that Si-OH-Al groups exposed at the external surface in delaminated materials (e.g., ITQ-2) are probably converted into additional AlOH Brønsted acid sites and that they are IR-invisible, most likely due to the very low absorption coefficient of their IR band. Some protons, acidic enough to protonate bases such as pyridine, do not manifest themselves as Si-OH-Al or Al-OH groups because of heterogenization of the OH groups and will be further elaborated when discussing the acid strength of 2D zeolites. In the comparison between OH group frequencies, the issue was raised as to whether these groups are located in the internal supercages of **MWW** (in the 3D structure) or in their halves (cavities) at the external surfaces of the layers. In this context, when investigating the acid properties of MCM-22 and MCM-36 zeolites by 2,4-dimethylquinoline adsorption, Laforge et al.[236,253] suggested that the frequency of the latter differed from 3620 cm^{-1} (Figure 6, a), albeit without providing a specific position.[236] Yet, most authors, following the assignment given by Bevilacqua et al.,[254] assume that there is no difference in frequency.

In addition to the concentration and accessibility of Brønsted acid sites, FTIR spectroscopy of adsorbed probe molecules makes it possible to determine the acid strength distribution—one of the important characteristics of zeolite catalysts. The comparative strength of acid sites in 2D and 3D zeolites remains controversial in the literature, with opposing conclusions—Brønsted acid sites are reported as either stronger or weaker for layered structures. Therefore, this strength must be quantified.

One of the methods for quantifying the strength of Brønsted acid sites is based on the temperature of desorption of strong bases, but this method has some drawbacks, and the results may depend on the instrument and the determination protocol. An alternative method uses weakly basic probes that can form hydrogen bonds with acid centers. The parameter measured in this method is the value of the red shift of the IR band that corresponds to the O−H stretching vibration. Many factors affect this interaction, including the basicity of the probe itself and the position of the active center, that is, whether the active center is located deep within the microporous channel of the zeolite, at the pore mouth, or at the surface of a layer. The results of Gilson et al.[255] and others have shown that probes such as CO, N_2, and acetonitrile respond differently depending on the size of the channels (e.g., 12- or 8-rings).[256,257] The interpretation of these confinement effects causes problems when analyzing 3D zeolites and should be compounded for 2D zeolites because of the increased ratio of external to internal surfaces.

An alternative approach was proposed by Arean et al.,[258] who suggested that the enthalpy change of the hydrogen bond formation (ΔH^0) is a much better indicator of the strength of OH groups than the red shifts of IR maxima. The ΔH^0 values were determined using variable-temperature IR (VTIR) spectroscopy, and compared with adsorption calorimetry results, and periodic DFT calculations. The enthalpy values were −22.5 (for CO) and −14.5 (for N_2) kJ/mol for H-MCM-22, and 20 and 13 kJ/mol for MCM-56. According to these calculations, 3D MCM-22 is a stronger acid than lamellar MCM-56, and overall **MWW** zeolites are weaker acids than **MFI** or **FER**. The values of the red shift upon formation of the hydrogen bond with CO indicate the opposite trend, that is, they are higher for **MWW**, with ca. 320 cm^{-1} (**MWW**) vs 303 cm^{-1} (**MFI**) and 297 cm^{-1} (**FER**).

The strength of acid sites in zeolite layers was calculated using embedded cluster QM/MM (quantum mechanics/molecular mechanics) calculations by Rybicki and Sauer.[259] The authors determined absolute deprotonation energies for Brønsted acid sites, Si-OH-Al groups, located in ultrathin 2D zeolites (1042−1091 kJ/mol), and the bulk H-**CHA** (1233 kJ/mol). The most important conclusion was that the deprotonation energies of 2D zeolites are much lower than those of their 3D counterparts, indicating higher strength of acid sites in 2D vs 3D zeolites. In addition, the acidity of ultrathin or single layer zeolites strongly depends on the actual layer thickness because the dielectric constant is much lower for 2D than for analogous bulk samples (i.e., 1.8 vs 2.9). As a result, the charge formed upon deprotonation is less screened in layered zeolites and can be stabilized by electrostatic interactions with neighboring ions. Thus, the acidity of 2D materials defined as deprotonation energies is much higher than that suggested by OH frequency shifts upon adsorption of base molecules. The same conclusion was drawn by Grajciar et al.,[260] who established that the

https://dx.doi.org/10.1021/acscatal.0c05332
ACS Catal. 2021, 11, 2366−2396

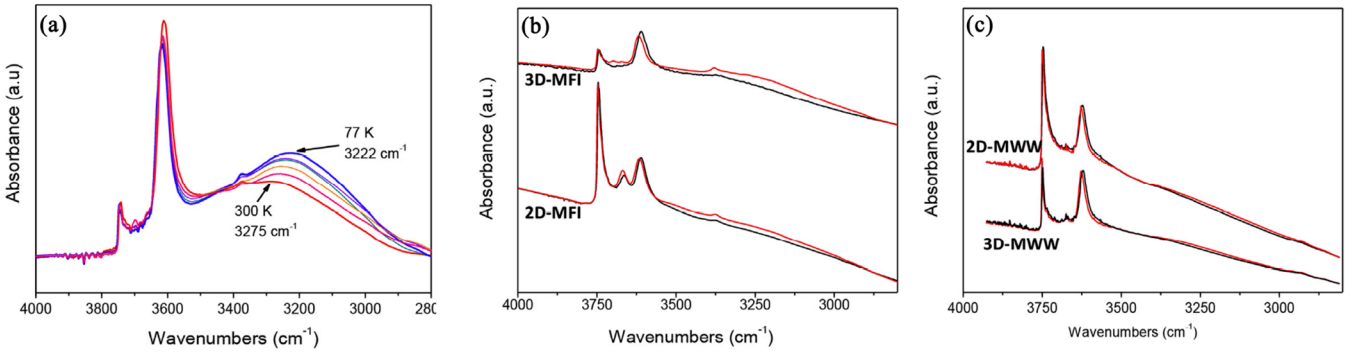

Figure 8. O−H vibrational bands of 3D **MFI** zeolite at various temperatures from liquid nitrogen to room temperature (a) and the changes in the IR spectra of OH vibrations with temperature on **MFI** (b) and **MWW** (c) zeolites. Red spectra were recorded at liquid nitrogen temperature and black ones at RT. Reproduced with permission from ref 260. Copyright 2019 Elsevier.

magnitude of OH frequency shifts upon hydrogen-bond formation (CO adsorption) is mostly affected by the absence of the "effect from the top", that is, less effective dispersion interactions. In line with this correlation, Sauer[261] showed that the adsorption energies of ammonia and (to some extent) pyridine were almost the same for 2D and 3D materials (adsorption energy for NH_3 −160 kJ/mol on a 2D structure vs −159 kJ/mol on a 3D structure, and for pyridine −145 kJ/mol on a 2D structure vs −182 kJ/mol on a 3D structure) even if the deprotonation energy, a measure of the intrinsic acid strength of a given site, was lower for 2D than for 3D materials. This effect may be compensated for by the properties of the conjugated acid−base pair. A deprotonated zeolite is a base conjugated with a protonated zeolite (an acid), so the stronger the acidic OH, the weaker its deprotonated form, thereby it binds ammonium ion (acid conjugated with an NH_3 base) less strongly. An additional but weaker effect results from the local environment around a given OH group. Boscoboinik et al.[262] studied interactions with probe molecules that are weak bases, CO and ethene, and found the same results as those observed when using stronger bases.

The preceding discussion on the overall acid strength of 2D zeolites in comparison with their 3D counterparts indicated two factors with opposite effects—the smaller effective dielectric constant at the surface of 2D zeolites, which results in lower deprotonation energies (higher acid strength), and weaker stabilization of chemisorbed molecules, due to missing "effect from the top". Computations have shown dissimilarities in proton distribution around individual framework positions (affecting the intrinsic acidity) between layered and bulk **MFI**/**MWW**, but the total effect on the average change upon transition from 3D to 2D character is close to negligible. These findings are in line with characteristics such as O−H/C−O stretching frequencies or CO adsorption heats detected experimentally.[199,260]

More striking differences between lamellar and conventional zeolites, identified in simulations and experiments, include changes in the concentration of BAS that are located inside the zeolite layer and which form intrazeolite hydrogen bonds, with framework oxygen across the ring and with a characteristic IR maximum below 3525 cm^{-1} (i.e., 3222 cm^{-1}, Figure 8).

The fraction of proton sites that participate in such hydrogen bonding is lower in layered forms of **MFI** than in the fully condensed zeolites (−20%), with virtually no changes in **MWW**.[260] In general, more significant surface effects (change in proton distribution or number of intrazeolite H-bonds) upon 3D → 2D transition were observed in the **MFI** topology characterized by 3 times higher silanol density, albeit with a lower layer thickness (2.0 nm) than **MWW** (2.5 nm) because more acid sites are close to the surface in the former. Similar conclusions were also drawn by Treps et al.,[263] who calculated (using the DFT) the stability of several surface species of **MFI**, such as nanoslabs and nanosheets. They also concluded that the pore-mouth Si-OH-Al groups are stabilized by the formation of additional hydrogen bonds, which cannot form inside the micropores because the distances separating the atoms are too long.

The comparison between 3D and 2D zeolites based on the concentration of external acid sites (Table 3) shows that the share of external sites may range from 17 to 100% (MCM-56) or from 30 to 100% (**MFI**). These values frequently do not correlate with the external area, thus suggesting that other intrinsic parameters and the synthesis procedure may also account for differences between 3D and 2D zeolites.

Temperature-programmed desorption of amines (especially n- and isopropylamine) is an interesting alternative to measure the acid sites concentration.[264,265] Alkylammonium ions, formed when alkyl amines are protonated by Brønsted acid sites, decompose to ammonia and olefin, and the measured Brønsted acid sites concentration are independent of a particular amine.[266] However, to the best of our knowledge, this method has not been used so far to investigate the acid sites concentration for 2D zeolites.

The following comparative analysis and discussion of the differences in catalytic behavior of 2D and 3D zeolites is focused on strong Brønsted and Lewis acid sites as the most influential active centers. However, often the role of other functionality in zeolites, in particular silanols, cannot be ignored. Moreover, the acidic nature of silanols located in a large quantity on the external surface of 2D zeolites can be different as it can be affected by the closely located Brønsted acid sites.[267] Internal and external silanols are also characterized by different activity which can be crucial for deactivation. For example, in methanol-to-propylene reaction isolated silanols in the pore affect the formation and diffusion of the intermediates and are thus responsible for the coke deposition, while external silanols do not promote this process to such extent.[268]

5.2.2. Cracking as a Probe Reaction for Strong Brønsted Acid Sites. Hydrocarbon cracking is among the most important and demanding industrial processes that rely on zeolites. Cracking of model compounds has been extensively studied to assess the effect of various channel systems and their accessibility on activity and product distribution. Since alkane cracking is

https://dx.doi.org/10.1021/acscatal.0c05332
ACS Catal. 2021, 11, 2366−2396

catalyzed by relatively strong acid sites, this process can be used to evaluate the distribution of such sites between inner and outer crystal surfaces. Several types of molecules (decalin, tetralin, as well as di- and triisopropyl benzenes − DIPB and TIPB) have been utilized to assess the external acidity of both **MFI** and **MWW** families of zeolites. By comparing 2D and 3D zeolites of the same type, the difference in the rates of cracking reactions can be related to differences either in the population of internal/external acid centers or in their strength. For example, decalin does not diffuse into the microporous channels of **MWW** or **MFI** zeolites but instead is transformed at 12-ring cavities on the outer surface of **MWW**. In another example, the activity of delaminated ITQ-2 is higher than that of bulk MCM-22 in the decaline conversion (TON = 58 vs 2.5 $g{\cdot}\mu mol^{-1}{\cdot}h^{-1}$).[269] Similarly, thanks to its higher external surface, nanolayered **MFI** outperforms its 3D analogue in the same reaction (16% vs 2% decalin conversion for 2D vs 3D **MFI**).[194]

In early studies of delaminated **MWW**-type materials, zeolites with similar concentrations of active centers but different architectures (2D ITQ-2 and 3D MCM-22) were tested in the cracking of *n*-decane (small molecule, which can penetrate into micropores) and DIPB.[152] The advantage of more exposed external surface of ITQ-2 was not significant when cracking *n*-decane; however, in the same reaction, the 2D zeolite provides a higher liquid/gas product than the bulk analogue due to easier diffusion of primary products from ITQ-2 pores exposed to the surface. As a result, the heavier compounds that are initially formed escape from the reaction space and avoid undergoing undesired secondary transformations. The decreasing concentration of active sites resulting from preparation of a 2D **MWW** such as MCM-36 with added inert silica as pillars, plays a significant role and may be responsible for reduced *n*-decane cracking activity.[174] When using heavier substrates, the advantages of layered catalysts stand out. In the cracking of DIPB/vacuum gasoil, delaminated **MWW** showed higher activity (with rate constants of 0.18/0.06 s^{-1} for DIPB/gasoil) than 3D **MWW** (0.11/0.03 s^{-1}). Despite its decreased total number of active sites, MCM-36 with well-developed mesoporosity outperforms MCM-22 in terms of conversion and ratio of liquid (diesel and gasoline)-to-gaseous products due to the increased fraction of highly accessible external acid centers. Another advantage of catalysts based on 2D zeolites is their typically longer lifetime because the amount of coke formed on the surface of ITQ-2 is lower thanks to the unobstructed desorption of the products.

The cracking of bulk molecules of different types, including TIPB and branched polyethylene, was studied on **MFI** zeolites with a multilamellar or disordered monolayered (unilamellar) architecture.[47,270] The latter catalyst exhibited higher conversion (85%) than the multilamellar material (45%) and bulk **MFI** (27%). For layered **MFI** materials, the TIPB conversion correlates with the ratio of external-to-internal BAS. The fraction of active centers on the outer surface and at the pore mouth can be controlled by the preparation method and incorporation of additional elements (e.g., boron).[270]

5.2.3. Using Alkylation to Probe the Reactivity of External Acid Sites. Friedel−Crafts alkylation is a common pathway to specialty and fine chemicals, and zeolites are frequently used as green catalysts in these reactions. Zeolites with an **MWW** topology have shown great benefits and have been applied in the large-scale synthesis of ethylbenzene and cumene for its suitable confinement of targeted monosubstituted products but insufficient space for further alkylation near the active sites located in surface cups.[38] As the activity of the **MWW** zeolite improves with the development of external surface, the alkylation of benzene proceeds at higher yields over the layered forms (MCM-56, ITQ-2, UZM-8) than over the conventional 3D MCM-22 catalysts.[271] While ethylbenzene/cumene syntheses by Friedel−Crafts alkylation of benzene are important industrially oriented processes, the alkylation of aromatics with benzyl alcohol is a useful and convenient model reaction to probe the active sites of zeolites because benzyl alcohol can participate not only in C- but also in O-alkylation (etherification) reactions. Toluene alkylation with isopropyl alcohol provided also interesting comparison between nanosheet MFI and the 3D analogue.[245,272,273] Both **MWW** and **MFI** zeolites were studied in these reactions using molecules with different sizes (most frequently, benzene or mesitylene).

Large differences in external surface reactivity were noticed between **MWW** and **MFI** for reactions involving bulky molecules (Figure 9, left).[274] The active centers located on external surfaces were found to play a key role in both C- and O-alkylation processes for the reaction of benzyl alcohol with mesitylene. The acid sites responsible for the activity of pillared **MWW** in both reactions are located only on the external surface, as confirmed by total deactivation when external sites were poisoned by bulky base molecules (DTBP). For pillared **MFI**, etherification can also be catalyzed by internal acid sites considering that O-alkylation, unlike C-alkylation, is not completely suppressed upon surface poisoning. The external surface of **MFI** zeolite appeared to be less active than that of **MWW** in C-alkylation, whereas the rates of O-alkylation over the active centers on the outer surface are similar for zeolites of both types. The significant difference in C-alkylation rates was explained by the difference in external surface features: **MFI** layers have pores with 10-ring windows and are characterized by high concentration of surface silanols, whereas **MWW** layers have 12-ring cavities and relatively low concentration of surface silanols (compared with **MFI**). As a consequence, mesitylene can be accommodated within the **MWW** cavities more easily than in the external surface of **MFI** that facilitates alkylation with benzyl alcohol.

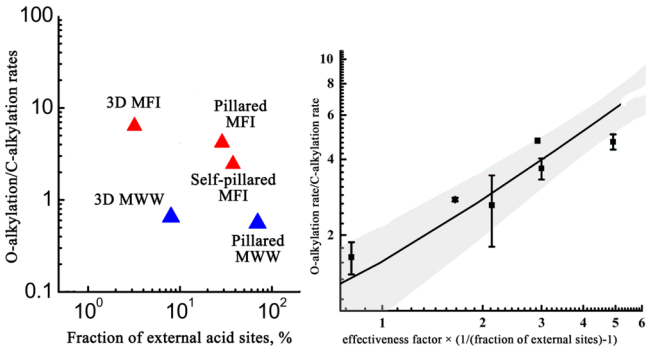

Figure 9. Reaction of benzyl alcohol with mesitylene. Left: Variation of the ratio between the rates of the etherification and alkylation reactions as a function of the fraction of external acid sites in **MFI** and **MWW** catalysts. Adapted with permission from ref 274. Copyright 2014 Elsevier. Right: Same parameter of **MFI** materials with different layer thicknesses versus the hierarchical-structure related factor. Adapted with permission from ref 275. Copyright 2019 Wiley-VCH.

A similar conclusion was reached in a study comparing self-pillared zeolite **MFI** with 3D **MWW** (Figure 9, right).[275] The benzyl alcohol etherification reaction over self-pillared **MFI**,

https://dx.doi.org/10.1021/acscatal.0c05332
ACS Catal. 2021, 11, 2366−2396

which contains layers with different thickness, was found to proceed at different rates. In the absence of micropore diffusion resistance, increasing the layer thickness elevates the ratio between O-/C-alkylation reaction rates because of the decreased fraction of acid sites on the external surface. The highest selectivity to the product of O-alkylation over self-pillared **MFI** was achieved for a characteristic diffusion length of approximately 10 nm. Both the selectivity to the C-alkylation product and C-alkylation reaction rate (0.034 vs 0.002 s^{-1} for **MWW** vs **MFI**, at similar etherification reaction rates 2.5−2.6·10^{-3} s^{-1}) were higher for surface active sites in **MWW**. The increase in the alkylation rate constant was again related to the differences in features of the surface between the **MFI** and **MWW** topologies.

Since in **MWW** both C-alkylation and O-alkylation are limited to the active sites on external surface, benzene alkylation with benzyl alcohol is also a good tool to differentiate **MWW** materials by their exposed external surface. The catalytic behavior of materials with high (MIT-1), moderate (MCM-56), and low (MCM-22) total pore volume (1.0−0.6−0.3 cm^3/g, respectively) and external surface (513−219−121 m^2/g, respectively) were compared in this reaction.[79] The activity correlates with the external surface area and concentration of active centers on the outer surface, and therefore, MIT-1 exhibited the highest activity (with yield of the C-alkylation product over MIT-1 reaching 65%, in comparison with 19% for MCM-22 and MCM-56). Atomic layer deposition of Si or Al in pillared **MWW**/**MFI** materials was performed toward tailoring the external acid sites responsible for C-alkylation.[276] The modification with silicon decreased the population of external acid sites, whereas aluminum deposition increased the number of surface centers. However, because of weak acid strength of the acid sites, conversion through alkylation remained unchanged. Simultaneously, both deposition procedures (Si and Al) affect the selectivity of external acid sites in both C- and O-alkylation over **MWW**: the rate constants of alkylation are higher, whereas those of etherification are lower than the corresponding rates of the unmodified pillared zeolite.

The methods for generating active sites (direct synthesis or postsynthesis) and permanent mesoporosity (delamination or pillaring) can affect the activity of layered zeolites in alkylation with benzyl alcohol. Postsynthesis addition of acid sites on the external surfaces of layered zeolites and the use of different pillaring procedures have not been efficient in enhancing activity thus far. To compare different methods for pillaring layered **MFI**, a procedure with multiple steps and a one-step treatment using mass transport through the vapor phase were compared by Wei et al.[277] As a simpler and shorter procedure (in the laboratory; large-scale manufacture is hard to imagine industrially), the vapor-phase approach is technically preferable. The catalytic performance of the pillared zeolites from both techniques was virtually identical.

Direct syntheses of delaminated 2D zeolites were much more efficient than postsynthesis treatments. Several groups compared the conventional, postsynthetically prepared ITQ-2 with analogue materials prepared directly in alkylation reactions. Postsynthetic delamination (conventional approach) adversely affected the framework integrity of the zeolite and thus its activity in alkylation with benzyl alcohol, independently of the concentration of acid sites in the material.[216] The preparation of the 2D zeolite in one step using an additional surfactant (cetyltrimethylammonium) allowed the introduction of additional aluminum sites at 12-ring cavities acting as external BAS. Reaction rates normalized to the concentration of external active centers reveal that directly synthesized **MWW** is more active (TON = 2750 $mol_{benzyl\ alcohol}$·$mol_{acid\ sites}^{-1}$ for an optimized sample) than ITQ-2 obtained by postsynthesis exfoliation (TON = 750 $mol_{benzyl\ alcohol}$·$mol_{acid\ sites}^{-1}$). The low activity of ITQ-2 is attributed to the high content of defective Al sites detected by 1D and 2D ^{27}Al MAS NMR. In another reaction, benzene alkylation with propene, the initial activity of "delaminated" **MWW** (ITQ-2_{direct}) directly synthesized in the presence of two SDAs was higher than the activity of MCM-22 and MCM-56 zeolites but similar to that of traditionally prepared ITQ-$2_{postsynthesis}$.[81] Despite not affecting product selectivity, the method of 2D **MWW** synthesis significantly affects the deactivation rate, with deactivation constants decreasing in the following order: MCM-56 ≫ MCM-22 > ITQ-2_{direct} ≥ ITQ-$2_{postsynthesis}$. When comparing the directly synthesized and conventionally prepared ITQ-2, all catalytic parameters (activity, selectivity, lifetime) are similar for both materials.

5.2.4. MTP and MTH: Negative Impact of Noncontrolled External Acidity. The methanol-to-propylene (MTP) reaction is one of the series of industrially relevant methanol-to-olefins (MTO) processes closely related to methanol-to-gasoline (MTG) and -hydrocarbons (MTH) technologies. The first step in the overall mechanism of all these reactions is methanol conversion into dimethyl ether (DME) followed by C−C bond formation reactions, resulting in a mixture of products (olefins, aliphatic, or aromatics, depending on the conditions and the type of catalyst).[278] After the formation of DME, the complex process of hydrocarbons formation can proceed through either direct route[279] (with relatively high activation barriers, takes place at the initial stages) or hydrocarbon pool route[280] when species formed at the initial stages (different types of species corresponding to arene, alkene, or alkane cycles or pools) are combined, providing the final products by reactions with relatively low activation barriers. Among aluminosilicate zeolites (in addition to the silicoaluminophosphate SAPO-34 with **CHA** topology), **MFI** is the only type of catalyst considered for this process due to superior activity and selectivity. Therefore, zeolites with **MWW** topology are not discussed in this section.

Most studies have aimed to develop an **MFI** crystal architecture to solve particular issues with the MTP reaction such as fast catalyst deactivation and relatively low selectivity to propylene. High methanol conversion and selectivity to propylene are the key parameters that are controlled when optimizing catalysts for MTP reactions. From the fundamental point of view, the MTP reaction is a good example of the evolution of ideas about the applicability of different forms of zeolites (from bulk to hierarchical and then to 2D) for this class of reactions.

The first step of MTP or MTH, DME formation, is independent of accessibility to acid sites and diffusion restrictions and does not require strong acid sites.[281] The small methanol molecules (0.37 nm) can easily diffuse through the 10-ring windows (0.55 nm) in **MFI** zeolite to reach acid sites located in micropores. The comparison of the catalytic behavior of layered and bulk **MFI** indicated that activity correlates with total acid concentration. As 2D and 3D zeolites have significantly different fractions of internal and external acid sites, this result confirms the same impact of those sites on the rate of DME formation. Although the acid sites on the external surface did not provide higher reaction rates, they were more stable against steam treatment, thus resulting in less

https://dx.doi.org/10.1021/acscatal.0c05332
ACS Catal. 2021, 11, 2366−2396

deterioration and dealumination of the acid sites. These processes are important because amorphous Al-containing materials are inactive in DME synthesis.[282]

Despite the insignificant effect on the rate of DME formation, decreasing the diffusion constraints improves the selectivity toward propylene. At lower residence times, olefin can diffuse from the pores of a zeolite, thus avoiding secondary transformations. These conditions increase the selectivity to propylene and improve the catalyst lifetime, as exemplified by zeolite nanoparticles (selectivity was improved from 43% to 49% for bulk **MFI** vs **MFI** nanoparticles).[283] The development of **MFI** materials with decreased size along one crystallographic direction (i.e., 3D → 2D trend, but the thicknesses does not approach the 2D limits) yielded materials with higher activity than conventional zeolites.[284] **MFI** with a thinner *b*-axis morphology (100 nm thickness) was prepared in a fluoride medium and had a higher pore volume and external surface area than the conventional zeolite. In the MTP process, this modified **MFI** exhibited improved initial selectivity to propylene (45 vs 38%) and deactivation resistance. The superior performance of the modified **MFI** was related to the shorter *b*-axis path and to intracrystalline secondary mesoporosity both facilitating diffusion of propylene.

For the MTH reaction on **MFI**, the presence of mesopores was also initially considered advantageous, so the development of secondary mesoporosity was often the goal in the catalyst design.[285] As a result, catalyst stability significantly increased during the MTH process (the period before 50% conversion drop was extended from 39 to 132 h) with the development of mesoporosity in the **MFI** family.[286] Moreover, an approximately linear relationship was found between mesoporosity and lifetime. Bulk **MFI** is deactivated faster than the zeolite with enhanced mesoporosity due to the preferential formation of carbon deposits inside the micropores. Accordingly, selective removal of Al from the external surface did not change the internal/external coke ratio. Simultaneously, dealumination of internal surface of the catalyst increased its resistance to deactivation. Therefore, the mesoporosity of **MFI** should be maximized to improve catalyst stability and activity.

This subject has been reinvestigated to understand whether the origin of **MFI** activity in MTH and its deactivation behavior are related to active centers situated in micropores or at the external surface of nanolayered **MFI**.[287] For this purpose, catalytic reactions were performed with and without a poisoning agent, bulk triphenylphospine oxide, affecting only external acid sites. When using the poison, the reaction rate remains unchanged, indicating that catalysis occurs inside micropores and that Al centers on the external surface do not participate in the desired transformation despite being Brønsted type acid sites of relatively high strength. Concomitantly, these surface active centers are strong enough to catalyze secondary hydrocarbon cracking and alkylation reactions. Thus, internal active centers catalyze propylene formation with the effect of transition-state selectivity, whereas the external acid sites are responsible for the deposition of carbonaceous species and catalyst deactivation.

In the MTP reaction, **MFI** nanosheets with an increased concentration of external acid sites are deactivated more quickly.[270] The higher ratio of strong/weak centers on the crystal exterior is the reason for the fast **MFI** zeolite deactivation due to coke formation, thereby decreasing the accessibility to Al sites. Thus, pore system characteristics, acid strength, and the location of active sites must be optimized for MTP and related reactions. Such an optimization was attempted when designing seed-fused **MFI** nanosheets (hybrid of lamellar and bulk **MFI**) using a seed-induced method.[270] The resulting materials showed longer lifetimes than the pure nanosheets (168−226 h vs 103 h for materials of similar composition) with the highest mesopore volume and the lowest layer thickness, which was related to the decreased particle size and optimized distribution of acid sites. Seed-fused nanosheets showed increased micropore volume at decreased external surface area. By optimizing acid strength and diffusion properties, such hybrid materials showed improved selectivity to propylene (up to 49%) and total selectivity to light olefins (C_2−C_4, up to 81%) in comparison with pure nanosheets (45% and 78%) or physical mixture (46% and 79%, respectively).

5.3. MFI and MWW as Model Layered Lewis-Acid Zeolite Catalysts. 5.3.1. Probing Lewis Acidity in 2D Zeolites. Lewis acid sites in zeolites are classified into three types:[288] (i) coordinatively unsaturated extra-framework or "framework-associated" Al atoms; (ii) metal cations at ion-exchange positions; and (iii) intrinsic centers related to framework tetravalent elements (Ti, Sn, Zr, and others).

The first type of Lewis centers, Al-associated Lewis acid sites, are a deviation from an ideal tetrahedral structure due to dissociation of the framework Si−O−Al bonds. This generates either complete or partial extra-framework species, resulting in "framework-associated" Al species. Lewis acid sites are not as uniform as the Brønsted acid sites because they are affected by various factors. The pathways that are involved in the origin and classification of Lewis acid sites are presented in an excellent review written by Ravi et al.[289] Lewis acid sites cannot be observed directly by IR and can be detected only via interaction with basic molecules. CO is the most often used probe for the simplicity of its own spectrum, high absorption coefficient of C−O vibrations, and strong influence of the electrostatic field on the spectrum of adsorbed CO molecules.[290] Besides the bands of physically adsorbed CO (2138 cm^{-1}) and CO interacting with silanol groups (2156 cm^{-1}) and BAS (2175 cm^{-1}), **MWW** materials show two bands of adsorbed CO: one at 2230 cm^{-1}, for LAS, associated with partial framework Al species, and another at 2243 cm^{-1}, for very strong LAS, related to highly coordinatively unsaturated Al^{3+} cations. The 2243 cm^{-1} band may be assigned to Al^{3+} of small aluminum oxide clusters formed by complete dealumination[252] or by dehydroxylation of the pyramidal aluminum, typical of **MWW** structures (Figure 10a). The former is also observed in 2D **MFI**,[244] but the latter has never been observed in this structure (Figure 10).

An additional band of CO adsorbed on Lewis acid sites, at 2190 cm^{-1}, was reported by Wu et al.[203] for mono- and multilamellar (but not bulk) **MFI**. The authors concluded that Al atoms were more heterogeneous in the nanolayered zeolites than in regular **MFI**.

Co-adsorptions of hexamethylenimine and pivalonitrile with CO were used to determine the location of Lewis acid sites in **MWW**-type zeolites, including Al-MCM-22 with the template removed by acid-treatment and with an interlayer-expanded derivative.[291] For Al-MCM-22 and its expanded form, the Lewis centers characterized by CO vibrations at 2227 and 2220 cm^{-1} were found only at the external surfaces of the **MWW** layers and inside the channels that were expanded by silylation. In the acid-treated sample, additional LAS were generated, located in the interlayer 10-ring micropores (CO vibrations at 2227 cm^{-1}). The authors concluded that all Lewis acid sites were either framework, tetrahedral Al species, or octahedral, extraframework Al and that these sites only differed by location, not by chemical

https://dx.doi.org/10.1021/acscatal.0c05332
ACS Catal. 2021, 11, 2366−2396

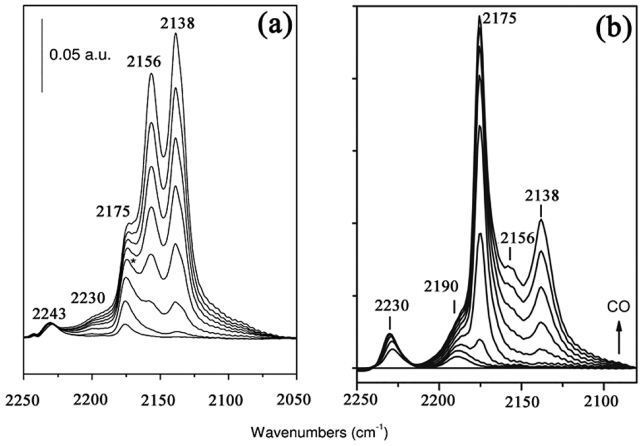

Figure 10. FTIR spectra of dehydrated ITQ-2 (a) and 2D **MFI** (b) at 77 K as a function of the CO coverage. Reproduced with permission from refs 252 and refs 203. Copyrights 2003 and 2014 Elsevier.

character. For other **MWW** series (MCM-22, MCM-56, and UJM-1), LAS were found only at internal surfaces.[208] Samples activated at moderate temperatures (450−480 °C) had very few Lewis acid sites detected by pyridine (30−90 μmol/g), and no interaction with pivalonitrile was observed, even after pivalonitrile adsorption at high temperature, which allowed its adsorption to micropores. Only in materials dehydroxylated at high temperature did the LAS give the small-intensity IR band at 2317 cm^{-1} and only after pivalonitrile adsorption at high temperature; therefore, these sites had to be located in micropores. Unfortunately, in this work, CO was not used as the secondary probe for Lewis acidity.

The comparison between these two works[208,291] on **MWW** materials suggests that Lewis acid sites may form both at the external layer surfaces and inside micropores upon thermal treatment in the presence of template, whereas thermal dehydroxylation in the absence of the template produces exclusively internal Lewis acid sites.

Lewis acid sites can be detected using also other approaches such as ^{31}P MAS NMR with trimethyl phosphine oxide (TMPO) as a probe molecule.[79] The peak observed at 53 ppm may be associated with TMPO coordinated to Lewis acid sites in the MIT-1 material, but another report did not observe this peak in **MWW** samples, regardless of the presence or absence of Lewis acid sites.[216] Since MIT-1 has a much more open structure (house-of-cards), it can in fact admit TMPO to its Lewis acid sites, whereas access may be problematic in the standard **MWW** materials. A similar dichotomy in the detection of Lewis acid sites using pivalonitrile was reported by Matsunaga[291] and by Gil.[208]

The second type of Lewis acid sites related to cations in ion-exchange positions was considered from experimental and theoretical points of view in relation to both 2D and 3D forms of zeolites of **MWW** and **MFI** topologies containing Li^+ cations.[77] Depending on the zeolite topology, the effect of changing layer connectivity (2D or 3D) on cation Lewis acidity, evaluated based on the interaction with CO (IR frequencies and adsorption enthalpies), was either negligible (**MWW**) or significant (**MFI**). This result was related to the surface density of silanols, which is 3 times higher in 2D **MFI** than in **MWW**, thus inducing much deeper changes in the state of Li^+ cation in 2D **MFI** than in the 3D form. Lewis site strength decreases as the Si−OH population (and layer flexibility) increases because this improves Li^+ coordination with the framework.

The sites of the third type, related to tetravalent elements in zeolite frameworks, are Lewis acid sites that can be active in various redox transformations, including biomass processing. The difference of catalytic behavior of 2D and 3D zeolites possessing the sites of this type are discussed in sections 5.3.2 and 5.3.3. Despite rapidly increasing the range of catalytic functions played by LAS incorporated in zeolite frameworks, their exact structure remains controversial.[292] One of the reasons complicating the understanding of local structure of Lewis centers related to four-valent metals is their relatively high chemical and structural flexibility, which results in a wide variety of possible site configurations. This variability becomes even more complicated as additional components appear in the system (e.g., under catalytic conditions), affecting the state of LAS by coordinating or deconstructing (often reversibly) chemical interactions. In a fully connected configurations (either perfect or distorted tetrahedral), $M(OSi)_4$ are referred to as 'closed' sites, whereas once one Si−O−M bond is broken, these sites are termed 'open' $M(OSi)_3OH$. Computational studies for Ti analogues of 'closed'-'open' centers and sites potentially formed upon deeper hydrolysis revealed that the second and further steps of $M(OSi)_3OH$ hydrolysis are energetically unfavorable, whereas bond breaking and the formation of a hydroxyl group in the first step suffices for framework relaxation/stabilization.[293] Specific features of M(IV) Lewis centers depend on the type of zeolite framework, through its influence on possible bond distances and angles, and on the type of central element, which determines the preferred geometry and energy of interaction with surrounding molecules.[201] Despite the diversity and dynamic nature of LAS in zeolites, some of them can be observed directly. For example, EXAFS and XANES have been used to confirm the nearly tetrahedral symmetry of Ti LAS in the TS-1 zeolite, in good agreement with theoretical findings.[294] The incorporation of Sn atoms, which are larger than Ti atoms, elongated the Sn−O distance in comparison with Ti−O (0.191 vs 0.179 nm), thereby distorting the zeolite framework.[295]

Both theoretical and experimental evidence supports the generation of 'open' sites in Sn- and Zr-substituted zeolites.[296] Brønsted acid centers can be relatively easy distinguished by the acid strength. In contrast, similar differentiation of Lewis acid sites is both challenging and probe-dependent because of significant variations in the energy of metal−base interactions and its dependence on the nature of the central element and on the properties of the probe. To estimate the relative strengths of 'closed' $M(OSi)_4$ centers, the lowest unoccupied molecular orbital (LUMO) energies, Fukui functions and absolute electronegativity/hardness were evaluated as descriptors of Lewis acidity using **MFI** zeolite as a model,[297] albeit without establishing a clear correlation between the mentioned intrinsic descriptors and experimental data. Conversely, estimations using NH_3 adsorption energies established the following order of acid strength for Lewis sites in **MFI**: Ge < Ti < Pb ≤ Sn ≤ Zr, with a good correlation between the intrinsic chemical descriptor (Mulliken electronegativity) of the metal center and the ^{15}N NMR chemical shift of pyridine adsorbed on the respective site.[298] The ^{15}N-pyridine adsorption/^{15}N NMR combination made it possible to investigate metal−probe adducts and was used for both qualitative (acid strength) and quantitative characterization of Lewis centers in zeolites containing various elements in tetrahedral positions. The

https://dx.doi.org/10.1021/acscatal.0c05332
ACS Catal. 2021, 11, 2366−2396

estimated strength of Lewis acid sites increased in the following order: Ti < Hf < Zr < Nb < Ta < Sn.

5.3.2. Biomass Transformation: From Brønsted to Lewis Sites. Biomass is considered a renewable raw substrate for a wide range of applications, mainly related to the manufacture of biobased fuels and chemicals via diverse chemical routes.[299−301] The application of zeolites for such catalytic processes is complicated by the complex biomass composition and multiple functionalities, which enable interactions with the metal centers and interfere with the behavior of the catalysts or even with poisoning. In addition, biomass typically contains a large fraction of water, which potentially affects the zeolite structure by hydrolysis, leaching and structural transformation, among other processes. Biomass containing heavy or highly reactive constituents also have carbon deposition tendency, thus shortening the lifetime of catalysts. The catalytic performance of layered zeolites in comparison to their 3D analogues depends on the type of reaction. Thus, 2D zeolite catalyst may show the following: (i) enhanced activity (e.g., in catalytic pyrolysis of biomass); (ii) no significant effect (as in the case of isomerization of particular terpenes); or even (iii) worse overall performance (e.g., in epoxidation of small-size linear alkenes), which are discussed in this section.

Thermal pyrolysis is used for biomass decomposition, forming different fractions of products in different states: solid (biochar), liquid (bio-oil), and light gaseous products. Applying a zeolite catalyst during pyrolysis helps to transform biomass raw materials more deeply and gently than without a catalyst.[302] The higher the concentration and strength of acid sites, the higher the activity in a wide range of reactions, including simple elimination (dehydration, decarboxylation, and decarbonylation), C−C bond breaking, polymerization, and aromatization, which decrease the amount of oxygen in the resulting bio-oil.[301] The chemistry of product pools will also differ between catalytic and noncatalytic pyrolysis, particularly regarding the formation of a higher fraction of aromatics and furans instead of oxygen-rich polyfunctional alcohols and ketones upon pyrolysis of cellulose and xylan, or lighter phenolics and aromatics instead of heavy phenolics upon lignin conversion. However, a major disadvantage of catalytic pyrolysis is the high rate of coke formation, but this problem was partly alleviated when applying hierarchical or 2D zeolites.[303−305] Layered zeolites demonstrate better catalytic activity and lifetime than 3D analogues or purely mesoporous materials with relatively weak acid sites. Zeolites with both **MFI** and **MWW** topologies were used to compare the performance of 2D vs 3D in catalytic pyrolysis. An **MFI** nanosheet catalyst with surface area, micropore volume, and number of acid sites comparable to those of a commercial **MFI** was applied to cellulose pyrolysis vapor upgrading. The yields of hydrocarbons and particularly aromatics were similar (33−34 and 26−28%, respectively) over both types of catalysts, but the 2D materials increased molecular transport, thus showing that mesopores have a positive impact on catalyst lifetime. Yet, the coke content was higher on nanosheets than on conventional **MFI** (0.22 vs 0.11 g/g catalyst at the same biomass/catalyst loading) because the increased accessibility of acid centers also facilitated coke precursors.[306]

Unilamellar **MFI** was also used to upgrade pyrolysis vapors formed upon cellulose, hemicellulose, or lignin treatment.[305] As strong acidity is required for upgrading through cracking and deoxygenation reactions, the 2D zeolite catalyst improved the quality of the resulting bio-oil by increasing the yield of more valuable products. For example, in cellulose pyrolysis, the use of layered **MFI** decreased the undesired fraction of oxygenates from >90% to <40% at the optimized catalyst content, and from 50+% to less than 30% in xylan pyrolysis. For similar reasons, layered-type **MWW** catalysts (e.g., ITQ-2) outperform their 3D analogues, as shown by their higher aromatics yield or deoxygenation degree.[307]

Considering the above, in catalytic pyrolysis, 2D zeolites generally perform better than their 3D counterparts, regardless of zeolite type or differences in acid properties. However, the trend is sometimes different when 2D and 3D zeolites are used to process biomass derivatives. Because of their increased external area, 2D zeolites should be suitable catalyst for the aldol condensation of various carbonyl-containing substances that appear in the gas fraction upon biomass thermal treatment. Therefore, 2D and 3D forms of zeolites with an **MWW** topology (MCM-56 and MCM-36 vs MCM-22 and MCM-49) were studied in condensation of furfural and acetone.[308] At comparable selectivity to the targeted condensation products, MCM-22 showed the highest conversion (over 60%), which was attributed to the highest total concentration of acid sites in supercages and on the external surface even though MCM-22 is supposed to have fewer Al on the external surface. Among 2D zeolites, MCM-36 exhibited the lowest conversion (30−35%) and was rapidly deactivated, which was attributed to easier coke formation on the external acid sites. These results contrast with the MCM-36 performance in isobutane/butene alkylation, whose prolonged performance is ascribed to delayed coking because of open access to acid sites.[41]

Lewis acid zeolites are widely applied in isomerization reactions, where crystal dimensionality (3D or 2D) determines the type of transformation. The latter can be either sensitive (e.g., sugars isomerization over Sn active sites) or practically insensitive (e.g., terpenoids isomerization over Ti active sites) to the extent of the external surface in layered materials. Sn-containing pillared[309] and self-pillared[310] **MFI** materials with increased accessibility of active centers were efficient catalysts in mono- and disaccharide isomerization. In glucose-to-fructose isomerization, both 3D and pillared 2D zeolites produced high fructose yields (>50%) and selectivity (approximately 70%) at similar glucose conversions (75% after 24 h). However, the 50% fructose yield was achieved after 8 h over 2D vs 24 h over 3D catalysts, respectively. These results can be easily attributed to facilitated diffusion in pillared zeolites considering the similar acidic properties of the two catalysts, which have been confirmed by FTIR. In maltose-to-maltulose isomerization, the 2D analogue shows higher targeted product yields than its bulk (3D) Sn-**MWW**, albeit with similar selectivity. Thus, in the isomerization of sugars, decreasing zeolite layer thickness has virtually no effect on selectivity but enhances conversion.

In addition to isomerization reactions, Sn-substituted zeolites were used in Baeyer−Villiger oxidation. 2D Sn-**MWW** prepared by postsynthesis treatment of a layered precursor outperformed bulk Sn-**MWW** (approximately 10% gain in conversion at the same selectivity >99%) in the Baeyer−Villiger oxidation of 2-adamantanone.[311] Similarly to zeolites with the **MWW** topology, Sn-**MFI** composed of nanosheets was also tested in the same Baeyer−Villiger reaction, outperforming bulk Sn-**MFI** in terms of activity ($TOF_{nanosheets}$ = 86 h^{-1}, TOF_{bulk} = 9 h^{-1}) at a similar selectivity of over 98%.[312]

The difference in catalytic behavior between Ti-containing 2D and 3D zeolites in isomerization reactions is exemplified by the α-pinene oxide transformation to campholenic aldehyde.[313,314] The 3D Ti-**MWW** zeolites exhibited the highest

https://dx.doi.org/10.1021/acscatal.0c05332
ACS Catal. 2021, 11, 2366−2396

yield of targeted aldehyde (up to 96% over Ti-MCM-22 catalysts with different Si/Ti ratios). Ti-MCM-36 is just slightly less active than the bulk analogue (91% yield) but significantly outperforms Ti-containing **MFI**, aluminosilicate, and mesoporous materials. The exceptionally high selectivity of **MWW**-type catalysts to campholenic aldehyde, independently of their dimensionality, was attributed to the presence of the predominant fraction of tetrahedrally coordinated titanium sites in the framework and their optimal concentration, without BAS facilitating undesired transformations. The slightly lower activity of Ti-substituted pillared **MWW** can be attributed to the still small (but higher than MCM-22) fraction of penta- and hexacoordinated Ti that does not catalyze α-pinene oxide isomerization similarly to the oxidation reactions.[180]

5.3.3. Oxidation Reactions: Key Role of the Metal Center State. As mentioned above for isomerization reactions involving Lewis acid sites, the coordination and distribution of Ti atoms, in addition to their accessibility, affect redox processes catalyzed by Ti sites. Simultaneously, if the coordination of Ti is appropriate for a reaction, 2D zeolites almost invariably outperform 3D analogues.[200] In the epoxidation of relatively active cyclic alkenes (C_6, C_8), layered Ti-**MFI** showed higher activity than purely microporous Ti-**MFI** (TS-1) when using *tert*-butyl hydroperoxide as oxidant (TOF = 61.9 vs 0.2 h^{-1} for C_6). When using aqueous H_2O_2, this difference was less pronounced (TOF = 15.3 and 7.2 h^{-1}).[315] In the epoxidation of propylene with cumene hydroperoxide, which requires even more open reaction spaces, 2D Ti-**MFI** totally outperformed conventional **MFI** (conversion values are 20.0 and 0.8%, respectively). The catalytic performance of layered titanosilicate was enhanced via postsynthetic NH_4F-treatment, which increased surface hydrophobicity through the interaction between surface silanol groups and fluoride. As a result, the conversion values approximately doubled (11% before vs 25% after for C_6 and 9% vs 15% for C_8) and selectivity toward epoxide improved (69% vs 43% for C_6 and 95% vs 91% for C_8).[316] Specifically, in this transformation, the Ti sites on the outer surface usually show lower catalytic activity than inner centers, as reflected in the reduced efficiency of epoxidation of linear 1-hexene (conversion is 20% for 3D vs 14% for 2D catalysts). Since hydrophobization has no effect on the intrinsic acidity of active sites, fluorination does not improve the conversion of such a reactant (13%), thus underscoring the "limitation" of 2D materials in the transformation of small molecules. In contrast to **MFI**, 2D **MWW** derivatives outperform conventional 3D **MWW** not only in the transformation of C_5−C_{12} cycloalkenes (for example, for C_{12} TON_{2D} = 57, TON_{3D} = 9) but also in the epoxidation of linear 1- and 2-hexenes (for 1-hexene TON_{2D} = 1390, TON_{3D} = 934).[317]

In addition to the appropriate coordination state, usually considered a necessary condition for successful epoxidation reactions, Ti confinement has been recently shown to play a key role as well.[318] Chelated Ti sites with enforced tetrahedral coordination (by using a bulk calixarene ligand) were selectively anchored on the external surface of **MWW** layers to mimic (i) unconfined terminal sites, (ii) partly confined positions at surface cavities, or (iii) the mixture of both. Confining environments provided 5-fold higher reaction rates in cyclo-C_6 epoxidation than sites where reaction events are unconfined. All types of sites activation enthalpies of the formation of kinetically relevant transition states were similar, whereas entropic barriers increased in the absence of confinement, in line with previous reports on similar enthalpic but lower entropic barriers for transformations in completely confining environments.[319] Although the studied material is not truly a Ti-**MWW** zeolite and thus does not completely represent its behavior during the catalytic process, the reaction rates for the mixture of Ti environments match the values typical of confined sites but differ from the intermediate values between two extreme states. This result suggests that Ti sites can move during a catalytic experiment from unconfined terminal framework positions to partly confined sites located in **MWW** surface pockets. MCM-56 is a **MWW** material with Al atoms located on the surface in "pyramidal" sites. Such atoms may be replaced by Ti to produce pyramidal TiOH groups, via Al removal by nitric acid, followed by calcination and treatment with titanium diisopropoxide bis(acetylacetonate).[320] In the resulting catalysts, three types of Ti moieties were identified in uncalcined materials—tetrahedral in the framework, five or six-coordinated Ti on the surface, presumably in pyramidal sites, and oxide-like clusters. After calcination, such surface Ti-atoms were converted into tetrahedral sites terminated by OH group and were the most active, resulting in the highest relative conversion of methyl phenyl sulfide per Ti content. In conclusion, these studies confirmed the potential of open, surface TiOH species for oxidation catalysis.

Considering the prevailing trend in zeolite catalysis, the advantages of 2D derivatives, if present, can be characterized as quantitative—the reactions proceed in basically the same manner but 2D derivatives favor the yield or the selectivities. A rare example of qualitative switch has been observed in cerium-exchanged **MWW** materials.[188] More specifically, IEZ-MWW with a slightly expanded interlayer distance can adsorb greater amounts of Ce^{3+} than both 3D MCM-22 and 2D MCM-56, acquiring a new type of activity at room temperature, CO-to-CO_2 conversion, which Ce-MCM-22 lacks. Such a change is particularly valuable because the possible performance debit of 3D vs 2D (quantitative) can be offset simply by increasing the catalyst volume (favored by the additional cost and labor of preparing 2D forms). To match the qualitative change offered by 2D, the only alternative may be another catalyst.

SUMMARY AND PERSPECTIVES

The possible existence of layered forms was not considered during the initial development of zeolites when the fundamental foundations and principal practical applications were established. In fact, there was a sharp boundary between 3D and 2D structures, reinforced by significant differences in fundamental characteristics. Layered zeolites represent a shift in a long-held concept with far reaching consequences, both fundamental and practical.

Layered zeolites are often regarded as one of the different modifications that can solve accessibility problems and diffusional constrains, which limit the applicability of conventional microporous catalysts. In a broader fundamental perspective, layered zeolites represent an expansion of the traditional view of frameworks as extended 3D networks, together forming a seamless 2D-3D continuum. In practical terms, 2D forms allow modifications and the creation of new forms and (molecularly mixed) compositions previously impossible to prepare. These capabilities are illustrated herein by the **MWW** and **MFI** materials, as models for replication and expansion with other frameworks that have been and will continue to be prepared in 2D forms. The assumption is that layered forms are possible for most and maybe all frameworks.

https://dx.doi.org/10.1021/acscatal.0c05332
ACS Catal. 2021, 11, 2366−2396

The layered zeolites **MFI** and **MWW** have produced almost 20 different layered forms, some common for both, including 9 by direct synthesis. Several reports have demonstrated that layered forms can perform better than conventional 3D zeolites, but most remain unconfirmed under conditions suitable for commercial uses, for example, in a bound form, and in comparison to commercial benchmarks. The practical uses of 2D zeolites can be also hindered by the additional costs and labor, so the quantitative advantage (yield and selectivity) may not justify substitution of existing catalysts. Instead, some qualitative changes displayed by a 2D zeolite form but not by the 3D parent may be the preferred route of development, as shown by CO-to-CO_2 oxidation by Ce-IEZ-MCM-22 (interlayer expanded zeolite (IEZ)), for which Ce-MCM-22(conventional 3D from) is inert.

Despite major advances in 2D **MWW** and **MFI**, there are still many basic open problems. For example, there is no **MFI** equivalent of the **MWW** precursor (MCM-22P). In addition, other frameworks can show forms and behavior similar to the two model systems, but other factors related to the framework itself (surface silanol concentration) may nevertheless play a key role and limit the options. A recent advance has been the liquid exfoliation of **MWW** into a liquid dispersion of monolayers. Thanks to this groundbreaking achievement, monolayers can be used as reagents to prepare suitable advanced materials at will, subject to favorable interactions and compatibility. The fundamental properties of 2D zeolites vs 3D, such as intrinsic activity and stability, among others, are still not firmly established, and conflicting results have been reported, most likely because many factors control the preparation, in addition to the test conditions.

The discovered coexistence of 2D and 3D structures for zeolites has implications for other solids both 2D and 3D by encouraging consideration of analogous circumstances not only with other 3D solids but also in the opposite direction—3D structures that can be made from classical 2D solids. From a long-term perspective, even lower-dimensional materials (e.g., 1D) may be used as precursors to materials with 2 or more dimensions. Yet, such systems are not easy to handle with and remain outside the current state of the art, for now, but declaring their impossibility a priori would be presumptuous. The evolution of 2D zeolites led to some unusual or unexpected phenomena or materials. However, this pattern is common to any scientific endeavor as new findings often seem to be obvious in hindsight and could have been anticipated if a broader analysis had been performed. Paradigmatic examples include interlayer expanded zeolites,[140] which have not been identified with other layered solids, and the generation of new zeolites structures, previously "unfeasible", by layer rearrangement.[30]

AUTHOR INFORMATION

Corresponding Authors

Barbara Gil − *Faculty of Chemistry, Jagiellonian University, 30-387 Kraków, Poland*; Email: barbara.k.gil@uj.edu.pl

Jiří Čejka − *Department of Physical and Macromolecular Chemistry, Faculty of Sciences, Charles University, 128 43 Prague 2, Czech Republic*; orcid.org/0000-0003-1400-1031; Email: jiri.cejka@natur.cuni.cz

Authors

Mariya Shamzhy − *Department of Physical and Macromolecular Chemistry, Faculty of Sciences, Charles University, 128 43 Prague 2, Czech Republic*; orcid.org/0000-0002-1979-6817

Maksym Opanasenko − *Department of Physical and Macromolecular Chemistry, Faculty of Sciences, Charles University, 128 43 Prague 2, Czech Republic*

Wieslaw J. Roth − *Faculty of Chemistry, Jagiellonian University, 30-387 Kraków, Poland*; orcid.org/0000-0002-4090-8043

Complete contact information is available at: https://pubs.acs.org/10.1021/acscatal.0c05332

Notes

The authors declare no competing financial interest.

ACKNOWLEDGMENTS

Czech authors would like to thank the OP VVV "Excellent Research Teams", project no. CZ.02.1.01/0.0/0.0/15_003/0000417 − CUCAM. J.Č. acknowledges the support of the Czech Science Foundation to the project EXPRO (19-27551X). M.S. thanks the Czech Science Foundation for the Project No. 20-12099S. M.O. acknowledges the support of Primus Research Program of the Charles University (project number PRIMUS/17/SCI/22 "Soluble zeolites"). B.G. acknowledges the support from National Science Centre Poland, grant no. 2016/21/B/ST5/00858. The authors acknowledge Dr. Carlos V. Melo for editing the manuscript.

REFERENCES

(1) Fermoso, J.; Hernando, H.; Jana, P.; Moreno, I.; Přech, J.; Ochoa-Hernandez, C.; Pizarro, P.; Coronado, J. M.; Čejka, J.; Serrano, D. P. Lamellar and Pillared ZSM-5 Zeolites Modified with MgO and ZnO for Catalytic Fast-Pyrolysis of Eucalyptus Woodchips. *Catal. Today* **2016**, *277*, 171−181.

(2) Přech, J.; Pizarro, P.; Serrano, D. P.; Čejka, J. From 3D to 2D Zeolite Catalytic Materials. *Chem. Soc. Rev.* **2018**, *47* (22), 8263−8306.

(3) Suib, S. L.; Přech, J.; Čejka, J.; Kuwahara, Y.; Mori, K.; Yamashita, H. Some Novel Porous Materials for Selective Catalytic Oxidations. *Mater. Today* **2020**, *32*, 244−259.

(4) Masters, A. F.; Maschmeyer, T. Zeolites - from Curiosity to Cornerstone. *Microporous Mesoporous Mater.* **2011**, *142* (2−3), 423−438.

(5) O'Hare, D. Inorganic Intercalation Compounds. In *Inorg. Mater.*, 2nd ed.; Bruce, D. W., O'Hare, D., Eds. Wiley: New York, 1997; pp 172−254.

(6) Van Der Voort, P.; Leus, K.; De Canck, E. *Introduction to Porous Materials*; Wiley: Hoboken, NJ, 2019; pp 75−118.

(7) Rouquerol, J.; Rouquerol, F.; Llewellyn, P.; Maurin, G.; Sing, K. S. W. *Adsorption by Powders and Porous Solids: Principles, Methodology and Applications*; Elsevier Science: 2013; pp 1−646.

(8) Fechete, I.; Wang, Y.; Védrine, J. C. The Past, Present and Future of Heterogeneous Catalysis. *Catal. Today* **2012**, *189* (1), 2−27.

(9) Čejka, J.; Corma, A.; Zones, S. I. *Zeolites and Catalysis: Synthesis, Reactions and Applications*; Wiley: 2010; p 881.

(10) Kresge, C. T.; Leonowicz, M. E.; Roth, W. J.; Vartuli, J. C.; Beck, J. S. Ordered Mesoporous Molecular Sieves Synthesized by a Liquid-Crystal Template Mechanism. *Nature* **1992**, *359* (6397), 710−712.

(11) Kresge, C. T.; Roth, W. J. The Discovery of Mesoporous Molecular Sieves from the Twenty Year Perspective. *Chem. Soc. Rev.* **2013**, *42* (9), 3663−3670.

(12) Yaghi, O. M.; O'Keeffe, M.; Ockwig, N. W.; Chae, H. K.; Eddaoudi, M.; Kim, J. Reticular Synthesis and the Design of New Materials. *Nature* **2003**, *423* (6941), 705−714.

(13) Auerbach, S. M.; Carrado, K. A.; Dutta, P. K. *Handbook of Layered Materials*; Marcel Dekker: New York, 2004; pp 1−664.

(14) Alberti, G.; Constantino, U. Layered Solids and Their Intercalation Chemistry. In *Comprehensive Supramolecular Chemistry,*

Solid-State Supramolecular Chemistry: Two- and Three-Dimensional Inorganic Networks; Alberti, G., Bein, T., Eds.; Pergamon: Oxford, 1996; Vol. 7, pp 1−23.
(15) Kulprathipanja, S. *Zeolites in Industrial Separation and Catalysis*; Wiley: 2010; pp 61−73.
(16) Vogt, E. T. C.; Whiting, G. T.; Chowdhury, A. D.; Weckhuysen, B. M., Zeolites and Zeotypes for Oil and Gas Conversion. In *Adv. Catal.*; Jentoft, F. C., Ed.; Elsevier: 2015; Vol. *58*, pp 143−314.
(17) Vogt, E. T. C.; Weckhuysen, B. M. Fluid Catalytic Cracking: Recent Developments on the Grand Old Lady of Zeolite Catalysis. *Chem. Soc. Rev.* **2015**, *44* (20), 7342−7370.
(18) Baerlocher, C.; McCusker, L. B. International Zeolite Association, Database of Zeolite Structures. See the following: http://www.iza-structure.org/databases/.
(19) Smith, J. V. Topochemistry of Zeolites and Related Materials. 1. Topology and Geometry. *Chem. Rev. (Washington, DC, U. S.)* **1988**, *88* (1), 149−182.
(20) Breck, D. W. *Zeolite Molecular Sieves: Structure, Chemistry, and Use*; Wiley: New York, 1973; pp 1−771.
(21) Haag, W. O.; Lago, R. M.; Weisz, P. B. The Active Site of Acidic Aluminosilicate Catalysts. *Nature* **1984**, *309* (5969), 589−591.
(22) Gleichmann, K.; Unger, B.; Brandt, A. Manufacturing of Industrial Zeolite Molecular Sieves. *Chem. Ing. Tech.* **2017**, *89* (7), 851−862.
(23) Deutschmann, O.; Knözinger, H.; Kochloefl, K.; Turek, T., Heterogeneous Catalysis and Solid Catalysts. In *Ullmann's Encyclopedia of Industrial Chemistry*; Wiley: 2009; pp 1−110.
(24) Čejka, J.; Millini, R.; Opanasenko, M.; Serrano, D. P.; Roth, W. J. Advances and Challenges in Zeolite Synthesis and Catalysis. *Catal. Today* **2020**, *345*, 2−13.
(25) Müller-Warmuth, W.; Schöllhorn, R. *Progress in Intercalation Research*; Kluwer: Dordrecht, 1994; pp 223−271.
(26) Nicolosi, V.; Chhowalla, M.; Kanatzidis, M. G.; Strano, M. S.; Coleman, J. N. Liquid Exfoliation of Layered Materials. *Science* **2013**, *340* (6139), 1226419.
(27) Clearfield, A.; Perry, H. P.; Gagnon, K. J., Porous Pillared Clays and Layered Phosphates. In *Comprehensive Inorganic Chemistry II (Second ed.): From Elements to Applications*; Reedijk, J., Poeppelmeier, K., Eds.; Elsevier: 2013; Vol. *5*, pp 169−211.
(28) Ernst, S.; Hartmann, M.; Tontisirin, S.; Bohlmann, W. Characterization and Catalytic Evaluation of Zeolite MCM-71. In *Molecular Sieves: From Basic Research to Industrial Applications*; Čejka, J., Žilková, N., Nachtigall, P., Eds.; Elsevier: 2005; Vol. *158*, pp 1287−1294.
(29) Dorset, D. L.; Roth, W. J.; Kennedy, G. J.; Dhingra, S. S. Crystal Structure of MCM-71 - a New Zeolite in the Mordenite Group. *Z. Kristallogr. - Cryst. Mater.* **2008**, *223* (7), 456−460.
(30) Mazur, M.; Wheatley, P. S.; Navarro, M.; Roth, W. J.; Položij, M.; Mayoral, A.; Eliášová, P.; Nachtigall, P.; Čejka, J.; Morris, R. E. Synthesis of 'Unfeasible' Zeolites. *Nat. Chem.* **2016**, *8* (1), 58−62.
(31) Roth, W. J.; Gil, B.; Makowski, W.; Marszalek, B.; Eliášová, P. Layer Like Porous Materials with Hierarchical Structure. *Chem. Soc. Rev.* **2016**, *45* (12), 3400−3438.
(32) Opanasenko, M.; Roth, W. J.; Čejka, J. Two-Dimensional Zeolites in Catalysis: Current Status and Perspectives. *Catal. Sci. Technol.* **2016**, *6*, 2467−2484.
(33) Osada, M.; Sasaki, T. Nanosheet Architectonics: A Hierarchically Structured Assembly for Tailored Fusion Materials. *Polym. J. (Tokyo, Jpn.)* **2015**, *47* (2), 89−98.
(34) Ma, R.; Sasaki, T. Two-Dimensional Oxide and Hydroxide Nanosheets: Controllable High-Quality Exfoliation, Molecular Assembly, and Exploration of Functionality. *Acc. Chem. Res.* **2015**, *48* (1), 136−143.
(35) Wang, L.; Sasaki, T. Titanium Oxide Nanosheets: Graphene Analogues with Versatile Functionalities. *Chem. Rev. (Washington, DC, U. S.)* **2014**, *114* (19), 9455−9486.
(36) Ma, R.; Sasaki, T. Nanosheets of Oxides and Hydroxides: Ultimate 2D Charge-Bearing Functional Crystallites. *Adv. Mater. (Weinheim, Ger.)* **2010**, *22* (45), 5082−5104.
(37) Leonowicz, M. E.; Lawton, J. A.; Lawton, S. L.; Rubin, M. K. MCM-22 - a Molecular Sieve with 2 Independent Multidimensional Channel Systems. *Science* **1994**, *264* (5167), 1910−1913.
(38) Degnan, T. F., Jr.; Smith, C. M.; Venkat, C. R. Alkylation of Aromatics with Ethylene and Propylene: Recent Development in Commercial Processes. *Appl. Catal., A* **2001**, *221*, 283−294.
(39) Degnan, T. F. Recent Progress in the Development of Zeolitic Catalysts for the Petroleum Refining and Petrochemical Manufacturing Industries. *Stud. Surf. Sci. Catal.* **2007**, *170*, 54−65.
(40) Lawton, S. L.; Fung, A. S.; Kennedy, G. J.; Alemany, L. B.; Chang, C. D.; Hatzikos, G. H.; Lissy, D. N.; Rubin, M. K.; Timken, H. K. C.; Steuernagel, S.; Woessner, D. E. Zeolite MCM-49: A Three-Dimensional MCM-22 Analogue Synthesized by In Situ Crystallization. *J. Phys. Chem.* **1996**, *100* (9), 3788−3798.
(41) Roth, W. J.; Kresge, C. T.; Vartuli, J. C.; Leonowicz, M. E.; Fung, A. S.; McCullen, S. B. MCM-36: The First Pillared Molecular Sieve with Zeolite Properties. *Stud. Surf. Sci. Catal.* **1995**, *94*, 301−308.
(42) Whittam, T. V. Zeolites Nu-6(1) and Nu-6(2). U.S. Patent 4397825 1983.
(43) Iler, R. K. Ion Exchange Properties of a Crystalline Hydrated Silica. *J. Colloid Sci.* **1964**, *19* (7), 648−657.
(44) Schreyeck, L.; Caullet, P.; Mougenel, J.-C.; Guth, J.-L.; Marler, B. A Layered Microporous Aluminosilicate Precursor of FER-type Zeolite. *J. Chem. Soc., Chem. Commun.* **1995**, *21*, 2187−2188.
(45) Schreyeck, L.; Caullet, P.; Mougenel, J. C.; Guth, J. L.; Marler, B. Prefer: A New Layered (Alumino) Silicate Precursor of FER-Type Zeolite. *Microporous Mater.* **1996**, *6* (5−6), 259−271.
(46) Na, K.; Choi, M.; Park, W.; Sakamoto, Y.; Terasaki, O.; Ryoo, R. Pillared MFI Zeolite Nanosheets of a Single-Unit-Cell Thickness. *J. Am. Chem. Soc.* **2010**, *132* (12), 4169−4177.
(47) Choi, M.; Na, K.; Kim, J.; Sakamoto, Y.; Terasaki, O.; Ryoo, R. Stable Single-Unit-Cell Nanosheets of Zeolite MFI as Active and Long-Lived Catalysts. *Nature* **2009**, *461* (7261), 246−249.
(48) Opanasenko, M.; Shamzhy, M.; Wang, Y. Z.; Yan, W. F.; Nachtigall, P.; Čejka, J. Synthesis and Post-Synthesis Transformation of Germanosilicate Zeolites. *Angew. Chem., Int. Ed.* **2020**, *59*, 19380−19389.
(49) Heard, C. J.; Grajciar, L.; Uhlik, F.; Shamzhy, M.; Opanasenko, M.; Čejka, J.; Nachtigall, P. Zeolite (in)Stability under Aqueous or Steaming Conditions. *Adv. Mater. (Weinheim, Ger.)* **2020**, *32*, 2003264.
(50) Eliášová, P.; Opanasenko, M.; Wheatley, P. S.; Shamzhy, M.; Mazur, M.; Nachtigall, P.; Roth, W. J.; Morris, R. E.; Čejka, J. The ADOR Mechanism for the Synthesis of New Zeolites. *Chem. Soc. Rev.* **2015**, *44* (20), 7177−7206.
(51) Park, W.; Yu, D.; Na, K.; Jelfs, K. E.; Slater, B.; Sakamoto, Y.; Ryoo, R. Hierarchically Structure-Directing Effect of Multi-Ammonium Surfactants for the Generation of MFI Zeolite Nanosheets. *Chem. Mater.* **2011**, *23* (23), 5131−5137.
(52) Kim, Y.; Kim, K.; Ryoo, R. Cooperative Structure Direction of Diammonium Surfactants and Sodium Ions to Generate MFI Zeolite Nanocrystals of Controlled Thickness. *Chem. Mater.* **2017**, *29* (4), 1752−1757.
(53) Eder, F.; He, Y.; Nivarthy, G.; Lercher, J. A. Sorption of Alkanes on Novel Pillared Zeolites; Comparison between MCM-22 and MCM-36. *Recl. Trav. Chim. Pays-Bas* **1996**, *115* (11/12), 531−535.
(54) Roth, W. J. Synthesis of Delaminated and Pillared Zeolitic Materials. *Stud. Surf. Sci. Catal.* **2007**, *168*, 221−239.
(55) Roth, W. J.; Čejka, J. Two-Dimensional Zeolites: Dream or Reality? *Catal. Sci. Technol.* **2011**, *1* (1), 43−53.
(56) Marler, B.; Gies, H. Hydrous Layer Silicates as Precursors for Zeolites Obtained through Topotactic Condensation: A Review. *Eur. J. Mineral.* **2012**, *24* (3), 405−428.
(57) Ramos, F. S. O.; de Pietre, M. K.; Pastore, H. O. Lamellar Zeolites: An Oxymoron? *RSC Adv.* **2013**, *3* (7), 2084−2111.
(58) Díaz, U.; Corma, A. Layered Zeolitic Materials: An Approach to Designing Versatile Functional Solids. *Dalton Trans.* **2014**, *43* (27), 10292−10316.
(59) Xu, L.; Wu, P. Diversity of Layered Zeolites: From Synthesis to Structural Modifications. *New J. Chem.* **2016**, *40* (5), 3968−3981.

https://dx.doi.org/10.1021/acscatal.0c05332
ACS Catal. 2021, 11, 2366−2396

(60) Schulman, E.; Wu, W.; Liu, D. X. Two-Dimensional Zeolite Materials: Structural and Acidity Properties. *Materials* **2020**, *13* (8), 1822.
(61) Roth, W. J.; Nachtigall, P.; Morris, R. E.; Čejka, J. Two-Dimensional Zeolites: Current Status and Perspectives. *Chem. Rev. (Washington, DC, U. S.)* **2014**, *114* (9), 4807−4837.
(62) Rubin, M. K.; Chu, P. Composition of Synthetic Porous Crystalline Material, Its Synthesis and Use. U.S. Patent US4954325A 1990.
(63) Blake, A. J.; Franklin, K. R.; Lowe, B. M. Preparation and Properties of Piperazine Silicate (EU-19) and a Silica Polymorph (EU-20). *J. Chem. Soc., Dalton Trans.* **1988**, No. 10, 2513−2517.
(64) Millini, R.; Carluccio, L. C.; Carati, A.; Bellussi, G.; Perego, C.; Cruciani, G.; Zanardi, S. ERS-12: A New Layered Tetramethylammonium Silicate Composed by Ferrierite Layers. *Microporous Mesoporous Mater.* **2004**, *74* (1−3), 59−71.
(65) Marler, B.; Wang, Y.; Song, J.; Gies, H. Topotactic Condensation of Layer Silicates with Ferrierite-Type Layers Forming Porous Tectosilicates. *Dalton Trans.* **2014**, *43* (27), 10396−10416.
(66) Roth, W. J.; Gil, B.; Makowski, W.; Sławek, A.; Grzybek, J.; Kubů, M.; Čejka, J. Interconversion of the CDO Layered Precursor ZSM-55 between FER and CDO Frameworks by Controlled Deswelling and Reassembly. *Chem. Mater.* **2016**, *28* (11), 3616−3619.
(67) Roth, W. J.; Dorset, D. L.; Kennedy, G. J. Discovery of New MWW Family Zeolite EMM-10: Identification of EMM-10P as the Missing MWW Precursor with Disordered Layers. *Microporous Mesoporous Mater.* **2011**, *142* (1), 168−177.
(68) Položij, M.; Thang, H. V.; Rubeš, M.; Eliášová, P.; Čejka, J.; Nachtigall, P. Theoretical Investigation of Layered Zeolites with MWW Topology: MCM-22P vs. MCM-56. *Dalton Trans.* **2014**, *43* (27), 10443−10450.
(69) Fung, A. S.; Lawton, S. L.; Roth, W. J. Synthetic Layered MCM-56, Its Synthesis and Use. U.S. Patent US5362697A, 1994.
(70) Roth, W. J. MCM-22 Zeolite Family and the Delaminated Zeolite MCM-56 Obtained in One-Step Synthesis. *Stud. Surf. Sci. Catal.* **2005**, *158A and B*, 19−26.
(71) Juttu, G. G.; Lobo, R. F. Characterization and Catalytic Properties of MCM-56 and MCM-22 Zeolites. *Microporous Mesoporous Mater.* **2000**, *40* (1−3), 9−23.
(72) Goergen, S.; Fayad, E.; Laforge, S.; Magnoux, P.; Rouleau, L.; Patarin, J. Synthesis of Layered MCM-22(P) in the Presence of Hexamethonium Cations and Its Transformation into EUO- and MWW-Type Zeolites. *J. Porous Mater.* **2011**, *18* (5), 639−650.
(73) Smeets, S.; Berkson, Z. J.; Xie, D.; Zones, S. I.; Wan, W.; Zou, X.; Hsieh, M.-F.; Chmelka, B. F.; McCusker, L. B.; Baerlocher, C. Well-Defined Silanols in the Structure of the Calcined High-Silica Zeolite SSZ-70: New Understanding of a Successful Catalytic Material. *J. Am. Chem. Soc.* **2017**, *139* (46), 16803−16812.
(74) Archer, R. H.; Carpenter, J. R.; Hwang, S. J.; Burton, A. W.; Chen, C. Y.; Zones, S. I.; Davis, M. E. Physicochemical Properties and Catalytic Behavior of the Molecular Sieve SSZ-70. *Chem. Mater.* **2010**, *22* (8), 2563−2572.
(75) Roth, W. J.; Čejka, J.; Millini, R.; Montanari, E.; Gil, B.; Kubů, M. Swelling and Interlayer Chemistry of Layered MWW Zeolites MCM-22 and MCM-56 with High Al Content. *Chem. Mater.* **2015**, *27* (13), 4620−4629.
(76) Grzybek, J.; Kubů, M.; Roth, W. J.; Gil, B.; Čejka, J.; Kasneryk, V. Structural Transformation and Chemical Modifications of the Unusual Layered Zeolite MWW Form SSZ-70. *Catal. Today* **2020**, *354*, 133−140.
(77) Ho, T. V.; Nachtigall, P.; Grajciar, L. The Lewis Acidity of Three- and Two-Dimensional Zeolites: The Effect of Framework Topology. *Catal. Today* **2018**, *304*, 12−21.
(78) Camblor, M. A.; Corma, A.; Díaz-Cabañas, M.-J.; Baerlocher, C. Synthesis and Structural Characterization of MWW Type Zeolite ITQ-1, the Pure Silica Analog of MCM-22 and SSZ-25. *J. Phys. Chem. B* **1998**, *102* (1), 44−51.
(79) Luo, H. Y.; Michaelis, V. K.; Hodges, S.; Griffin, R. G.; Roman-Leshkov, Y. One-Pot Synthesis of MWW Zeolite Nanosheets Using a Rationally Designed Organic Structure-Directing Agent. *Chem. Sci.* **2015**, *6* (11), 6320−6324.
(80) Grzybek, J.; Roth, W. J.; Gil, B.; Korzeniowska, A.; Mazur, M.; Čejka, J.; Morris, R. E. A New Layered MWW Zeolite Synthesized with the Bifunctional Surfactant Template and the Updated Classification of Layered Zeolite Forms Obtained by Direct Synthesis. *J. Mater. Chem. A* **2019**, *7* (13), 7701−7709.
(81) Margarit, V. J.; Martínez-Armero, M. E.; Navarro, M. T.; Martínez, C.; Corma, A. Direct Dual-Template Synthesis of MWW Zeolite Monolayers. *Angew. Chem., Int. Ed.* **2015**, *54* (46), 13724−13728.
(82) Xu, L.; Ji, X.; Jiang, J.-G.; Han, L.; Che, S.; Wu, P. Intergrown Zeolite MWW Polymorphs Prepared by the Rapid Dissolution−Recrystallization Route. *Chem. Mater.* **2015**, *27* (23), 7852−7860.
(83) Archer, R. H.; Zones, S. I.; Davis, M. E. Imidazolium Structure Directing Agents in Zeolite Synthesis: Exploring Guest/Host Relationships in the Synthesis of SSZ-70. *Microporous Mesoporous Mater.* **2010**, *130* (1), 255−265.
(84) Choi, M.; Cho, H. S.; Srivastava, R.; Venkatesan, C.; Choi, D.-H.; Ryoo, R. Amphiphilic Organosilane-Directed Synthesis of Crystalline Zeolite with Tunable Mesoporosity. *Nat. Mater.* **2006**, *5*, 718−723.
(85) Kennedy, G. J.; Lawton, S. L.; Rubin, M. K. 29Si MAS NMR Studies of a High Silica Form of the Novel Molecular Sieve: MCM-22. *J. Am. Chem. Soc.* **1994**, *116* (24), 11000−11003.
(86) Bennett, J. M.; Chang, C. D.; Lawton, S. L.; Leonowicz, M. E.; Lissy, D. N.; Rubin, M. K. Synthetic Porous Crystalline MCM-49, Its Synthesis and Use. U.S. Patent US5236575A, 1993.
(87) Argauer, R. J.; Landolt, G. R. Crystalline Zeolite ZSM-5 and Method of Preparing the Same. U.S. Patent US3702886A, 1972.
(88) Kokotailo, G. T.; Lawton, S. L.; Olson, D. H.; Meier, W. M. Structure of Synthetic Zeolite ZSM-5. *Nature* **1978**, *272* (5652), 437−438.
(89) Flanigen, E. M.; Bennett, J. M.; Grose, R. W.; Cohen, J. P.; Patton, R. L.; Kirchner, R. M.; Smith, J. V. Silicalite, a New Hydrophobic Crystalline Silica Molecular Sieve. *Nature* **1978**, *271* (5645), 512−516.
(90) Chu, P. Crystalline Zeolite ZSM-11. U.S. Patent US3709979A, 1973.
(91) Kokotailo, G. T.; Chu, P.; Lawton, S. L.; Meier, W. M. Synthesis and Structure of Synthetic Zeolite ZSM-11. *Nature* **1978**, *275* (5676), 119−120.
(92) Vaughan, P. A. Crystal Structure of Zeolite Ferrierite. *Acta Crystallogr.* **1966**, *21*, 983.
(93) Graham, R. P. D. On Ferrierite, a New Zeolitic Mineral, from British Columbia; with Notes on Some Other Canadian Minerals. *Proc. & Trans. R. Soc. Canada* **1918**, *12* (Sec IV), 185−190.
(94) Ikeda, T.; Akiyama, Y.; Oumi, Y.; Kawai, A.; Mizukami, F. The Topotactic Conversion of a Novel Layered Silicate into a New Framework Zeolite. *Angew. Chem., Int. Ed.* **2004**, *43* (37), 4892−4896.
(95) Dorset, D. L.; Kennedy, G. J. Crystal Structure of MCM-65: An Alternative Linkage of Ferrierite Layers. *J. Phys. Chem. B* **2004**, *108* (39), 15216−15222.
(96) Araki, T. Crystal-Structure of a Cesium Aluminosilicate, $Cs[AlSi_5O_{12}]$. *Z. Kristallogr.* **1980**, *152* (3−4), 207−213.
(97) Zanardi, S.; Alberti, A.; Cruciani, G.; Corma, A.; Fornés, V.; Brunelli, M. Crystal Structure Determination of Zeolite Nu-6(2) and Its Layered Precursor Nu-6(1). *Angew. Chem., Int. Ed.* **2004**, *43* (37), 4933−4937.
(98) Wang, Y. X.; Gies, H.; Marler, B.; Muller, U. Synthesis and Crystal Structure of Zeolite RUB-41 Obtained as Calcination Product of a Layered Precursor: A Systematic Approach to a New Synthesis Route. *Chem. Mater.* **2005**, *17* (1), 43−49.
(99) Brooke, H. J. On the Comptonite of Vesuvius, the Brewsterite of Scotland, the Stilbite and the Heulandite. *Edinburgh Philos. J.* **1822**, *6*, 112−115.
(100) Merkle, A. B.; Slaughter, M. Crystal Structure of Heulandite $(Ca,Na_2)Al_2Si_7O_{18}\cdot 6H_2O$. *Am. Mineral.* **1967**, *52* (1−2), 273−276.
(101) Thomson, T. A Chemical Analysis of Sodalite, a New Mineral from Greenland. *Med. Phys. J.* **1811**, *26*, 303−308.

https://dx.doi.org/10.1021/acscatal.0c05332
ACS Catal. 2021, 11, 2366−2396

(102) Marler, B.; Stroter, N.; Gies, H. The Structure of the New Pure Silica Zeolite RUB-24, $Si_{32}O_{64}$, Obtained by Topotactic Condensation of the Intercalated Layer Silicate RUB-18. *Microporous Mesoporous Mater.* **2005**, *83* (1−3), 201−211.
(103) Lesch, D. A.; Wilson, S. T. Crystalline Aluminophosphate of the Molecular-Sieve Type, and Method for Its Preparation. $AlPO_4$−41. European Patent 0254075 A1, 1988.
(104) Bennett, J. M.; Kirchner, R. M. The Structure of as-Synthesized $ALPO_4$−16 Determined by a New Framework Modeling Method and Rietveld Refinement of Synchrotron Powder Diffraction Data. *Zeolites* **1991**, *11* (5), 502−506.
(105) Rubin, M. K. Synthetic Crystal MCM-35. U.S. Patent US4981663A, 1991.
(106) Barrett, P. A.; Díaz-Cabañas, M. J.; Camblor, M. A. Crystal Structure of Zeolite MCM-35 (MTF). *Chem. Mater.* **1999**, *11* (10), 2919−2927.
(107) Vortmann, S.; Marler, B.; Gies, H.; Daniels, P. Synthesis and Crystal-Structure of the New Borosilicate Zeolite RUB-13. *Microporous Mater.* **1995**, *4* (2−3), 111−121.
(108) Roth, W. J.; Nachtigall, P.; Morris, R. E.; Wheatley, P. S.; Seymour, V. R.; Ashbrook, S. E.; Chlubná, P.; Grajciar, L.; Položij, M.; Zukal, A.; Shvets, O.; Čejka, J. A Family of Zeolites with Controlled Pore Size Prepared Using a Top-Down Method. *Nat. Chem.* **2013**, *5* (7), 628−633.
(109) Galli, E.; Gottardi, G. The Crystal Structure of Stilbite. *Mineral. Petrogr. Acta* **1966**, *12*, 1−10.
(110) Davis, T. M.; Chen, C.-Y.; Žilková, N.; Vitvarova-Prochazkova, D.; Čejka, J.; Zones, S. I. The Importance of Channel Intersections in the Catalytic Performance of High Silica Stilbite. *J. Catal.* **2013**, *298*, 84−93.
(111) Morris, R. E.; Burton, A.; Bull, L. M.; Zones, S. I. SSZ-51 - a New Aluminophosphate Zeotype: Synthesis, Crystal Structure, NMR, and Dehydration Properties. *Chem. Mater.* **2004**, *16* (15), 2844−2851.
(112) Millini, R.; Perego, G.; Parker Jr, W. O.; Bellussi, G.; Carluccio, L. Layered Structure of ERB-1 Microporous Borosilicate Precursor and Its Intercalation Properties Towards Polar Molecules. *Microporous Mater.* **1995**, *4* (2−3), 221−230.
(113) Zones, S. I.; Holtermann, D. I.; Innes, R. A.; Pecoraro, T. A.; Santilli, D. S.; Ziemer, J. N. Zeolite SSZ-25. U.S. Patent US4826667A, 1989.
(114) Puppe, L.; Weisser, J. Crystalline Aluminosilicate PSH-3 and Its Process of Preparation. U.S. Patent US4439409A, 1984.
(115) Schmidt, J. E.; Xie, D.; Davis, M. E. High-Silica, Heulandite-Type Zeolites Prepared by Direct Synthesis and Topotactic Condensation. *J. Mater. Chem. A* **2015**, *3* (24), 12890−12897.
(116) Oberhagemann, U.; Bayat, P.; Marler, B.; Gies, H.; Rius, J. A Layer Silicate: Synthesis and Structure of the Zeolite Precursor RUB-15-$[N(CH_3)_4]_8[Si_{24}O_{52}(OH)_4]\cdot 20H_2O$. *Angew. Chem., Int. Ed. Engl.* **1996**, *35* (23−24), 2869−2872.
(117) Moteki, T.; Chaikittisilp, W.; Shimojima, A.; Okubo, T. Silica Sodalite without Occluded Organic Matters by Topotactic Conversion of Lamellar Precursor. *J. Am. Chem. Soc.* **2008**, *130* (47), 15780−15781.
(118) Wolf, F.; Schwieger, W. Ion-Exchange of Mono-Valent Cations in Synthetic Sodium Poly-Silicates with Layer Structure. *Z. Anorg. Allg. Chem.* **1979**, *457* (10), 224−228.
(119) Borbely, G.; Beyer, H. K.; Karge, H. G.; Schwieger, W.; Brandt, A.; Bergk, K. H. Chemical Characterization, Structural Features, and Thermal Behavior of Sodium and Hydrogen Octosilicate. *Clays Clay Miner.* **1991**, *39* (5), 490−497.
(120) Brenn, U.; Ernst, H.; Freude, D.; Herrmann, R.; Jähnig, R.; Karge, H. G.; Kärger, J.; König, T.; Mädler, B.; Pingel, U. T.; Prochnow, D.; Schwieger, W. Synthesis and Characterization of the Layered Sodium Silicate Ilerite. *Microporous Mesoporous Mater.* **2000**, *40* (1−3), 43−52.
(121) Vortmann, S.; Rius, J.; Siegmann, S.; Gies, H. Ab Initio Structure Solution from X-Ray Powder Data at Moderate Resolution: Crystal Structure of a Microporous Layer Silicate. *J. Phys. Chem. B* **1997**, *101* (8), 1292−1297.
(122) Wheatley, P. S.; Morris, R. E. Calcination of a Layered Aluminofluorophosphate Precursor to Form the Zeolitic AFO Framework. *J. Mater. Chem.* **2006**, *16* (11), 1035−1037.
(123) Asakura, Y.; Takayama, R.; Shibue, T.; Kuroda, K. Topotactic Conversion of beta-Helix-Layered Silicate into AST-Type Zeolite through Successive Interlayer Modifications. *Chem. - Eur. J.* **2014**, *20* (7), 1893−1900.
(124) Rojas, A.; Camblor, M. A. HPM-2, the Layered Precursor to Zeolite MTF. *Chem. Mater.* **2014**, *26* (2), 1161−1169.
(125) Schmidt, J. E.; Xie, D.; Davis, M. E. Synthesis of the RTH-Type Layer: The First Small-Pore, Two Dimensional Layered Zeolite Precursor. *Chem. Sci.* **2015**, *6* (10), 5955−5963.
(126) Chen, Y. P.; Huang, S. L.; Wang, X. G.; Zhang, L.; Wu, N. N.; Liao, F. H.; Wang, Y. Synthesis and Characterization of a Layered Silicogermanate PKU-22 and Its Topotactic Condensation to a Three-Dimensional STI-Type Zeolite. *Cryst. Growth Des.* **2017**, *17* (10), 5465−5473.
(127) Guo, P.; Afeworki, M. B. E.; Cao, G.; Yun, Y. F.; Sun, J. L.; Su, J.; Wan, W.; Zou, X. D. Synthesis and Structure of a Layered Fluoroaluminophosphate and Its Transformation to a Three-Dimensional Zeotype Framework. *Inorg. Chem.* **2018**, *57* (18), 11753−11760.
(128) Roth, W. J.; Dorset, D. L. Expanded View of Zeolite Structures and Their Variability Based on Layered Nature of 3-D Frameworks. *Microporous Mesoporous Mater.* **2011**, *142* (1), 32−36.
(129) Kubů, M.; Roth, W. J.; Greer, H. F.; Zhou, W.; Morris, R. E.; Přech, J.; Čejka, J. A New Family of Two-Dimensional Zeolites Prepared from the Intermediate Layered Precursor IPC-3P Obtained During the Synthesis of TUN Zeolite. *Chem. - Eur. J.* **2013**, *19* (41), 13937−13945.
(130) Rohde, L. M.; Lewis, G. J.; Miller, M. A.; Moscoso, J. G.; Gisselquist, J. L.; Patton, R. L.; Wilson, S. T.; Jan, D. Y. Crystalline aluminosilicate zeolitic composition: UZM-8. U.S. Patent US6756030B1, 2004.
(131) Na, K.; Park, W.; Seo, Y.; Ryoo, R. Disordered Assembly of MFI Zeolite Nanosheets with a Large Volume of Intersheet Mesopores. *Chem. Mater.* **2011**, *23* (5), 1273−1279.
(132) Wang, L. L.; Wang, Y.; Liu, Y. M.; Chen, L.; Cheng, S. F.; Gao, G. H.; He, M. Y.; Wu, P. Post-Transformation of MWW-Type Lamellar Precursors into MCM-56 Analogues. *Microporous Mesoporous Mater.* **2008**, *113* (1−3), 435−444.
(133) Zhao, Z.; Zhang, W.; Ren, P.; Han, X.; Müller, U.; Yilmaz, B.; Feyen, M.; Gies, H.; Xiao, F. S.; De Vos, D.; Tatsumi, T.; Bao, X. Insights into the Topotactic Conversion Process from Layered Silicate RUB-36 to FER-Type Zeolite by Layer Reassembly. *Chem. Mater.* **2013**, *25* (6), 840−847.
(134) Burton, A.; Accardi, R. J.; Lobo, R. F.; Falcioni, M.; Deem, M. W. MCM-47: A Highly Crystalline Silicate Composed of Hydrogen-Bonded Ferrierite Layers. *Chem. Mater.* **2000**, *12* (10), 2936−2942.
(135) Roth, W. J.; Kresge, C. T. Intercalation Chemistry of Nu-6(1), the Layered Precursor to Zeolite NSI, Leading to the Pillared Zeolite MCM-39(Si). *Microporous Mesoporous Mater.* **2011**, *144* (1−3), 158−161.
(136) Kresge, C. T.; Roth, W. J. Crystalline Oxide Material. U.S. Patent US5266541A, 1993.
(137) Rollmann, L. D.; Schlenker, J. L.; Lawton, S. L.; Kennedy, C. L.; Kennedy, G. J. MCM-69, a Novel Layered Analogue of EU-19. *Microporous Mesoporous Mater.* **2002**, *53* (1−3), 179−193.
(138) Moteki, T.; Chaikittisilp, W.; Sakamoto, Y.; Shimojima, A.; Okubo, T. Role of Acidic Pretreatment of Layered Silicate RUB-15 in Its Topotactic Conversion into Pure Silica Sodalite. *Chem. Mater.* **2011**, *23* (15), 3564−3570.
(139) Roth, W. J.; Shvets, O. V.; Shamzhy, M.; Chlubná, P.; Kubů, M.; Nachtigall, P.; Čejka, J. Postsynthesis Transformation of Three-Dimensional Framework into a Lamellar Zeolite with Modifiable Architecture. *J. Am. Chem. Soc.* **2011**, *133* (16), 6130−6133.
(140) Fan, W. B.; Wu, P.; Namba, S.; Tatsumi, T. A Titanosilicate That Is Structurally Analogous to an MWW-Type Lamellar Precursor. *Angew. Chem., Int. Ed.* **2004**, *43* (2), 236−240.

https://dx.doi.org/10.1021/acscatal.0c05332
ACS Catal. 2021, 11, 2366−2396

(141) Wu, P.; Ruan, J. F.; Wang, L. L.; Wu, L. L.; Wang, Y.; Liu, Y. M.; Fan, W. B.; He, M. Y.; Terasaki, O.; Tatsumi, T. Methodology for Synthesizing Crystalline Metallosilicates with Expanded Pore Windows through Molecular Alkoxysilylation of Zeolitic Lamellar Precursors. *J. Am. Chem. Soc.* **2008**, *130* (26), 8178−8187.
(142) Jiang, J. G.; Jia, L.; Yang, B.; Xu, H.; Wu, P. Preparation of Interlayer-Expanded Zeolite from Lamellar Precursor Nu-6(1) by Silylation. *Chem. Mater.* **2013**, *25* (23), 4710−4718.
(143) Gies, H.; Muller, U.; Yilmaz, B.; Tatsumi, T.; Xie, B.; Xiao, F. S.; Bao, X. H.; Zhang, W. P.; De Vos, D. Interlayer Expansion of the Layered Zeolite Precursor RUB-39: A Universal Method to Synthesize Functionalized Microporous Silicates. *Chem. Mater.* **2011**, *23* (10), 2545−2554.
(144) Asakura, Y.; Matsuo, Y.; Takahashi, N.; Kuroda, K. Ordered Silylation of Layered Silicate RUB-51 with Half-Sodalite Cages. *Bull. Chem. Soc. Jpn.* **2011**, *84* (9), 968−975.
(145) Verheyen, E.; Joos, L.; Van Havenbergh, K.; Breynaert, E.; Kasian, N.; Gobechiya, E.; Houthoofd, K.; Martineau, C.; Hinterstein, M.; Taulelle, F.; Van Speybroeck, V.; Waroquier, M.; Bals, S.; Van Tendeloo, G.; Kirschhock, C. E. A.; Martens, J. A. Design of Zeolite by Inverse Sigma Transformation. *Nat. Mater.* **2012**, *11* (12), 1059−1064.
(146) Roth, W. J.; Dorset, D. L.; Kennedy, G. J.; Yorke, T.; Helton, T. E. A Novel Molecular Sieve Composition EMM-12, a Method of Making and a Process of Using the Same. WO Patent 2010021795 (A1), 2010.
(147) Macedo, T. R.; Airoldi, C. Organofunctionalized RUB-18 from the Intercalated Precursor Cetyltrimethylammonium Cation. *Microporous Mesoporous Mater.* **2010**, *128* (1−3), 158−164.
(148) Kiba, S.; Itagaki, T.; Nakato, T.; Kuroda, K. Interlayer Modification of a Layered H-Octosilicate (H-RUB-18) with Methanol: Formation of a Highly Ordered Organosilicate Nanohybrid. *J. Mater. Chem.* **2010**, *20* (16), 3202−3210.
(149) Corma, A.; Diaz, U.; Domine, M. E.; Fornes, V. AlITQ-6 and TiITQ-6: Synthesis, Characterization, and Catalytic Activity. *Angew. Chem., Int. Ed.* **2000**, *39* (8), 1499−1501.
(150) Kawai, A.; Ikeda, T.; Kodaira, T.; Endo, A.; Mizukami, F. Preparation of Plate-Like Mesoporous Material from Layered Silicate RUB-15. *J. Nanosci. Nanotechnol.* **2013**, *13* (4), 2864−2870.
(151) Xu, L.; Ji, X.; Li, S.; Zhou, Z.; Du, X.; Sun, J.; Deng, F.; Che, S.; Wu, P. Self-Assembly of Cetyltrimethylammonium Bromide and Lamellar Zeolite Precursor for the Preparation of Hierarchical MWW Zeolite. *Chem. Mater.* **2016**, *28* (12), 4512−4521.
(152) Corma, A.; Fornes, V.; Pergher, S. B.; Maesen, T. L. M.; Buglass, J. G. Delaminated Zeolite Precursors as Selective Acidic Catalysts. *Nature* **1998**, *396* (6709), 353−356.
(153) Corma, A.; Fornes, V.; Diaz, U. ITQ-18 a New Delaminated Stable Zeolite. *Chem. Commun. (Cambridge, U. K.)* **2001**, No. 24, 2642−2643.
(154) Osada, S.; Iribe, A.; Kuroda, K. Exfoliation of Layered Octosilicate by Simple Cation Exchange with Didecyldimethylammonium Ions. *Chem. Lett.* **2013**, *42* (1), 80−82.
(155) Machoke, A. G.; Knoke, I. Y.; Lopez-Orozco, S.; Schmiele, M.; Selvam, T.; Marthala, V. R. R.; Spiecker, E.; Unruh, T.; Hartmann, M.; Schwieger, W. Synthesis of Multilamellar MFI-Type Zeolites under Static Conditions: The Role of Gel Composition on Their Properties. *Microporous Mesoporous Mater.* **2014**, *190*, 324−333.
(156) Chlubná, P.; Roth, W. J.; Greer, H. F.; Zhou, W. Z.; Shvets, O.; Zukal, A.; Čejka, J.; Morris, R. E. 3D to 2D Routes to Ultrathin and Expanded Zeolitic Materials. *Chem. Mater.* **2013**, *25* (4), 542−547.
(157) Zhang, X. Y.; Liu, D. X.; Xu, D. D.; Asahina, S.; Cychosz, K. A.; Agrawal, K. V.; Al Wahedi, Y.; Bhan, A.; Al Hashimi, S.; Terasaki, O.; Thommes, M.; Tsapatsis, M. Synthesis of Self-Pillared Zeolite Nanosheets by Repetitive Branching. *Science* **2012**, *336* (6089), 1684−1687.
(158) Kosuge, K.; Tsunashima, A. New Silica-Pillared Material Prepared from the Layered Silicic Acid of Ilerite. *J. Chem. Soc., Chem. Commun.* **1995**, No. 23, 2427−2428.
(159) Corma, A.; Diaz, U.; Garcia, T.; Sastre, G.; Velty, A. Multifunctional Hybrid Organic-Inorganic Catalytic Materials with a Hierarchical System of Well-Defined Micro- and Mesopores. *J. Am. Chem. Soc.* **2010**, *132* (42), 15011−15021.
(160) Ishii, R.; Shinohara, Y. Preparation of a Microporous Biphenyl-Pillared Layered Hybrid Material Using Organic-Bridged Alkoxysilane and Layered Silicic Acid. *J. Mater. Chem.* **2005**, *15* (5), 551−553.
(161) Opanasenko, M.; Parker, W. O.; Shamzhy, M.; Montanari, E.; Bellettato, M.; Mazur, M.; Millini, R.; Čejka, J. Hierarchical Hybrid Organic-Inorganic Materials with Tunable Textural Properties Obtained Using Zeolitic-Layered Precursor. *J. Am. Chem. Soc.* **2014**, *136* (6), 2511−2519.
(162) Roth, W. J.; Sasaki, T.; Wolski, K.; Song, Y.; Tang, D. M.; Ebina, Y.; Ma, R. Z.; Grzybek, J.; Kalahurska, K.; Gil, B.; Mazur, M.; Zapotoczny, S.; Čejka, J. Liquid Dispersions of Zeolite Monolayers with High Catalytic Activity Prepared by Soft-Chemical Exfoliation. *Sci. Adv.* **2020**, *6* (12), No. eaay8163.
(163) Varoon, K.; Zhang, X. Y.; Elyassi, B.; Brewer, D. D.; Gettel, M.; Kumar, S.; Lee, J. A.; Maheshwari, S.; Mittal, A.; Sung, C. Y.; Cococcioni, M.; Francis, L. F.; McCormick, A. V.; Mkhoyan, K. A.; Tsapatsis, M. Dispersible Exfoliated Zeolite Nanosheets and Their Application as a Selective Membrane. *Science* **2011**, *334* (6052), 72−75.
(164) Dakhchoune, M.; Villalobos, L. F.; Semino, R.; Liu, L. M.; Rezaei, M.; Schouwink, P.; Avalos, C. E.; Baade, P.; Wood, V.; Han, Y.; Ceriotti, M.; Agrawal, K. V. Gas-Sieving Zeolitic Membranes Fabricated by Condensation of Precursor Nanosheets. *Nat. Mater.* 2020, DOI: 10.1038/s41563-020-00822-2.
(165) Čejka, J.; Roth, W. J.; Opanasenko, M. Two-Dimensional Silica-Based Inorganic Networks. In *Comprehensive Supramolecular Chemistry II*; Gokel, G. W., Barbour, L., Atwood, J. L., Eds. Elsevier Science: 2017; Vol. 7, pp 475−501.
(166) Vogt, E. T. C.; Whiting, G. T.; Dutta Chowdhury, A.; Weckhuysen, B. M. Chapter Two - Zeolites and Zeotypes for Oil and Gas Conversion. In *Adv. Catal.*; Jentoft, F. C., Ed.; Academic Press: 2015; Vol. *58*, pp 143−314.
(167) Li, K. H.; Valla, J.; Garcia-Martinez, J. Realizing the Commercial Potential of Hierarchical Zeolites: New Opportunities in Catalytic Cracking. *ChemCatChem* **2014**, *6* (1), 46−66.
(168) Van Koningsveld, H.; Jansen, J. C.; Van Bekkum, H. The Monoclinic Framework Structure of Zeolite H-ZSM-5. Comparison with the Orthorhombic Framework of as-Synthesized ZSM-5. *Zeolites* **1990**, *10* (4), 235−42.
(169) Inayat, A.; Knoke, I.; Spiecker, E.; Schwieger, W. Assemblies of Mesoporous FAU-Type Zeolite Nanosheets. *Angew. Chem., Int. Ed.* **2012**, *51* (8), 1962−1965.
(170) Khaleel, M.; Wagner, A. J.; Mkhoyan, K. A.; Tsapatsis, M. On the Rotational Intergrowth of Hierarchical FAU/EMT Zeolites. *Angew. Chem., Int. Ed.* **2014**, *53* (36), 9456−9461.
(171) Jung, J.; Jo, C.; Cho, K.; Ryoo, R. Zeolite Nanosheet of a Single-Pore Thickness Generated by a Zeolite-Structure-Directing Surfactant. *J. Mater. Chem.* **2012**, *22* (11), 4637−4640.
(172) Jeon, M. Y.; Kim, D.; Kumar, P.; Lee, P. S.; Rangnekar, N.; Bai, P.; Shete, M.; Elyassi, B.; Lee, H. S.; Narasimharao, K.; Basahel, S. N.; Al-Thabaiti, S.; Xu, W. Q.; Cho, H. J.; Fetisov, E. O.; Thyagarajan, R.; DeJaco, R. F.; Fan, W.; Mkhoyan, K. A.; Siepmann, J. I.; Tsapatsis, M. Ultra-Selective High-Flux Membranes from Directly Synthesized Zeolite Nanosheets. *Nature* **2017**, *543* (7647), 690−694.
(173) Corma, A.; Diaz, U.; Domine, M. E.; Fornes, V. New Aluminosilicate and Titanosilicate Delaminated Materials Active for Acid Catalysis, and Oxidation Reactions Using H_2O_2. *J. Am. Chem. Soc.* **2000**, *122* (12), 2804−2809.
(174) Corma, A.; Fornes, V.; Martinez-Triguero, J.; Pergher, S. B. Delaminated Zeolites: Combining the Benefits of Zeolites and Mesoporous Materials for Catalytic Uses. *J. Catal.* **1999**, *186* (1), 57−63.
(175) Gil, B.; Makowski, W.; Marszalek, B.; Roth, W. J.; Kubů, M.; Čejka, J.; Olejniczak, Z. High Acidity Unilamellar Zeolite MCM-56 and Its Pillared and Delaminated Derivatives. *Dalton Trans.* **2014**, *43* (27), 10501−10511.
(176) Maheshwari, S.; Martínez, C.; Teresa Portilla, M.; Llopis, F. J.; Corma, A.; Tsapatsis, M. Influence of Layer Structure Preservation on

the Catalytic Properties of the Pillared Zeolite MCM-36. *J. Catal.* **2010**, *272* (2), 298−308.
(177) Theng, B. K. G. Polymer-Clay Nanocomposites. *Dev. Clay Sci.* **2012**, *4*, 201−241.
(178) Maheshwari, S.; Jordan, E.; Kumar, S.; Bates, F. S.; Penn, R. L.; Shantz, D. F.; Tsapatsis, M. Layer Structure Preservation During Swelling, Pillaring, and Exfoliation of a Zeolite Precursor. *J. Am. Chem. Soc.* **2008**, *130* (4), 1507−1516.
(179) Landis, M. E.; Aufdembrink, B. A.; Chu, P.; Johnson, I. D.; Kirker, G. W.; Rubin, M. K. Preparation of Molecular Sieves from Dense, Layered Metal Oxides. *J. Am. Chem. Soc.* **1991**, *113* (8), 3189−3190.
(180) Přech, J. Catalytic Performance of Advanced Titanosilicate Selective Oxidation Catalysts - a Review. *Catal. Rev.: Sci. Eng.* **2018**, *60* (1), 71−131.
(181) Přech, J.; Eliášová, P.; Aldhayan, D.; Kubů, M. Epoxidation of Bulky Organic Molecules over Pillared Titanosilicates. *Catal. Today* **2015**, *243*, 134−140.
(182) Wilde, N.; Přech, J.; Pelz, M.; Kubů, M.; Čejka, J.; Glaser, R. Accessibility Enhancement of TS-1-Based Catalysts for Improving the Epoxidation of Plant Oil-Derived Substrates. *Catal. Sci. Technol.* **2016**, *6* (19), 7280−7288.
(183) Přech, J.; Morris, R. E.; Čejka, J. Selective Oxidation of Bulky Organic Sulphides over Layered Titanosilicate Catalysts. *Catal. Sci. Technol.* **2016**, *6* (8), 2775−2786.
(184) Přech, J.; Čejka, J. UTL Titanosilicate: An Extra-Large Pore Epoxidation Catalyst with Tunable Textural Properties. *Catal. Today* **2016**, *277*, 2−8.
(185) Přech, J.; Carretero, M. A.; Čejka, J. Baeyer-Villiger Oxidation of Cyclic Ketones by Using Tin-Silica Pillared Catalysts. *ChemCatChem* **2017**, *9* (15), 3063−3072.
(186) Shamzhy, M.; Mazur, M.; Opanasenko, M.; Roth, W. J.; Čejka, J. Swelling and Pillaring of the Layered Precursor IPC-1P: Tiny Details Determine Everything. *Dalton Trans.* **2014**, *43* (27), 10548−10557.
(187) Opanasenko, M.; Shamzhy, M.; Yu, F. J.; Zhou, W. Z.; Morris, R. E.; Čejka, J. Zeolite-Derived Hybrid Materials with Adjustable Organic Pillars. *Chem. Sci.* **2016**, *7* (6), 3589−3601.
(188) Roth, W. J.; Makowski, W.; Marszalek, B.; Michorczyk, P.; Skuza, W.; Gil, B. Activity Enhancement of Zeolite MCM-22 by Interlayer Expansion Enabling Higher Ce Loading and Room Temperature CO Oxidation. *J. Mater. Chem. A* **2014**, *2* (38), 15722−15725.
(189) Ruan, J. F.; Wu, P.; Slater, B.; Zhao, Z. L.; Wu, L. L.; Terasaki, O. Structural Characterization of Interlayer Expanded Zeolite Prepared from Ferrierite Lamellar Precursor. *Chem. Mater.* **2009**, *21* (13), 2904−2911.
(190) Osada, M.; Sasaki, T. Exfoliated Oxide Nanosheets: New Solution to Nanoelectronics. *J. Mater. Chem.* **2009**, *19* (17), 2503−2511.
(191) Hartmann, M.; Machoke, A. G.; Schwieger, W. Catalytic Test Reactions for the Evaluation of Hierarchical Zeolites. *Chem. Soc. Rev.* **2016**, *45* (12), 3313−3330.
(192) Perez-Ramirez, J.; Verboekend, D.; Bonilla, A.; Abello, S. Zeolite Catalysts with Tunable Hierarchy Factor by Pore-Growth Moderators. *Adv. Funct. Mater.* **2009**, *19* (24), 3972−3979.
(193) Wei, R.; Yang, H.; Scott, J. A.; Aguey-Zinsou, K.-F.; Zhang, D. 2D Versus 3D MFI Zeolite: The Effect of Si/Al Ratio on the Accessibility of Acid Sites and Catalytic Performance. *Mater. Tod. Chem.* **2018**, *8*, 1−12.
(194) Seo, Y.; Cho, K.; Jung, Y.; Ryoo, R. Characterization of the Surface Acidity of MFI Zeolite Nanosheets by ^{31}P NMR of Adsorbed Phosphine Oxides and Catalytic Cracking of Decalin. *ACS Catal.* **2013**, *3* (4), 713−720.
(195) Fan, C.; Wang, Y.; Li, H.; Wang, X.; Sun, C.; Zhang, X.; Wang, C.; Wang, S. Seed-Induced Synthesis of Multilamellar ZSM-5 Nanosheets Directed by Amphiphilic Organosilane. *New J. Chem.* **2018**, *42* (20), 17043−17055.
(196) Qin, Z.; Pinard, L.; Benghalem, M. A.; Daou, T. J.; Melinte, G.; Ersen, O.; Asahina, S.; Gilson, J.-P.; Valtchev, V. Preparation of Single-Crystal "House-of-Cards"-Like ZSM-5 and Their Performance in Ethanol-to-Hydrocarbon Conversion. *Chem. Mater.* **2019**, *31* (13), 4639−4648.
(197) Jiang, L.; Li, X. Y.; Gong, Y. J.; Meng, X. L.; Zhang, L. M.; Zhai, Y. L.; Shang, S. M.; Meng, L. K. MCM-56 Stabilization Synthesis Using Auxiliary Tetraethylammounium Ions: Its Role to Inhibit Surface Si-O-Al Bridged Linkage and Retain Highly Delaminated Structure. *Microporous Mesoporous Mater.* **2020**, *302*, 110245.
(198) Corma, A.; Martínez, A.; Martínez-Soria, V. Catalytic Performance of the New Delaminated ITQ-2 Zeolite for Mild Hydrocracking and Aromatic Hydrogenation Processes. *J. Catal.* **2001**, *200* (2), 259−269.
(199) Hernandez-Tamargo, C. E.; Roldan, A.; de Leeuw, N. H. A Density Functional Theory Study of the Structure of Pure-Silica and Aluminium-Substituted MFI Nanosheets. *J. Solid State Chem.* **2016**, *237*, 192−203.
(200) Xu, L.; Sun, J. L. Recent Advances in the Synthesis and Application of Two-Dimensional Zeolites. *Adv. Energy Mater.* **2016**, *6* (17), 1600441.
(201) Shamzhy, M.; Opanasenko, M.; Concepcion, P.; Martinez, A. New Trends in Tailoring Active Sites in Zeolite-Based Catalysts. *Chem. Soc. Rev.* **2019**, *48* (4), 1095−1149.
(202) Bleken, B.-T. L.; Wragg, D. S.; Arstad, B.; Gunnæs, A. E.; Mouzon, J.; Helveg, S.; Lundegaard, L. F.; Beato, P.; Bordiga, S.; Olsbye, U.; Svelle, S.; Lillerud, K. P. Unit Cell Thick Nanosheets of Zeolite H-ZSM-5: Structure and Activity. *Top. Catal.* **2013**, *56* (9), 558−566.
(203) Wu, L.; Magusin, P. C. M. M.; Degirmenci, V.; Li, M.; Almutairi, S. M. T.; Zhu, X.; Mezari, B.; Hensen, E. J. M. Acidic Properties of Nanolayered ZSM-5 Zeolites. *Microporous Mesoporous Mater.* **2014**, *189*, 144−157.
(204) Lacarriere, A.; Luck, F.; Swierczynski, D.; Fajula, F.; Hulea, V. Methanol to Hydrocarbons over Zeolites with MWW Topology: Effect of Zeolite Texture and Acidity. *Appl. Catal., A* **2011**, *402* (1−2), 208−217.
(205) Liang, T. Y.; Chen, J. L.; Qin, Z. F.; Li, J. F.; Wang, P. F.; Wang, S.; Wang, G. F.; Dong, M.; Fan, W. B.; Wang, J. G. Conversion of Methanol to Olefins over H-ZSM-5 Zeolite: Reaction Pathway Is Related to the Framework Aluminum Siting. *ACS Catal.* **2016**, *6* (11), 7311−7325.
(206) Tempelman, C. H. L.; Portilla, M. T.; Martínez-Armero, M. E.; Mezari, B.; de Caluwé, N. G. R.; Martínez, C.; Hensen, E. J. M. One-Pot Synthesis of Nano-Crystalline MCM-22. *Microporous Mesoporous Mater.* **2016**, *220*, 28−38.
(207) Gil, B.; Marszalek, B.; Micek-Ilnicka, A.; Olejniczak, Z. The Influence of Si/Al Ratio on the Distribution of OH Groups in Zeolites with MWW Topology. *Top. Catal.* **2010**, *53* (19−20), 1340−1348.
(208) Gil, B.; Kalahurska, K.; Kowalczyk, A. A Study of the External and Internal Sites of 2D and 3D Zeolites through the FTIR Investigation of the Adsorption of Ammonia and Pivalonitrile. *Appl. Catal., A* **2019**, *578*, 63−69.
(209) Onida, B.; Geobaldo, F.; Testa, F.; Crea, F.; Garrone, E. FTIR Investigation of the Interaction at 77 K of Diatomic Molecular Probes on MCM-22 Zeolite. *Microporous Mesoporous Mater.* **1999**, *30* (1), 119−127.
(210) Meloni, D.; Laforge, S.; Martin, D.; Guisnet, M.; Rombi, E.; Solinas, V. Acidic and Catalytic Properties of H-MCM-22 Zeolites: 1. Characterization of the Acidity by Pyridine Adsorption. *Appl. Catal., A* **2001**, *215* (1), 55−66.
(211) Freude, D.; Hunger, M.; Pfeifer, H.; Schwieger, W. ^{1}H MAS NMR Studies on the Acidity of Zeolites. *Chem. Phys. Lett.* **1986**, *128* (1), 62−66.
(212) Pfeifer, H. Highly Resolved Solid-State Proton Magnetic Resonance Studies of Zeolites. *J. Chem. Soc., Faraday Trans. 1* **1988**, *84* (11), 3777−3783.
(213) Delitala, C.; Alba, M. D.; Becerro, A. I.; Delpiano, D.; Meloni, D.; Musu, E.; Ferino, I. Synthesis of MCM-22 Zeolites of Different Si/Al Ratio and Their Structural, Morphological and Textural Characterisation. *Microporous Mesoporous Mater.* **2009**, *118* (1), 1−10.

https://dx.doi.org/10.1021/acscatal.0c05332
ACS Catal. 2021, 11, 2366−2396

(214) Zhao, Q.; Chen, W.-H.; Huang, S.-J.; Wu, Y.-C.; Lee, H.-K.; Liu, S.-B. Discernment and Quantification of Internal and External Acid Sites on Zeolites. *J. Phys. Chem. B* **2002**, *106* (17), 4462−4469.
(215) Zheng, A. M.; Liu, S. B.; Deng, F. P-31 NMR Chemical Shifts of Phosphorus Probes as Reliable and Practical Acidity Scales for Solid and Liquid Catalysts. *Chem. Rev. (Washington, DC, U. S.)* **2017**, *117* (19), 12475−12531.
(216) Zhou, Y.; Mu, Y.; Hsieh, M.-F.; Kabius, B.; Pacheco, C.; Bator, C.; Rioux, R. M.; Rimer, J. D. Enhanced Surface Activity of MWW Zeolite Nanosheets Prepared Via a One-Step Synthesis. *J. Am. Chem. Soc.* **2020**, *142* (18), 8211−8222.
(217) Hernandez-Tamargo, C. E.; Roldan, A.; de Leeuw, N. H. DFT Modeling of the Adsorption of Trimethylphosphine Oxide at the Internal and External Surfaces of Zeolite MFI. *J. Phys. Chem. C* **2016**, *120* (34), 19097−19106.
(218) Zheng, A. M.; Chen, L.; Yang, J.; Zhang, M. J.; Su, Y. C.; Yue, Y.; Ye, C. H.; Deng, F. Combined DFT Theoretical Calculation and Solid-State NMR Studies of Al Substitution and Acid Sites in Zeolite MCM-22. *J. Phys. Chem. B* **2005**, *109* (51), 24273−24279.
(219) Webster, C. E.; Drago, R. S.; Zerner, M. C. Molecular Dimensions for Adsorptives. *J. Am. Chem. Soc.* **1998**, *120* (22), 5509−5516.
(220) Sing, K. S. W.; Williams, R. T. The Use of Molecular Probes for the Characterization of Nanoporous Adsorbents. *Part. Part. Syst. Char.* **2004**, *21* (2), 71−79.
(221) Góra-Marek, K.; Tarach, K.; Choi, M. 2,6-Di-Tert-Butylpyridine Sorption Approach to Quantify the External Acidity in Hierarchical Zeolites. *J. Phys. Chem. C* **2014**, *118* (23), 12266−12274.
(222) Bortnovsky, O.; Melichar, Z.; Sobalík, Z.; Wichterlová, B. Quantitative Analysis of Aluminium and Iron in the Framework of Zeolites. *Microporous Mesoporous Mater.* **2001**, *42* (1), 97−102.
(223) Lad, J. B.; Makkawi, Y. T. Adsorption of Dimethyl Ether (DME) on Zeolite Molecular Sieves. *Chem. Eng. J. (Amsterdam, Neth.)* **2014**, *256*, 335−346.
(224) Datka, J.; Gil, B.; Kubacka, A. Heterogeneity of OH Groups in NaH-Mordenites: Effect of Na/H Exchange Degree. *Zeolites* **1997**, *18* (4), 245−249.
(225) Gora-Marek, K.; Derewinski, M.; Sarv, P.; Datka, J. IR and NMR Studies of Mesoporous Alumina and Related Aluminosilicates. *Catal. Today* **2005**, *101* (2), 131−138.
(226) Thibault-Starzyk, F.; Gil, B.; Aiello, S.; Chevreau, T.; Gilson, J. In Situ Thermogravimetry in an Infrared Spectrometer: An Answer to Quantitative Spectroscopy of Adsorbed Species on Heterogeneous Catalysts. *Microporous Mesoporous Mater.* **2004**, *67* (1), 107−112.
(227) Emeis, C. A. Determination of Integrated Molar Extinction Coefficients for Infrared Absorption Bands of Pyridine Adsorbed on Solid Acid Catalysts. *J. Catal.* **1993**, *141* (2), 347−354.
(228) Bevilacqua, M.; Busca, G. A Study of the Localization and Accessibility of Brønsted and Lewis Acid Sites of H-Mordenite through the FT-IR Spectroscopy of Adsorbed Branched Nitriles. *Catal. Commun.* **2002**, *3* (11), 497−502.
(229) Sadowska, K.; Gora-Marek, K.; Datka, J. Accessibility of Acid Sites in Hierarchical Zeolites: Quantitative IR Studies of Pivalonitrile Adsorption. *J. Phys. Chem. C* **2013**, *117* (18), 9237−9244.
(230) Thibault-Starzyk, F.; Stan, I.; Abello, S.; Bonilla, A.; Thomas, K.; Fernandez, C.; Gilson, J.-P.; Perez-Ramirez, J. Quantification of Enhanced Acid Site Accessibility in Hierarchical Zeolites - the Accessibility Index. *J. Catal.* **2009**, *264* (1), 11−14.
(231) Onfroy, T.; Clet, G.; Houalla, M. Quantitative IR Characterization of the Acidity of Various Oxide Catalysts. *Microporous Mesoporous Mater.* **2005**, *82* (1−2), 99−104.
(232) Nesterenko, N. S.; Thibault-Starzyk, F.; Montouillout, V.; Yuschenko, V. V.; Fernandez, C.; Gilson, J. P.; Fajula, F.; Ivanova, I. I. Accessibility of the Acid Sites in Dealuminated Small-Port Mordenites Studied by FTIR of Co-Adsorbed Alkylpyridines and CO. *Microporous Mesoporous Mater.* **2004**, *71* (1−3), 157−166.
(233) Ordomsky, V. V.; Murzin, V. Y.; Monakhova, Y. V.; Zubavichus, Y. V.; Knyazeva, E. E.; Nesterenko, N. S.; Ivanova, I. I. Nature, Strength and Accessibility of Acid Sites in Micro/Mesoporous Catalysts Obtained by Recrystallization of Zeolite BEA. *Microporous Mesoporous Mater.* **2007**, *105* (1), 101−110.
(234) Tukur, N. M.; Al-Khattaf, S. Catalytic Transformation of 1,3,5-Trimethylbenzene over a USY Zeolite Catalyst. *Energy Fuels* **2007**, *21* (5), 2499−2508.
(235) Lakiss, L.; Vicente, A.; Gilson, J.-P.; Valtchev, V.; Mintova, S.; Vimont, A.; Bedard, R.; Abdo, S.; Bricker, J. Probing the Brønsted Acidity of the External Surface of Faujasite-Type Zeolites. *ChemPhysChem* **2020**, *21* (16), 1873−1881.
(236) Ayrault, P.; Datka, J.; Laforge, S.; Martin, D.; Guisnet, M. Characterization of the Internal and External Acidity of H-MCM-22 Zeolites. *J. Phys. Chem. B* **2004**, *108* (36), 13755−13763.
(237) Korzeniowska, A.; Grzybek, J.; Kalahurska, K.; Kubů, M.; Roth, W. J.; Gil, B. The Structure-Catalytic Activity Relationship for the Transient Layered Zeolite MCM-56 with MWW Topology. *Catal. Today* **2020**, *345*, 116−124.
(238) Roth, W. J.; Chlubná, P.; Kubů, M.; Vitvarová, D. Swelling of MCM-56 and MCM-22P with a New Medium — Surfactant−Tetramethylammonium Hydroxide Mixtures. *Catal. Today* **2013**, *204*, 8−14.
(239) Wu, Y.; Emdadi, L.; Qin, D.; Zhang, J.; Liu, D. Quantification of External Surface and Pore Mouth Acid Sites in Unit-Cell Thick Pillared MFI and Pillared MWW Zeolites. *Microporous Mesoporous Mater.* **2017**, *241*, 43−51.
(240) Chlubná, P.; Roth, W. J.; Zukal, A.; Kubů, M.; Pavlatová, J. Pillared MWW Zeolites MCM-36 Prepared by Swelling MCM-22P in Concentrated Surfactant Solutions. *Catal. Today* **2012**, *179* (1), 35−42.
(241) Laforge, S.; Ayrault, P.; Martin, D.; Guisnet, M. Acidic and Catalytic Properties of MCM-22 and MCM-36 Zeolites Synthesized from the Same Precursors. *Appl. Catal., A* **2005**, *279*, 79−88.
(242) He, Y. J.; Nivarthy, G. S.; Eder, F.; Seshan, K.; Lercher, J. A. Synthesis, Characterization and Catalytic Activity of the Pillared Molecular Sieve MCM-36. *Microporous Mesoporous Mater.* **1998**, *25* (1), 207−224.
(243) Corma, A.; Fornes, V.; Guil, J. M.; Pergher, S.; Maesen, T. L. M.; Buglass, J. G. Preparation, Characterisation and Catalytic Activity of ITQ-2, a Delaminated Zeolite. *Microporous Mesoporous Mater.* **2000**, *38* (2−3), 301−309.
(244) Lønstad Bleken, B.-T.; Mino, L.; Giordanino, F.; Beato, P.; Svelle, S.; Lillerud, K. P.; Bordiga, S. Probing the Surface of Nanosheet H-ZSM-5 with FTIR Spectroscopy. *Phys. Chem. Chem. Phys.* **2013**, *15* (32), 13363−13370.
(245) Jo, C.; Ryoo, R.; Žilková, N.; Vitvarová, D.; Čejka, J. The Effect of MFI Zeolite Lamellar and Related Mesostructures on Toluene Disproportionation and Alkylation. *Catal. Sci. Technol.* **2013**, *3* (8), 2119−2129.
(246) Korde, A.; Min, B.; Almas, Q.; Chiang, Y. D.; Nair, S.; Jones, C. W. Effect of Si/Al Ratio on the Catalytic Activity of Two-Dimensional MFI Nanosheets in Aromatic Alkylation and Alcohol Etherification. *ChemCatChem* **2019**, *11* (18), 4548−4557.
(247) Corma, A.; Corell, C.; PerezPariente, J.; Guil, J. M.; GuilLopez, R.; Nicolopoulos, S.; Calbet, J. G.; ValletRegi, M. Adsorption and Catalytic Properties of MCM-22: The Influence of Zeolite Structure. *Zeolites* **1996**, *16* (1), 7−14.
(248) Armaroli, T.; Bevilacqua, M.; Trombetta, M.; Milella, F.; Alejandre, A. G.; Ramirez, J.; Notari, B.; Willey, R. J.; Busca, G. A Study of the External and Internal Sites of MFI-Type Zeolitic Materials through the FTIR Investigation of the Adsorption of Nitriles. *Appl. Catal., A* **2001**, *216* (1−2), 59−71.
(249) Montanari, T.; Bevilacqua, M.; Busca, G. Use of Nitriles as Probe Molecules for the Accessibility of the Active Sites and the Detection of Complex Interactions in Zeolites through IR Spectroscopy. *Appl. Catal., A* **2006**, *307* (1), 21−29.
(250) Kadam, S. A.; Shamzhy, M. V. IR Operando Study of Ethanol Dehydration over MFI Zeolites: Structure−Activity Relationships. *J. Phys. Chem. C* **2018**, *122* (42), 24055−24067.
(251) Gil, B.; Roth, W. J.; Grzybek, J.; Korzeniowska, A.; Olejniczak, Z.; Elias, M.; Opanasenko, M.; Čejka, J. The Effect of Hot Liquid Water

https://dx.doi.org/10.1021/acscatal.0c05332
ACS Catal. 2021, 11, 2366−2396

Treatment on the Properties and Catalytic Activity of MWW Zeolites with Various Layered Structures. *Catal. Today* **2018**, *304*, 22−29.
(252) Onida, B.; Borello, L.; Bonelli, B.; Geobaldo, F.; Garrone, E. IR Study of the Acidity of ITQ-2, an "All-Surface" Zeolitic System. *J. Catal.* **2003**, *214* (2), 191−199.
(253) Laforge, S.; Martin, D.; Guisnet, M. m-Xylene Transformation over H-MCM-22 Zeolite. 2. Method for Determining the Catalytic Role of the Three Different Pore Systems. *Microporous Mesoporous Mater.* **2004**, *67* (2), 235−244.
(254) Bevilacqua, M.; Meloni, D.; Sini, F.; Monaci, R.; Montanari, T.; Busca, G. A Study of the Nature, Strength, and Accessibility of Acid Sites of H-MCM-22 Zeolite. *J. Phys. Chem. C* **2008**, *112* (24), 9023−9033.
(255) Gilson, J.-P.; Fernandez, C.; Thibault-Starzyk, F. New Insights on Zeolite Chemistry by Advanced IR and NMR Characterization Tools. *J. Mol. Catal. A: Chem.* **2009**, *305* (1), 54−59.
(256) Marie, O.; Massiani, P.; Thibault-Starzyk, F. Infrared Evidence of a Third Brønsted Site in Mordenites. *J. Phys. Chem. B* **2004**, *108* (16), 5073−5081.
(257) Chenevarin, S.; Thibault-Starzyk, F. Two-Dimensional IR Pressure-Jump Spectroscopy of Adsorbed Species for Zeolites. *Angew. Chem., Int. Ed.* **2004**, *43* (9), 1155−1158.
(258) Arean, C. O.; Delgado, M. R.; Nachtigall, P.; Thang, H. V.; Rubeš, M.; Bulánek, R.; Chlubná-Eliášová, P. Measuring the Brønsted Acid Strength of Zeolites − Does It Correlate with the O−H Frequency Shift Probed by a Weak Base? *Phys. Chem. Chem. Phys.* **2014**, *16* (21), 10129−10141.
(259) Rybicki, M.; Sauer, J. Acidity of Two-Dimensional Zeolites. *Phys. Chem. Chem. Phys.* **2015**, *17* (41), 27873−27882.
(260) Thang, H. V.; Vaculik, J.; Přech, J.; Kubů, M.; Čejka, J.; Nachtigall, P.; Bulanek, R.; Grajciar, L. The Brønsted Acidity of Three- and Two-Dimensional Zeolites. *Microporous Mesoporous Mater.* **2019**, *282*, 121−132.
(261) Sauer, J. Brønsted Activity of Two-Dimensional Zeolites Compared to Bulk Materials. *Faraday Discuss.* **2016**, *188*, 227−234.
(262) Boscoboinik, J. A.; Yu, X.; Emmez, E.; Yang, B.; Shaikhutdinov, S.; Fischer, F. D.; Sauer, J.; Freund, H. J. Interaction of Probe Molecules with Bridging Hydroxyls of Two-Dimensional Zeolites: A Surface Science Approach. *J. Phys. Chem. C* **2013**, *117* (26), 13547−13556.
(263) Treps, L.; Gomez, A.; de Bruin, T.; Chizallet, C. Environment, Stability and Acidity of External Surface Sites of Silicalite-1 and ZSM-5 Micro and Nano Slabs, Sheets, and Crystals. *ACS Catal.* **2020**, *10* (5), 3297−3312.
(264) Parrillo, D. J.; Gorte, R. J. Characterization of Acidity in H-ZSM-5, H-ZSM-12, H-Mordenite, and H-Y Using Microcalorimetry. *J. Phys. Chem.* **1993**, *97* (34), 8786−8792.
(265) Pereira, C.; Gorte, R. J. Method for Distinguishing Brønsted-Acid Sites in Mixtures of H-ZSM-5, H-Y and Silica-Alumina. *Appl. Catal., A* **1992**, *90* (2), 145−157.
(266) Kresnawahjuesa, O.; Gorte, R. J.; de Oliveira, D.; Lau, L. Y. A Simple, Inexpensive, and Reliable Method for Measuring Brønsted-Acid Site Densities in Solid Acids. *Catal. Lett.* **2002**, *82* (3−4), 155−160.
(267) Brauer, P.; Situmorang, O.; Ng, P. L.; D'Agostino, C. Effect of Al Content on the Strength of Terminal Silanol Species in ZSM-5 Zeolite Catalysts: A Quantitative DRIFTS Study without the Use of Molar Extinction Coefficients. *Phys. Chem. Chem. Phys.* **2018**, *20* (6), 4250−4262.
(268) Meng, X. J.; Zhang, M. X.; Chen, C. L.; Li, C. Y.; Xiong, W.; Li, M. Insights into the Role of Silanols in Methanol to Propene Reaction over Silicalite-2 Zeolite through Post-Treatments. *Appl. Catal., A* **2018**, *558*, 122−130.
(269) Corma, A.; Gonzalez-Alfaro, V.; Orchilles, A. V. Decalin and Tetralin as Probe Molecules for Cracking and Hydrotreating the Light Cycle Oil. *J. Catal.* **2001**, *200* (1), 34−44.
(270) Shang, Y. S.; Wang, W. G.; Zhai, Y. L.; Song, Y.; Zhao, X. M.; Ma, T.; Wei, J. H.; Gong, Y. J. Seed-Fused ZSM-5 Nanosheet as a Superior MTP Catalyst: Synergy of Micro/Mesopore and Inter/External Acidity. *Microporous Mesoporous Mater.* **2019**, *276*, 173−182.
(271) Cha, S. H.; Lee, J.; Shin, J.; Hong, S. B. Zeolite UZM-8: Synthesis, Characterization, and Catalytic Properties in Isopropylation of Benzene with 2-Propanol. *Top. Catal.* **2015**, *58* (7−9), 537−544.
(272) Wichterlova, B.; Čejka, J. Mechanism of N-Propyltoluene Formation in C3 Alkylation of Toluene: The Effect of Zeolite Structural Type. *J. Catal.* **1994**, *146* (2), 523−529.
(273) Žilková, N.; Shamzhy, M.; Shvets, O.; Čejka, J. Transformation of Aromatic Hydrocarbons over Isomorphously Substituted UTL: Comparison with Large and Medium Pore Zeolites. *Catal. Today* **2013**, *204*, 22−29.
(274) Liu, D. X.; Zhang, X. Y.; Bhan, A.; Tsapatsis, M. Activity and Selectivity Differences of External Brønsted Acid Sites of Single-Unit-Cell Thick and Conventional MFI and MWW Zeolites. *Microporous Mesoporous Mater.* **2014**, *200*, 287−290.
(275) Xu, D. D.; Abdelrahman, O.; Ahn, S. H.; Guefrachi, Y.; Kuznetsov, A.; Ren, L. M.; Hwang, S.; Khaleel, M.; Al Hassan, S.; Liu, D. X.; Hong, S. B.; Dauenhauer, P.; Tsapatsis, M. A Quantitative Study of the Structure-Activity Relationship in Hierarchical Zeolites Using Liquid-Phase Reactions. *AIChE J.* **2019**, *65* (3), 1067−1075.
(276) Wu, Y. Q.; Lu, Z.; Emdadi, L.; Oh, S. C.; Wang, J.; Lei, Y.; Chen, H. Y.; Tran, D. T.; Lee, I. C.; Liu, D. X. Tuning External Surface of Unit-Cell Thick Pillared MFI and MWW Zeolites by Atomic Layer Deposition and Its Consequences on Acid-Catalyzed Reactions. *J. Catal.* **2016**, *337*, 177−187.
(277) Wei, L.; Song, K.; Wu, W.; Holdren, S.; Zhu, G.; Shulman, E.; Shang, W.; Chen, H.; Zachariah, M. R.; Liu, D. Vapor-Phase Strategy to Pillaring of Two-Dimensional Zeolite. *J. Am. Chem. Soc.* **2019**, *141* (22), 8712−8716.
(278) Gogate, M. R. Methanol-to-Olefins Process Technology: Current Status and Future Prospects. *Pet. Sci. Technol.* **2019**, *37* (5), 559−565.
(279) Chowdhury, A. D.; Houben, K.; Whiting, G. T.; Mokhtar, M.; Asiri, A. M.; Al-Thabaiti, S. A.; Basahel, S. N.; Baldus, M.; Weckhuysen, B. M. Initial Carbon-Carbon Bond Formation During the Early Stages of the Methanol-to-Olefin Process Proven by Zeolite-Trapped Acetate and Methyl Acetate. *Angew. Chem., Int. Ed.* **2016**, *55* (51), 15840−15845.
(280) Chowdhury, A. D.; Paioni, A. L.; Houben, K.; Whiting, G. T.; Baldus, M.; Weckhuysen, B. M. Bridging the Gap between the Direct and Hydrocarbon Pool Mechanisms of the Methanol-to-Hydrocarbons Process. *Angew. Chem., Int. Ed.* **2018**, *57* (27), 8095−8099.
(281) Olsbye, U.; Svelle, S.; Bjorgen, M.; Beato, P.; Janssens, T. V. W.; Joensen, F.; Bordiga, S.; Lillerud, K. P. Conversion of Methanol to Hydrocarbons: How Zeolite Cavity and Pore Size Controls Product Selectivity. *Angew. Chem., Int. Ed.* **2012**, *51* (24), 5810−5831.
(282) Kim, K.; Ryoo, R.; Jang, H. D.; Choi, M. Spatial Distribution, Strength, and Dealumination Behavior of Acid Sites in Nanocrystalline MFI Zeolites and Their Catalytic Consequences. *J. Catal.* **2012**, *288*, 115−123.
(283) Zhang, Q.; Chen, G. R.; Wang, Y. Y.; Chen, M. Y.; Guo, G. Q.; Shi, J.; Luo, J.; Yu, J. H. High-Quality Single-Crystalline MFI-Type Nanozeolites: A Facile Synthetic Strategy and MTP Catalytic Studies. *Chem. Mater.* **2018**, *30* (8), 2750−2758.
(284) Zhang, L. L.; Song, Y.; Li, G. D.; Zhang, Q.; Zhang, S. L.; Xu, J.; Deng, F.; Gong, Y. J. F-Assisted Synthesis of a Hierarchical ZSM-5 Zeolite for Methanol to Propylene Reaction: A b-Oriented Thinner Dimensional Morphology. *RSC Adv.* **2015**, *5* (75), 61354−61363.
(285) Bjorgen, M.; Joensen, F.; Holm, M. S.; Olsbye, U.; Lillerud, K. P.; Svelle, S. Methanol to Gasoline over Zeolite H-ZSM-5: Improved Catalyst Performance by Treatment with NaOH. *Appl. Catal., A* **2008**, *345* (1), 43−50.
(286) Kim, J.; Choi, M.; Ryoo, R. Effect of Mesoporosity against the Deactivation of MFI Zeolite Catalyst During the Methanol-to-Hydrocarbon Conversion Process. *J. Catal.* **2010**, *269* (1), 219−228.
(287) Kim, W.; Ryoo, R. Probing the Catalytic Function of External Acid Sites Located on the MFI Nanosheet for Conversion of Methanol to Hydrocarbons. *Catal. Lett.* **2014**, *144* (7), 1164−1169.

https://dx.doi.org/10.1021/acscatal.0c05332
ACS Catal. 2021, 11, 2366−2396

(288) Busca, G.; Gervasini, A. Chapter One - Solid Acids, Surface Acidity and Heterogeneous Acid Catalysis. In *Adv. Catal.*; Song, C., Ed.; Academic Press: 2020; Vol. *67*, pp 1−90.
(289) Ravi, M.; Sushkevich, V. L.; van Bokhoven, J. A. Towards a Better Understanding of Lewis Acidic Aluminium in Zeolites. *Nat. Mater.* **2020**, *19* (10), 1047−1056.
(290) Hadjiivanov, K. I.; Vayssilov, G. N. Characterization of Oxide Surfaces and Zeolites by Carbon Monoxide as an IR Probe Molecule. *Adv. Catal.* **2002**, *47*, 307−511.
(291) Matsunaga, Y.; Yamazaki, H.; Imai, H.; Yokoi, T.; Tatsumi, T.; Kondo, J. N. Hexamethyleneimine and Pivalonitrile as Location Probe Molecules of Lewis Acid Sites on MWW-Type Zeolites. *Microporous Mesoporous Mater.* **2015**, *206*, 86−94.
(292) Luo, H. Y.; Lewis, J. D.; Roman-Leshkov, Y. Lewis Acid Zeolites for Biomass Conversion: Perspectives and Challenges on Reactivity, Synthesis, and Stability. In *Annual Review of Chemical and Biomolecular Engineering*; Prausnitz, J. M., Ed.; Annual Reviews: 2016; Vol. *7*, pp 663−692.
(293) To, J.; Sokol, A. A.; French, S. A.; Catlow, C. R. A. Formation of Active Sites in TS-1 by Hydrolysis and Inversion. *J. Phys. Chem. C* **2007**, *111* (40), 14720−14731.
(294) Bordiga, S.; Bonino, F.; Damin, A.; Lamberti, C. Reactivity of Ti(IV) Species Hosted in TS-1 Towards H_2O_2-H_2O Solutions Investigated by Ab Initio Cluster and Periodic Approaches Combined with Experimental XANES and EXAFS Data: A Review and New Highlights. *Phys. Chem. Chem. Phys.* **2007**, *9* (35), 4854−4878.
(295) Bare, S. R.; Kelly, S. D.; Sinkler, W.; Low, J. J.; Modica, F. S.; Valencia, S.; Corma, A.; Nemeth, L. T. Uniform Catalytic Site in Sn-Beta-Zeolite Determined Using X-Ray Absorption Fine Structure. *J. Am. Chem. Soc.* **2005**, *127* (37), 12924−12932.
(296) Moliner, M. State of the Art of Lewis Acid-Containing Zeolites: Lessons from Fine Chemistry to New Biomass Transformation Processes. *Dalton Trans.* **2014**, *43* (11), 4197−4208.
(297) Yang, G.; Zhou, L. J.; Han, X. W. Lewis and Brønsted Acidic Sites in M^{4+}-Doped Zeolites (M = Ti, Zr, Ge, Sn, Pb) as Well as Interactions with Probe Molecules: A DFT Study. *J. Mol. Catal. A: Chem.* **2012**, *363*, 371−379.
(298) Gunther, W. R.; Michaelis, V. K.; Griffin, R. G.; Roman-Leshkov, Y. Interrogating the Lewis Acidity of Metal Sites in Beta Zeolites with N-15 Pyridine Adsorption Coupled with MAS NMR Spectroscopy. *J. Phys. Chem. C* **2016**, *120* (50), 28533−28544.
(299) Perego, C.; Bosetti, A. Biomass to Fuels: The Role of Zeolite and Mesoporous Materials. *Microporous Mesoporous Mater.* **2011**, *144* (1−3), 28−39.
(300) Khan, W.; Jia, X. C.; Wu, Z. J.; Choi, J.; Yip, A. C. K. Incorporating Hierarchy into Conventional Zeolites for Catalytic Biomass Conversions: A Review. *Catalysts* **2019**, *9* (2), 127.
(301) Serrano, D. P.; Melero, J. A.; Morales, G.; Iglesias, J.; Pizarro, P. Progress in the Design of Zeolite Catalysts for Biomass Conversion into Biofuels and Bio-Based Chemicals. *Catal. Rev.: Sci. Eng.* **2018**, *60* (1), 1−70.
(302) Rahman, M. M.; Liu, R. H.; Cai, J. M. Catalytic Fast Pyrolysis of Biomass over Zeolites for High Quality Bio-Oil - a Review. *Fuel Process. Technol.* **2018**, *180*, 32−46.
(303) Chen, L. Y.; Ma, X. Q.; Tang, F. F.; Li, Y.; Yu, Z. S.; Chen, X. F. Comparison of Catalytic Effect on Upgrading Bio-Oil Derived from Co-Pyrolysis of Water Hyacinth and Scrap Tire over Multilamellar MFI Nanosheets and HZSM-5. *Bioresour. Technol.* **2020**, *312*, 123592.
(304) Ishihara, A. Preparation and Reactivity of Hierarchical Catalysts in Catalytic Cracking. *Fuel Process. Technol.* **2019**, *194*, 106116.
(305) Lee, H. W.; Park, S. H.; Jeon, J. K.; Ryoo, R.; Kim, W.; Suh, D. J.; Park, Y. K. Upgrading of Bio-Oil Derived from Biomass Constituents over Hierarchical Unilamellar Mesoporous MFI Nanosheets. *Catal. Today* **2014**, *232*, 119−126.
(306) Xu, M. Z.; Mukarakate, C.; Iisa, K.; Budhi, S.; Menart, M.; Davidson, M.; Robichaud, D. J.; Nimlos, M. R.; Trewyn, B. G.; Richards, R. M. Deactivation of Multilayered MFI Nanosheet Zeolite During Upgrading of Biomass Pyrolysis Vapors. *ACS Sustainable Chem. Eng.* **2017**, *5* (6), 5477−5484.
(307) Naqvi, S. R.; Uemura, Y.; Yusup, S.; Nishiyama, N.; Naqvi, M. Catalytic Consequences of Micropore Topology on Biomass Pyrolysis Vapors over Shape Selective Zeolites. In *8th International Conference on Applied Energy*; Yan, J., Sun, F., Chou, S. K., Desideri, U., Li, H., Campana, P., Xiong, R., Eds.; Elsevier: 2017; Vol. *105*, pp 557−561.
(308) Kikhtyanin, O.; Chlubná, P.; Jindrova, T.; Kubicka, D. Peculiar Behavior of MWW Materials in Aldol Condensation of Furfural and Acetone. *Dalton Trans.* **2014**, *43* (27), 10628−10641.
(309) Ren, L. M.; Guo, Q.; Orazov, M.; Xu, D. D.; Politi, D.; Kumar, P.; Alhassan, S. M.; Mkhoyan, K. A.; Sidiras, D.; Davis, M. E.; Tsapatsis, M. Pillared Sn-MWW Prepared by a Solid-State-Exchange Method and Its Use as a Lewis Acid Catalyst. *ChemCatChem* **2016**, *8* (7), 1274−1278.
(310) Ren, L. M.; Guo, Q.; Kumar, P.; Orazov, M.; Xu, D. D.; Alhassan, S. M.; Mkhoyan, K. A.; Davis, M. E.; Tsapatsis, M. Self-Pillared, Single-Unit-Cell Sn-MFI Zeolite Nanosheets and Their Use for Glucose and Lactose Isomerization. *Angew. Chem., Int. Ed.* **2015**, *54* (37), 10848−10851.
(311) Liu, G. Q.; Jiang, J. G.; Yang, B. T.; Fang, X. Q.; Xu, H.; Peng, H. G.; Xu, L.; Liu, Y. M.; Wu, P. Hydrothermal Synthesis of MWW-Type Stannosilicate and Its Post-Structural Transformation to MCM-56 Analogue. *Microporous Mesoporous Mater.* **2013**, *165*, 210−218.
(312) Luo, H. Y.; Bui, L.; Gunther, W. R.; Min, E.; Roman-Leshkov, Y. Synthesis and Catalytic Activity of Sn-MFI Nanosheets for the Baeyer-Villiger Oxidation of Cyclic Ketones. *ACS Catal.* **2012**, *2* (12), 2695−2699.
(313) Pitínová-Štekrová, M.; Eliášová, P.; Weissenberger, T.; Shamzhy, M.; Musilova, Z.; Čejka, J. Highly Selective Synthesis of Campholenic Aldehyde over Ti- MWW Catalysts by α-Pinene Oxide Isomerization. *Catal. Sci. Technol.* **2018**, *8* (18), 4690−4701.
(314) Štekrová, M.; Kubů, M.; Shamzhy, M.; Musilova, Z.; Čejka, J. Alpha-Pinene Oxide Isomerization: Role of Zeolite Structure and Acidity in the Selective Synthesis of Campholenic Aldehyde. *Catal. Sci. Technol.* **2018**, *8* (9), 2488−2501.
(315) Wang, J. G.; Xu, L.; Zhang, K.; Peng, H. G.; Wu, H. H.; Jiang, J. G.; Liu, Y. M.; Wu, P. Multilayer Structured MFI-Type Titanosilicate: Synthesis and Catalytic Properties in Selective Epoxidation of Bulky Molecules. *J. Catal.* **2012**, *288*, 16−23.
(316) Na, K.; Jo, C.; Kin, J.; Ahn, W. S.; Ryoo, R. MFI Titanosilicate Nanosheets with Single-Unit-Cell Thickness as an Oxidation Catalyst Using Peroxides. *ACS Catal.* **2011**, *1* (8), 901−907.
(317) Wu, P.; Nuntasri, D.; Ruan, J. F.; Liu, Y. M.; He, M. Y.; Fan, W. B.; Terasaki, O.; Tatsumi, T. Delamination of Ti-MWW and High Efficiency in Epoxidation of Alkenes with Various Molecular Sizes. *J. Phys. Chem. B* **2004**, *108* (50), 19126−19131.
(318) Grosso-Giordano, N. A.; Hoffman, A. S.; Boubnov, A.; Small, D. W.; Bare, S. R.; Zones, S. I.; Katz, A. Dynamic Reorganization and Confinement of Ti-IV Active Sites Controls Olefin Epoxidation Catalysis on Two-Dimensional Zeotypes. *J. Am. Chem. Soc.* **2019**, *141* (17), 7090−7106.
(319) Liu, Y. S.; Vjunov, A.; Shi, H.; Eckstein, S.; Camaioni, D. M.; Mei, D. H.; Barath, E.; Lercher, J. A. Enhancing the Catalytic Activity of Hydronium Ions through Constrained Environments. *Nat. Commun.* **2017**, *8*, 14113.
(320) Korzeniowska, A.; Grzybek, J.; Roth, W. J.; Kowalczyk, A.; Michorczyk, P.; Čejka, J.; Přech, J.; Gil, B. Incorporation of Ti as a Pyramidal Framework Site in the Mono-Layered MCM-56 Zeolite and Its Oxidation Activity. *ChemCatChem* **2019**, *11* (1), 520−527.

https://dx.doi.org/10.1021/acscatal.0c05332
ACS Catal. 2021, 11, 2366−2396